32000

National Library of Canada / Bibliothèque nationale du Canada

CANADIAN THESES ON MICROFICHE / THÈSES CANADIENNES SUR MICROFICHE

NAME OF AUTHOR/*NOM DE L'AUTEUR* JAMES LEWIS KENNEDY

TITLE OF THESIS/*TITRE DE LA THÈSE* THE DESIGN AND ANALYSIS OF AIRFOIL SECTIONS

UNIVERSITY/*UNIVERSITÉ* OF ALBERTA

DEGREE FOR WHICH THESIS WAS PRESENTED/*GRADE POUR LEQUEL CETTE THÈSE FUT PRÉSENTÉE* Ph.D.

YEAR THIS DEGREE CONFERRED/*ANNÉE D'OBTENTION DE CE GRADE* 1977

NAME OF SUPERVISOR/*NOM DU DIRECTEUR DE THÈSE* D. J. MARSDEN

Permission is hereby granted to the NATIONAL LIBRARY OF CANADA to microfilm this thesis and to lend or sell copies of the film.

The author reserves other publication rights, and neither the thesis nor extensive extracts from it may be printed or otherwise reproduced without the author's written permission.

L'autorisation est, par la présente, accordée à la BIBLIOTHÈQUE NATIONALE DU CANADA de microfilmer cette thèse et de prêter ou de vendre des exemplaires du film.

L'auteur se réserve les autres droits de publication; ni la thèse ni de longs extraits de celle-ci ne doivent être imprimés ou autrement reproduits sans l'autorisation écrite de l'auteur.

DATED/*DATÉ* 22 April 1977 SIGNED/*SIGNÉ* James L. Kennedy

PERMANENT ADDRESS/*RÉSIDENCE FIXE* 63 VIEWPARK DRIVE, RUTHERGLEN, GLASGOW, SCOTLAND.

NL-91 (3-74)

National Library of Canada

Cataloguing Branch
Canadian Theses Division

Ottawa, Canada
K1A 0N4

Bibliothèque nationale du Canada

Direction du catalogage
Division des thèses canadiennes

NOTICE

The quality of this microfiche is heavily dependent upon the quality of the original thesis submitted for microfilming. Every effort has been made to ensure the highest quality of reproduction possible.

If pages are missing, contact the university which granted the degree.

Some pages may have indistinct print especially if the original pages were typed with a poor typewriter ribbon or if the university sent us a poor photocopy.

Previously copyrighted materials (journal articles, published tests, etc.) are not filmed.

Reproduction in full or in part of this film is governed by the Canadian Copyright Act, R.S.C. 1970, c. C-30. Please read the authorization forms which accompany this thesis.

THIS DISSERTATION
HAS BEEN MICROFILMED
EXACTLY AS RECEIVED

AVIS

La qualité de cette microfiche dépend grandement de la qualité de la thèse soumise au microfilmage. Nous avons tout fait pour assurer une qualité supérieure de reproduction.

S'il manque des pages, veuillez communiquer avec l'université qui a conféré le grade.

La qualité d'impression de certaines pages peut laisser à désirer, surtout si les pages originales ont été dactylographiées à l'aide d'un ruban usé ou si l'université nous a fait parvenir une photocopie de mauvaise qualité.

Les documents qui font déjà l'objet d'un droit d'auteur (articles de revue, examens publiés, etc.) ne sont pas microfilmés.

La reproduction, même partielle, de ce microfilm est soumise à la Loi canadienne sur le droit d'auteur, SRC 1970, c. C-30. Veuillez prendre connaissance des formules d'autorisation qui accompagnent cette thèse.

LA THÈSE A ÉTÉ
MICROFILMÉE TELLE QUE
NOUS L'AVONS REÇUE

THE UNIVERSITY OF ALBERTA

The Design and Analysis of Airfoil Sections

by

© James Lewis Kennedy

A THESIS

SUBMITTED TO THE FACULTY OF GRADUATE STUDIES AND RESEARCH

IN PARTIAL FULFILMENT OF THE REQUIREMENTS FOR THE DEGREE

OF DOCTOR OF PHILOSOPHY

DEPARTMENT OF MECHANICAL ENGINEERING

EDMONTON, ALBERTA

SPRING, 1977

THE UNIVERSITY OF ALBERTA

FACULTY OF GRADUATE STUDIES AND RESEARCH

The undersigned certify that they have read, and recommend to the Faculty of Graduate Studies and Research, for acceptance, a thesis entitled "The Design and Analysis of Airfoil Sections" submitted by James Lewis Kennedy in partial fulfulment of the requirements for the degree of Doctor of Philosophy.

David Hawsden
Supervisor

Ronald Eck

J. D. Dale

David J. Wilson

G. W. Parkinson
External Examiner

Date 15 April 1977

ABSTRACT

The development of new airfoil sections with specific characteristics is made possible by numerical design procedures based on potential flow analysis methods. The properties of such sections can be predicted fairly well by combining boundary layer and potential flow analyses to form a viscous flow analysis technique. Progress in airfoil design depends largely on the development of these numerical tools and this thesis describes the development and application of such design and analysis methods.

A surface singularity, potential flow analysis method using a distribution of vorticity on the airfoil surface and a boundary condition specified in terms of the stream function is described. An important feature of this method is the trailing point Kutta condition which gives improved accuracy and allows for a substantial reduction in the number of surface elements needed for an accurate solution. Comparisons with exact test cases show that this method is much more efficient than previous surface singularity techniques.

An efficient, reliable potential flow design technique was developed from the analysis method. The application of the trailing point Kutta condition permits the design of airfoils with large rear loadings and contributes to the fast convergence of the iterative design procedure. The technique is powerful and flexible enough to handle complicated single and multi-component airfoil designs.

A viscous flow analysis method was constructed by taking the potential flow solution and correcting it for the effects of boundary layer displacement thickness using an equivalent airfoil technique.

The equivalent airfoil section has the same thickness distribution as the actual section but its camber line lies in the centre of the displacement surface about the section. The potential flow about the equivalent section is shown to provide a good approximation to the viscous flow about the actual section.

A practical form of the velocity distribution optimized for maximum lift coefficient was developed. The effect on this distribution of increasing the upper surface velocity at the trailing edge, which is equivalent to increasing the loading there, was found to be a dramatic increase in the optimum lift coefficient. A velocity distribution exhibiting a large lift coefficient was used to design a single component section for which viscous flow analysis predicted a lift coefficient of 3.72.

A model of this section was built and tested in the University of Alberta low turbulence wind tunnel at Reynolds numbers from 10^6 to 2×10^6. The model generated considerable rear loading and gave a maximum lift coefficient of 2.64. The discrepancy in lift coefficient arises from the viscous flow analysis being unable to account for the unusually large viscous effects present in this particular section. The approximations used in the equivalent airfoil technique are therefore not applicable in cases with such large rear loading. Suggestions are given for extending the capabilities of the viscous flow analysis to handle such difficult cases as well as more usual airfoil sections.

ACKNOWLEDGEMENTS

The author wishes to extend his appreciation to Dr. D. J. Marsden for providing the opportunity to undertake this research and for his guidance and supervision of this thesis. The financial support of both the National Research Council and the University of Alberta is gratefully acknowledged.

The assistance provided by Gerry Kiss in writing some of the computer routines, developing the wind tunnel testing apparatus and providing the data on the FX-61-163 model is also gratefully acknowledged.

Thanks are extended to the staff of the Mechanical Engineering Shop for their part in preparing the wind tunnel and model for the experimental tests. Special thanks are due to Ernie Telzerow for skillfully manufacturing a very accurate, beautifully finished test model. Thanks are also due to Tony Dyke for his assistance in programming the data acquisition system and for his considerable help in running the experimental tests.

Fellow graduate students are thanked for providing the stimulating atmosphere in which this work was conducted. The author also wishes to thank Daphne Cornelius for producing an excellently typed thesis and for correcting the many spelling errors in the original.

Finally, thanks are due to my wife, Marion, for her patience and understanding and for assisting in the drafting of the figures in the thesis.

TABLE OF CONTENTS

LIST OF TABLES

LIST OF FIGURES

LIST OF SYMBOLS

a,b	distances defined in Figure 2
c	element curvature, equation (46)
C	airfoil chord, also control point
C_d	dissipation integral
C_D	drag coefficient
C_f	skin friction coefficient
C_L	lift coefficient
C_{MQ}	quarter chord moment coefficient
C_p	pressure coefficient
E	velocity error, equation (22)
H, H^*	shape factors
K	influence coefficient (matrix element)
m	velocity distribution exponent, equation (41)
M	number of components in a wing section
N	number of surface elements on a component
P	pressure
P_{tw}	total pressure in wake
P_w	static pressure in wake
q	freestream dynamic pressure, $\frac{1}{2} \rho U_\infty^2$
r	radial distance between points, also distance defined in Figure 2
R	right hand side of matrix equation
Re	Reynolds number, $\frac{U_\infty C}{\nu}$
Re_x	Reynolds number based on x, $\frac{ux}{\nu}$

Re_θ	Reynolds number based on θ, $\frac{u\theta}{\nu}$
S	surface, also surface distance
t	distance defined in Figure 5
u,v	velocity components in boundary layer
U	velocity on airfoil surface
U_∞	freestream velocity
x,y	Cartesian co-ordinates

Greek Symbols

α	angle of attack
β	velocity distribution parameter, equation (40)
γ	vortex density
Γ	vortex strength
δ^*	displacement thickness
δ^{**}	energy thickness
Δ	element half length
$\Delta\psi$	difference in streamfunctions
ϵ_b	blockage correction factor
θ	momentum thickness
ν	kinematic viscosity
ξ,η	co-ordinate system in Figure 48
ρ	density
σ	pressure gradient parameter, equation (35)
τ	shear stress
ψ	streamfunction

Subscripts

i	index of control point
j	index of element
k	index of airfoil component
l	index of element end point
pr	value at start of turbulent pressure recovery region
r	rooftop value
te	trailing edge
tl	lower surface, adjacent to trailing edge
tp	trailing point
tu	upper surface, adjacent to trailing edge
u,l	upper, lower in Figure 22
o	stagnation conditions
∞	freestream conditions

Superscripts

r	required value
d	design iteration

CHAPTER I.

INTRODUCTION

In a country this size it is little wonder that aviation plays such an important role. Flying has, in fact, become an accepted part in the lives of most of the population. The scope of aviation here ranges from the fast transportation of large numbers of people over long distances to the use of hang gliders as a pleasure craft. Among all these modes of flight the great majority rely on airfoils to maintain the craft and its payload in the air. Just as there are a great variety of aircraft used today, so there are a great variety of airfoil sections.

The demands being made of all aircraft are continually being increased and this leads to increased demands being made of the airfoil sections which are used. To conduct the search for new, improved airfoil sections by purely experimental tests is not realistic. First, it is unlikely that trial and error techniques will provide the best sections. Second, the costs, in both time and money, of performing experimental tests are considerably greater than those of analyzing the section mathematically. There is therefore a need for the development of fast, accurate, reliable methods of analyzing and consequently designing airfoil sections.

The main thrust of aviation is to transport people as fast as possible. Low speed flight is however of great importance as it occurs in both the take-off and landing of aircraft. The low speeds which are demanded, largely for safety and economic reasons, require that the airfoil section develop high lift coefficients. It is therefore important that methods of increasing the lift coefficients of airfoil sections be examined thoroughly.

The major portion of the lift coefficient is due to the low pressure coefficients generated on the upper surface of a section. Liebeck and Ormsbee [1] have examined the theoretical problem of optimizing this pressure distribution to obtain maximum lift. Their results indicate that increases in the optimum lift coefficient can be expected if the pressure coefficient at the trailing edge of the upper surface is reduced. Preliminary potential flow results suggest that this is only possible if there is a corresponding increase in pressure coefficient at the trailing edge on the lower surface. This has the effect of adding some loading to the rear of the airfoil section, right up to the trailing edge. The possibility of increasing the lift coefficients of sections by developing large rear loadings is therefore interesting and attractive in its apparent simplicity. Interest in sections with high rear loadings is not confined to high lift sections. Large rear loadings may also be of help in high speed sections where a more even load distribution over the length of the section may be desirable.

Several analytical techniques of determining the properties of airfoil sections are available. These techniques posess varying degrees of sophistication and accuracy, however the basic part of all the techniques is the calculation of the potential flow about the section. The potential flow equations can themselves be solved by a great variety of techniques and an excellent discussion of the different methods available is given by Hess and Smith [2]. The technique which they used has, however, some drawbacks and to overcome these a better method must be developed. One particular problem arises from their application of the Kutta condition. This has been written as a condition specifying no load near the section trailing edge which is in conflict with the aim of

examining sections with large rear loading.

It was known, with foresight, that iterative procedures would be developed for the design and viscous flow analysis of sections. These will require an application of the potential flow analysis at each iteration. The potential flow method developed will therefore have to be particularly efficient if such procedures are to be performed with an affordable amount of computing effort.

The potential flow over the airfoil section will provide a fairly accurate model of the real flow around the section. Viscous effects must however be taken into consideration. It is therefore necessary to analyze the boundary layers which will develop on the airfoil surfaces. This analysis will provide the aerodynamicist with information regarding the transition from laminar to turbulent flow, the location, if any, of laminar and turbulent separation and the drag coefficient of the section.

A model of the full viscous flow over an airfoil section can be constructed by matching the outer potential flow solution to the boundary layer solution next to the airfoil surface. The use of the boundary layer displacement thickness, which can be calculated, permits the determination of the displacement surface about which potential flow can be assumed to occur. Such a viscous flow model is necessary for the prediction of the actual performance of airfoil sections.

The ultimate goal of airfoil theory is not simply to analyze sections to determine their characteristics but to design sections which have specific characteristics. With the advent of design methods, such as that of Chen [3], aerodynamicists are rapidly approaching their goal. These modern methods require the specification of the surface velocity

distribution about the section, and they design a section which gives that distribution, if it is possible. This is exactly what the airfoil designer wants as the aerodynamic characteristics of the section are determined by this surface velocity distribution.

A design method is an inverse of a potential flow analysis method and the characteristics of one are transferred to the other. The method to be developed must be efficient and reliable and must also be flexible enough to handle many of the constraints on geometry with which all aerodynamicists are beset. A specific requirement of the design method will be the ability to design sections with considerable rear loading. This can only be done correctly if the commonly used, no load Kutta condition is removed from the design method and replaced with a more suitable condition.

The surface velocity distributions which can be permitted on an airfoil surface are limited to those for which the boundary layer remains attached. To determine these distributions the boundary layer analysis used in the viscous flow model can be utilized. As a first step in examining the effects of rear loading on obtaining high lift coefficients a procedure following the lines of that of Liebeck and Ormsbee [1] can be used. This will provide the upper surface velocity distribution which gives the optimum lift coefficient. The possibility of obtaining such a velocity distribution on a single component section can be examined by applying the design method to the design of a section which will produce this distribution in potential flow.

The designed airfoil can be examined in the viscous flow analysis to determine the expected performance and especially to determine the effects of the viscous flow on the desired rear loading. The

design of any airfoil section exhibiting radically new characteristics cannot end with this analysis. A model of the section must therefore be tested experimentally to determine if the results of the analysis can be achieved in practice. This serves as a test of the analysis method under conditions not previously encountered with conventional airfoil sections.

The University of Alberta low turbulence wind tunnel provides such a test facility. The large size of this tunnel and the use of a data acquisition system makes possible the collection of accurate experimental data to compliment the theoretical results.

In summary, it is the object of this thesis to develop all the necessary analytical tools. These will be tested to ensure that they perform satisfactorily. They will then be applied to the problem of achieving high lift coefficients on a single component section using a large amount of rear loading. Finally, a model of such a high lift section will be manufactured and tested.

CHAPTER II

POTENTIAL FLOW ANALYSIS

2.1 Introduction

An efficient, reliable method for calculating the velocity distribution on the surface of airfoil sections is required as the first step in the design of such sections. Conformal transformation methods such as that of Theodorsen [4] can analyze sections of arbitrary shape. These methods are based on the theorem which states that it is always possible to transform the potential field around any closed contour into the potential field around a circle. Such methods are not simple and, as there is no such theorem for transforming the potential field around multi-component sections, one looks to surface singularity methods of analysis. These methods replace the potential flow field outside the airfoil contour with that about a set of singularities, sources or vortices, which satisfy the same boundary conditions. Surface singularity methods can deal easily with multi-component sections and are no less accurate than conformal transformation methods on single component cases.

The most widely used surface singularity method is that of Hess and Smith [2]. This method uses a distribution of sources and sinks on the surface of the airfoil section combined with a vorticity distribution to generate circulation. On the other hand the method of Martensen [5] simply uses a distribution of vortices on the airfoil surface. This latter method has been modified, and improved, by Wilkinson [6] who used it with some success as an integral part of his method of airfoil design. One distinct advantage of using a distribution of vortices alone is that the vortex density, which is determined directly, is equal to the surface

velocity.

The boundary condition which is applied in an airfoil analysis is that the solid surfaces of the airfoil section are streamlines. In the above methods [2,5,6] this condition has been written in terms of velocities. In the Hess and Smith [2] method, the normal velocity at the solid surface is required to be zero. In Martensen's [5] and Wilkinson's [6] methods, the tangential velocity at the interior of the solid surface is set equal to zero, which also results in the surface being a streamline. Such formulations result in Fredholm integral equations of the second kind. This thesis will adopt a boundary condition which requires that the stream function at points on the solid surface be a constant. This removes the problem of determining the normal or tangential directions to the solid surface. This boundary condition, combined with the use of surface vortices, has also been used by Goldstein and Jerison [7], as a part of a method of cascade design, and by Oellers [8] in a technique of analyzing cascades.

Chen [3] has analyzed and compared various surface singularity methods. He shows that the method of Hess and Smith [2] is very sensitive to the co-ordinates of the airfoil surface. He also found that the method of Martensen [5], when improved to handle thin airfoils, does not predict the correct circulation about the section tested. Chen [3] developed a method, based on that of Oellers [8], using surface vortices and the constant stream function boundary condition. This method showed none of the problems associated with the other two methods and was found to be faster also.

A major advantage of the methods of Oellers [8] and Chen [3] is that they are easily extended to provide an iterative method of airfoil

design. Chen [3] has developed such a design method and has demonstrated the power of this approach to the design of airfoil sections.

Mavriplis [9] has also developed a method of airfoil section analysis and design using distributed vortices and the constant stream function boundary condition. On an exact test case his analysis method gives more accurate results for the lift coefficient than does the Hess and Smith method. Mavriplis [9] and Chen [3] use similar iterative techniques to design airfoil sections, but they differ in the manner in which the influence coefficients are formulated and in the method of solution [10].

The method presented here is also a surface vorticity method using the constant stream function boundary condition. It is thought to be the simplest available and provides exceptional accuracy for little computing effort. These aspects make this method attractive to both established users of airfoil analysis techniques and to those who are just entering this field.

2.2 Surface Singularity Theory

In two dimensional, incompressible, irrotational flow the stream function, ψ, must satisfy Laplace's equation,

$$\frac{\partial^2 \psi}{\partial x^2} + \frac{\partial^2 \psi}{\partial y^2} = 0. \qquad (1)$$

This is the familiar equation of potential flow in two dimensions. For the flow over airfoil sections there can be no normal velocity at the solid surfaces, and thus each solid surface is a streamline of the flow. Since the stream functions ψ_k ($k = 1, \ldots M$) on the surfaces of the M components on a multi-component section are constants, the boundary

condition for equation (1) can be written as,

$$\psi = \psi_k, \text{ on the surface.} \tag{2}$$

The stream function for a uniform stream incident to the positive X axis at an angle α is given by,

$$\psi = y \cos \alpha - x \sin \alpha, \tag{3}$$

which satisfies equation (1). This equation, and all subsequent equations, are in dimensionless form. The distances are dimensionless with respect to the chord length C, the velocities with respect to the free stream velocity U_∞ and the stream functions with respect to the product $U_\infty C$.

The point vortex of strength Γ, located at (x_0, y_0), has the stream function,

$$\psi = -\frac{\Gamma}{2\pi} \ln (r), \tag{4}$$

where

$$r = \sqrt{(x-x_0)^2 + (y-y_0)^2}.$$

Equation (4) also satisfies (1), except at $r = 0$. Because of the linearity of equation (1) any collection of point vortices or any continuous distribution of them, as in Figure 1, that lies on the airfoil surface, S, will satisfy equation (1) in the region outside of S.

A general point on the surface S is designated S'. Vorticity having a density $\gamma(S')$ at S' is continuously distributed over the surface. The stream function at some point P due to this distribution is given by

$$\psi_P = \frac{-1}{2\pi} \int_{S'} \gamma(S') \ln r\,(P,S')\, d\,S'. \tag{5}$$

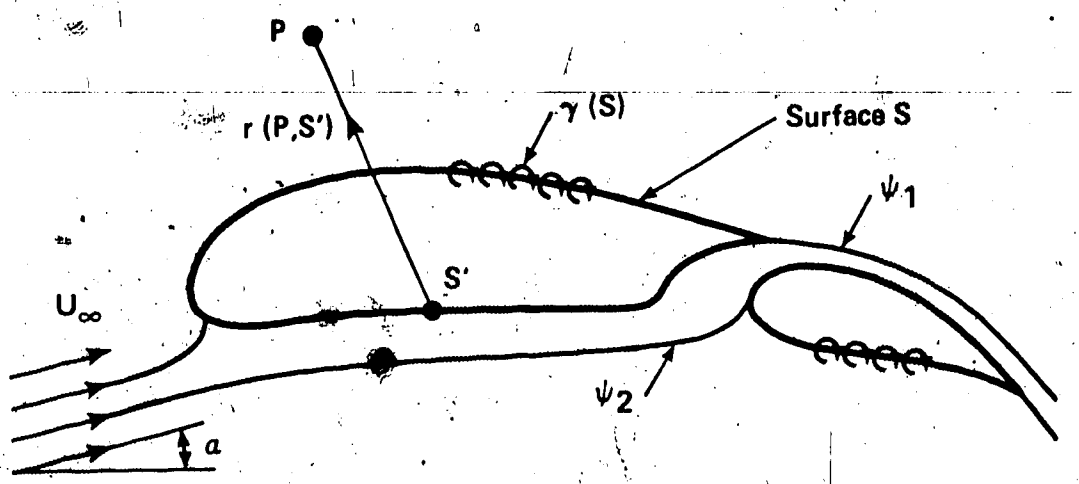

FIGURE 1 - VORTEX REPRESENTATION OF TWO COMPONENT AIRFOIL

When the point P lies on the surface S, equation (5) gives the stream function at the surface due to the distribution of vorticity on the surface.

Applying the boundary condition (2) to the combined flow due to a uniform stream plus the above distribution of vorticity one obtains

$$\psi_k = y_S \cos\alpha - x_S \sin\alpha - \frac{1}{2\pi}\int_{S'} \gamma(S')\, \ell n\, r(S,S')\, d.S' \qquad (6)$$

The airfoil surface is divided up in some manner into N small surface elements. On each of these there is a control point, C_i, located at (x_i, y_i), at which the boundary condition (6) is made to apply. Each element j has vorticity of density $\gamma(S_j)$ distributed on its surface. The integral in (6), over the whole surface S, is then replaced by a

summation of N integrals over the N surface elements. Applying (6) at the control point, C_i, one obtains,

$$\psi_k + \sum_{j=1}^{N} \frac{1'}{2\pi} \int_{S_j} \gamma(S_j) \ln r\,(C_i, S_j)\, d S_j = y_i \cos\alpha - x_i \sin\alpha. \tag{7}$$

There are N control points C_i and there is one such equation for each control point. The problem of potential flow over an airfoil section has therefore been reduced to that of solving these N simultaneous equations.

The results required of an airfoil analysis method are the surface velocities. Martensen [5] shows that the velocity in the interior of the wing is zero and the discontinuity in tangential velocity across a vortex sheet is equal to the density of the vortex sheet. Thus $\gamma(S_j)$ is equal to the surface velocity. In solving the equation (7) one therefore solves directly for the velocities on the airfoil surfaces.

At this point it is necessary to make some assumptions about the section geometry, the location of the control points, and the form of $\gamma(S_j)$ over each element j. The simplest approximation is to assume that the elements are straight lines with the control points at the element midpoints and that $\gamma(S_j)$ is a constant, γ_j, over each element.

Using the above approximations and applying equation (7) at each control point yields the system of equations,

$$\psi_k + \sum_{j=1}^{N} K_{ij}\, \gamma_j = R_i\,, \quad (i = 1, \ldots N) \tag{8}$$

where K_{ij} is the influence coefficient of the element j on control point i, R_i is the right hand side of (7) evaluated at control point i and ψ_k is the stream function for the airfoil component k. Using the

notation of figure 2, the influence coefficients can be written:

$$K_{ij} = \frac{1}{4\pi}\left\{(b+\Delta)\ \ell n\ (r_1^2) - (b-\Delta)\ \ell n\ (r_2^2) + 2a\ \tan^{-1}\left(\frac{2a\Delta}{a^2+b^2-\Delta^2}\right) - 4\Delta\right\}. \tag{9}$$

The details of the calculation of this equation are provided in Appendix 1. The right hand side is written,

$$R_i = (y_i \cos\alpha - x_i \sin\alpha). \tag{10}$$

The K_{ij} and R_i are purely functions of the co-ordinates of the surface elements and the angle of attack, α, of the free stream relative to the airfoil chord. The system of equations (8) is a set of N equations for the N unknown γ_j and M unknown ψ_k, where there are M components. The M additional equations required for a solution to this problem are termed the Kutta conditions and there is one for each component in the airfoil section.

The technique described so far makes use of the simplifying assumptions of straight line elements and constant vortex density on each element, which is referred to here as the basic method. Hess [11] has shown that for the Hess and Smith surface source method some improvement is obtained if one includes the effects of curved elements and varying source density over the element. The equations needed for curved surface elements and varying vortex density were developed to see if a similar improvement in accuracy could be obtained with the present method. An improvement in accuracy by the use of curved elements might allow a reduction in the number of control points needed, which would in turn reduce computing costs.

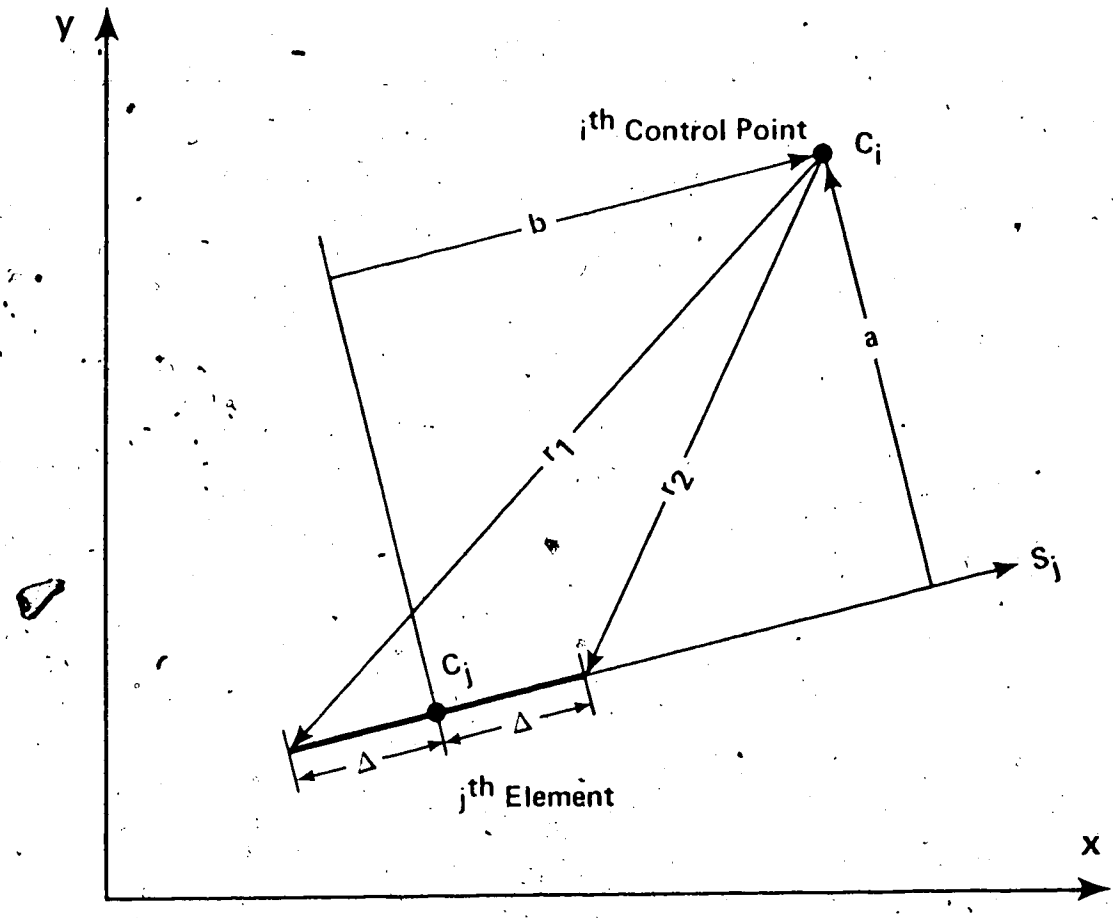

FIGURE 2 - NOTATION USED TO CALCULATE INFLUENCE COEFFICIENTS

The equation which must be solved is, again, equation (7). The procedure used to evaluate the integral in (7) is exactly that used by Hess [11]. The integral evaluation yields a series of terms the first of which is the constant vortex density, straight line element case analyzed above. The next two terms arise from a linear variation of the vortex density, and from approximating the surface shape with a parabolic curve rather than a straight line. Further terms in the series allow for nonlinear variations in the vorticity distribution and higher order curvature in the shape of the elements. Higher order terms become progressively less important and only those terms which give significant improvements in accuracy in the overall solution need be retained. Details of the method using higher order terms are given in Appendix 1. There it is shown that the higher order method is considerably more difficult to implement than the basic case. A comparison of the accuracy of the various possibilities is given in section 2.5.

2.3 The Kutta Condition

In the inviscid flow over any cylinder there are, in general, two stagnation points on the body. There is also an undetermined circulation about the body and hence, by the Kutta-Joukowski theorem, the net resultant force on the body is undetermined. Kutta and Joukowski independently arrived at a technique for determining the circulation which would exist on an airfoil section in a fluid of very small viscosity. This technique is known as the Kutta condition or as Joukowski's hypothesis, the former being used here.

Kutta and Joukowski were concerned with airfoil sections whose geometries are calculated by a conformal transformation technique known today as the Joukowski transformation. In this the flow over a circular

cylinder is mapped into the flow over an airfoil section with a cusped trailing edge. These sections have two stagnation points. One located near the leading edge and the other near the trailing edge. Also the velocity at the trailing edge will, in general, be infinite.

Both Kutta and Joukowski proposed that the circulation around the circular cylinder be adjusted so that one of the stagnation points in that flow be located at the point which will map into the airfoil trailing edge. In this case the infinite velocity and the stagnation point, occurring together at the trailing edge, cancel and yield a finite, non-zero velocity there. It has been shown by Milne-Thomson [12] that a concequence of this assumption is that the stagnation streamline leaves the cusped trailing edge tangent to it.

It is remarkable that this smooth flow from the trailing edge is observed in practice in unstalled airfoil sections. The photographs of flow visualisation studies of Prandtl and Tietjens [13] show this effect clearly. They also show the process of convection of vorticity from the airfoil at the initial stages of motion which sets up the correct amount of circulation. The Kutta condition is both mathematically necessary, to provide unique solutions to airfoil analyses, and has a clear physical basis.

For the analysis of airfoil sections using conformal transformation techniques locating a stagnation point at the point on the cylinder which maps into the airfoil trailing edge is generally used. For sections with wedge shaped trailing edges this results in zero velocity at the trailing edge.

In thin airfoil theory the section is replaced by a vortex sheet on its mean camber line. Here the velocity at the ends of the

of the sheet will be infinite if there is any vortex strength there. The Kutta condition in this case fixes the strength of the vorticity at the trailing edge at zero.

In his surface singularity method Wilkinson [6] shows that there is considerable numerical difficulty in setting the trailing edge velocity equal to zero. He therefore introduced the assumption that there is no load carried on the two elements adjacent to the trailing edge. The velocities on these two elements are therefore the same. This approximation gave reasonable results and has become the one most commonly used in surface singularity analysis.

This "no load" Kutta condition can be applied to the present method. As the vortex densities are identical to the surface velocities, counter-clockwise about the section, this can be written,

$$\gamma_{tu} = - \gamma_{t\ell}$$

or

$$\gamma_{tu} + \gamma_{t\ell} = 0 \qquad (11)$$

In general equation (11) is incorrect and, in order to minimise the errors it introduces, one is forced to use very small elements near the trailing edge. A better solution is to model the observed physical phenomena that the airflow leaves the trailing edge smoothly. This can be modeled by providing an additional control point just off the trailing edge. Such a Kutta condition was used successfully by Bhateley and Bradley [14].

The bisector of the trailing edge is extended into the free stream and a control point placed a small fraction of chord downstream of the trailing edge. It is then assumed that the streamline through

the other control points of that component also passes through this control point. Equation (7) then applies to these trailing control points, C_{tp}, and the Kutta condition can be written as,

$$\psi_k + \sum_{j=1}^{N} K_{tp,j} \gamma_j = R_{tp} \qquad (12)$$

There are M such trailing control points, one for each component, and hence M Kutta condition equations.

2.4. Method of Solution

Since the solution to the problem of potential flow over mutli-component airfoil sections is a simple extension to the single component case, only the latter is presented here in detail.

The first step in the solution is to define the elements which describe the airfoil surface. One obvious method of doing this is to let the supplied section co-ordinates be the end points of the surface elements. This has the disadvantage that there may be insufficient co-ordinates available or that they may be irregularly spaced. To overcome these problems the airfoil is divided up, from its leading edge at x = 0 to its trailing edge at x = 1, in a manner similar to that used by Wilkinson [6] and Stevens, Goradia and Braden [15]. The end points of the surface elements are located, as shown in Fig. 3, at x co-ordinates given by,

$$x_\ell = \frac{1}{2}[1 - \cos \phi_\ell], \quad (\ell = 0,1, \ldots N) \qquad (13)$$

where $\phi_\ell = \frac{2\pi\ell}{N}$. Here N must be an even number in order that an end point be located at the airfoil trailing edge.

This distribution of points provides, in general, the most

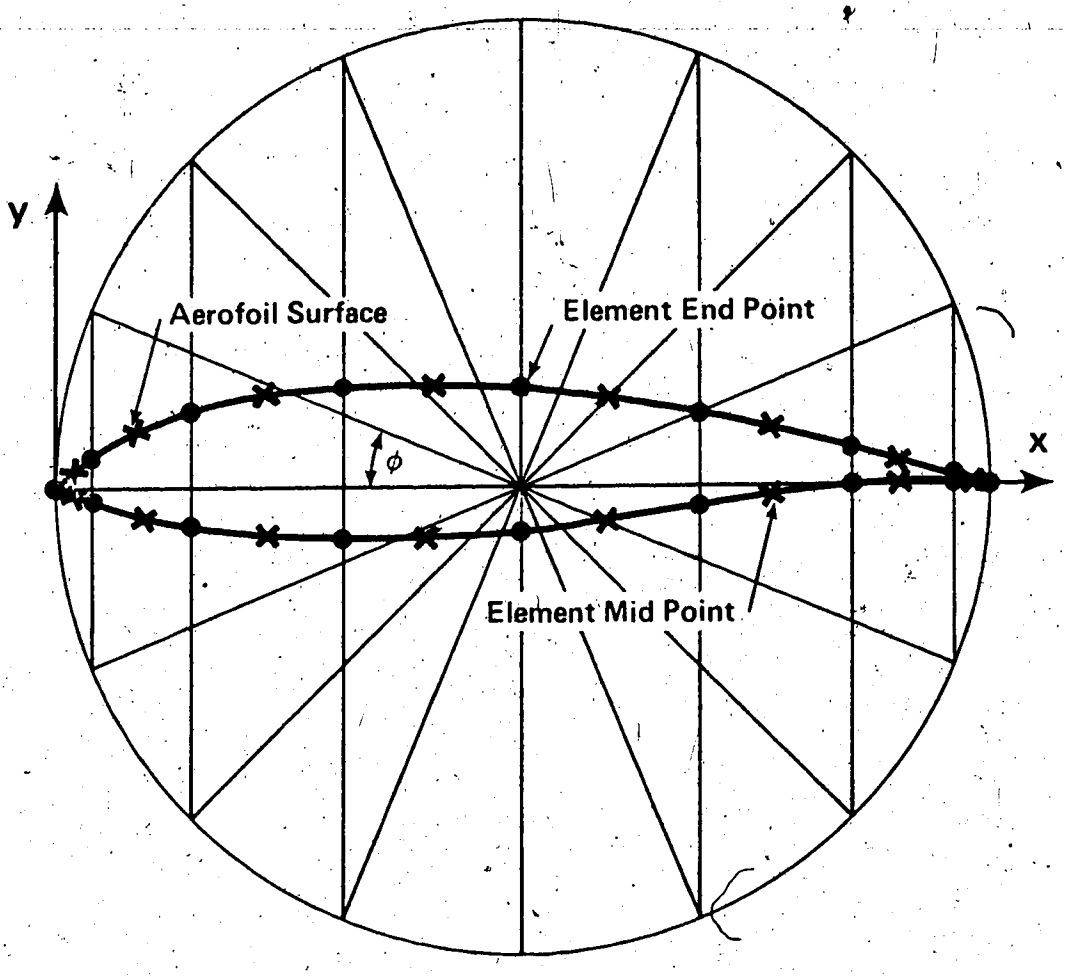

FIGURE 3 - LOCATION OF ELEMENTS ON AIRFOIL SURFACE

accurate solution because it concentrates the control points near the leading edge and trailing edge where the largest velocity gradients generally occur.

The corresponding co-ordinates y_ℓ of the element end points are determined by interpolation on the given airfoil data. The use of standard library computer subroutines for interpolation can sometimes give trouble depending on the distribution of the original airfoil co-ordinates. The use of a cubic spline function has been found to be the most reliable method. This gives smooth curves through the given points and can be easily and efficiently computed using the method of Ahlberg, Nilson and Walsh [16].

The infinite slope at the leading edge of a blunt nosed airfoil section is a source of some trouble for any polynomial interpolation technique. This can be overcome by rotating each surface of the airfoil through 30^0, as shown in Figure 4. The cubic spline method allows one to specify the slope at the leading edge, which in this case is tan 60^0. After interpolating on the rotated data one rotates the interpolated end points through -30^0 to restore the airfoil to its original position. This guarantees that the interpolated data contain the same blunt nosed characteristics as on the original data, which is especially important at large angles of attack. While this process is not strictly necessary it has been found to be very successful when data points near the nose are sparse or irregularly spaced.

The control points are taken as the mid points of each surface element, as shown in Figure 3. In the case where the trailing point Kutta condition is used an additional control point has to be generated. The bisector of the trailing edge is extended, as shown in Figure 5, and

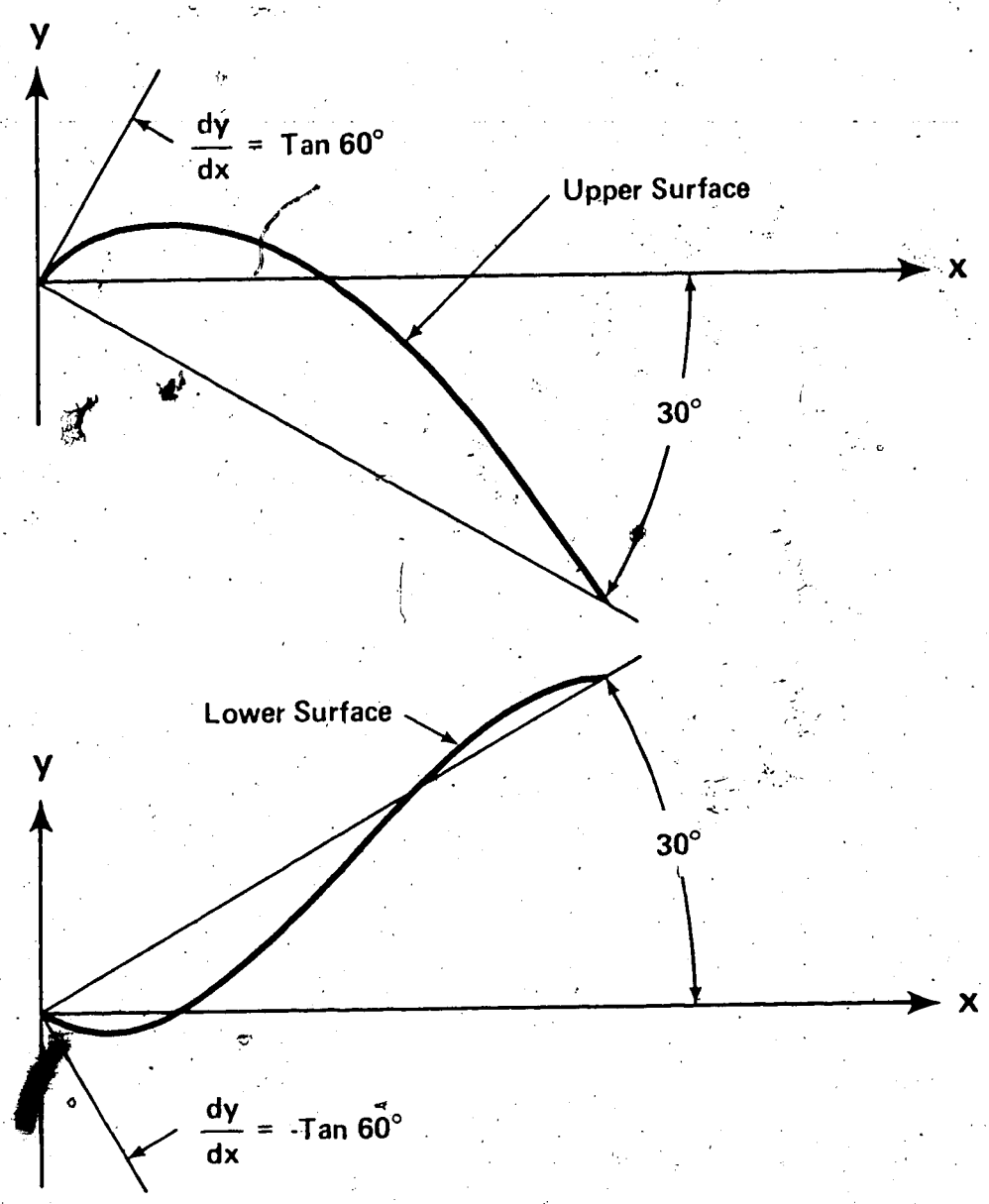

FIGURE 4 - ROTATION OF AIRFOIL SURFACES

the control point is located on this extension a distance 0.01 t from the trailing edge. This distance was found to give the most reliable results for a wide range of airfoil sections.

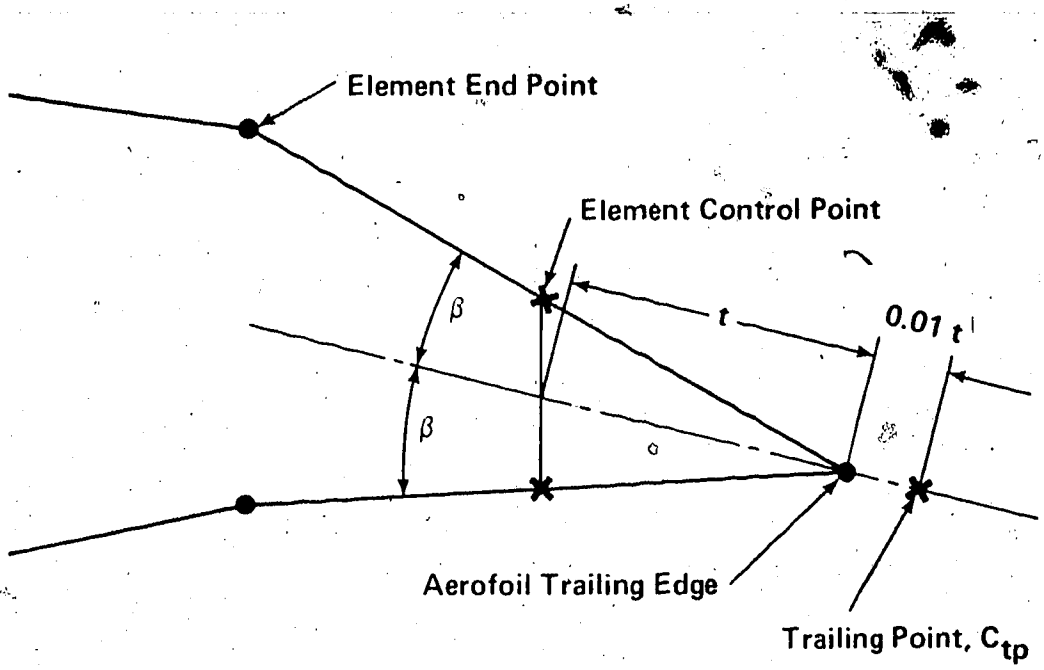

FIGURE 5 - LOCATION OF TRAILING CONTROL POINT

Having determined the location of the element end points and control points one can proceed to calculate the influence coefficients K_{ij}. For each element j, whose length is 2Δ, the distances a, b, r_1 and r_2 as defined in Figure 2 are calculated. Equation (9) is then used to calculate K_{ij}. In cases where $a^2 + b^2 - \Delta^2 \leq 0$ one can use the relation,

$$\tan^{-1}\left(\frac{2}{a^2+b^2-\Delta^2}\right) = \tan^{-1}\left(\frac{b+\Delta}{a}\right) - \tan^{-1}\left(\frac{b-\Delta}{a}\right) \qquad (14)$$

to determine which value of the arctangent should be used. The right hand side of (14) is considerably more accurate than the left hand side when calculating terms where a is small. This occurs frequently on slender airfoil sections and in the calculation of the influence coefficients due to adjacent elements. The calculation for R_i, equation (10), depends on both the location of control point C_i and the angle of attack α.

The system of equations (8) can be written in matrix form as,

$$\begin{matrix} i=1 \\ \\ i=N \end{matrix}\begin{bmatrix} \\ K_{ij} \\ \\ \end{bmatrix}\begin{bmatrix} \\ \gamma_j \\ \\ \end{bmatrix} + \begin{bmatrix} 1 \\ \cdot \\ \cdot \\ 1 \end{bmatrix} \psi_1 = \begin{bmatrix} \\ R_i \\ \\ \end{bmatrix} \quad (15)$$

The Kutta condition can be written as equation (11) or as equation (12). This becomes another equation in the system which then becomes,

$$\begin{matrix} i=1 \\ \\ \\ \\ i=N \\ i=N+1 \end{matrix}\begin{bmatrix} K_{1,1} & \cdots & K_{1,N} & 1 \\ \cdot & & \cdot & \cdot \\ \cdot & & \cdot & \cdot \\ \cdot & & \cdot & \cdot \\ \cdot & & \cdot & \cdot \\ K_{N,1} & \cdots & K_{N,N} & 1 \\ \text{Kutta condition} & & & \end{bmatrix}\begin{bmatrix} \gamma_1 \\ \cdot \\ \cdot \\ \cdot \\ \cdot \\ \gamma_N \\ \psi_1 \end{bmatrix} = \begin{bmatrix} \\ \\ R_i \\ \\ \\ \end{bmatrix} \quad (16)$$

The system of equations (16) is then solved for the N unknown vortex densities γ_j and the stream function ψ_1. For most single component airfoils N need not exceed 40, while 70 elements are sufficient for most two component airfoils. The system (16) is therefore generally small and dense, and Gaussian elimination is used in preference to iterative techniques.

The solutions are the dimensionless surface velocities at the control points and the dimensionless stream function. The pressure distribution, lift coefficient and pitching moment can be easily calculated from the velocities.

When this technique is extended to multi-component airfoil sections the point distribution (13) is first scaled to the chord of each individual component before being applied. It is then necessary to move each component to its correct location. This is done by specifying the amounts by which the leading edge of the component is translated and the angle through which the component is rotated. With the geometry thus defined, one can calculate the K_{ij} and R_i from (9) and (10).

The multi-component case gives rise to a different stream function for each component and each component has its own Kutta condition. For example a two component airfoil with N elements on each component gives rise to a system of equations which can be written,

$$
\begin{array}{r}
i=1 \\
\\
\\
i=N \\
i=N+1 \\
\\
\\
i=2N \\
\text{Kutta condition, component 1} \\
l=2N+2 \quad \text{Kutta condition, component 2}
\end{array}
\left[\begin{array}{cccccc}
K_{1,1} & \cdots & K_{1,2N} & 1 & 0 & \\
\vdots & & & \vdots & \vdots & \\
K_{N,1} & & K_{N,2N} & 1 & 0 & \\
K_{N+1,1} & & K_{N+1,2N} & 0 & 1 & \\
\vdots & & & \vdots & \vdots & \\
K_{2N,1} & \cdots & K_{2N,2N} & 0 & 1 & \\
\multicolumn{3}{c}{} & 1 & 0 & \\
\multicolumn{3}{c}{} & 0 & 1 &
\end{array}\right]
\left[\begin{array}{c}
\gamma_1 \\
\vdots \\
\gamma_N \\
\gamma_{N+1} \\
\vdots \\
\gamma_{2N} \\
\psi_1 \\
\psi_2
\end{array}\right]
=
\left[\begin{array}{c}
\\
\vdots \\
\\
R_i \\
\\
\vdots \\
\\
\\
\end{array}\right]
\qquad (17)
$$

Equation (17) is then solved by Gaussian elimination.

The right hand sides of (16) and (17), R_i, are the only terms which include the angle of attack α. In determining the flow over one airfoil section at a number of angles of attack one therefore need only

determine the coefficient matrix, K_{ij}, once. The column vectors R_i and γ_j can be replaced by matrices $R_{i\alpha}$ and $\gamma_{j\alpha}$ where each column of $R_{i\alpha}$ is calculated for a different angle of attack. After applying Gaussian elimination to this new system of equations each column of the solution matrix, $\gamma_{j\alpha}$, is the solution for a different angle of attack. This method of solution is a very efficient way to obtain the velocity distributions on an airfoil section at several angles of attack.

2.5 Results

The performance of this method is best tested against exact solutions for known airfoils obtained by a conformal transformation technique. In the case of single element airfoils Karman - Trefftz sections are used as a test.

A comparison was made between results using equations (11) and (12) for the Kutta condition and between these and the exact solution. In the case of airfoils with small camber at low angles of attack the two surface velocities γ_{tu} and $-\gamma_{t\ell}$ are very close in magnitude. Here (11) is quite adequate and gives results almost identical to those obtained using (12). Both methods gave excellent agreement with the exact solution for such cases.

Moderate and highly cambered airfoil sections, however, show a marked difference in magnitude between γ_{tu} and $\gamma_{t\ell}$. Under these conditions equation (11) can not be expected to be an accurate Kutta condition. Figure 6 shows that the use of equation (11) does indeed result in considerable errors in the calculated velocity distribution. The velocities on the upper surface of the airfoil are too low, while those on the lower surface are too high. Much more accurate results are obtained with equation (12). With the sparse distribution of points used it is difficult to model the highly curved nose section accurately.

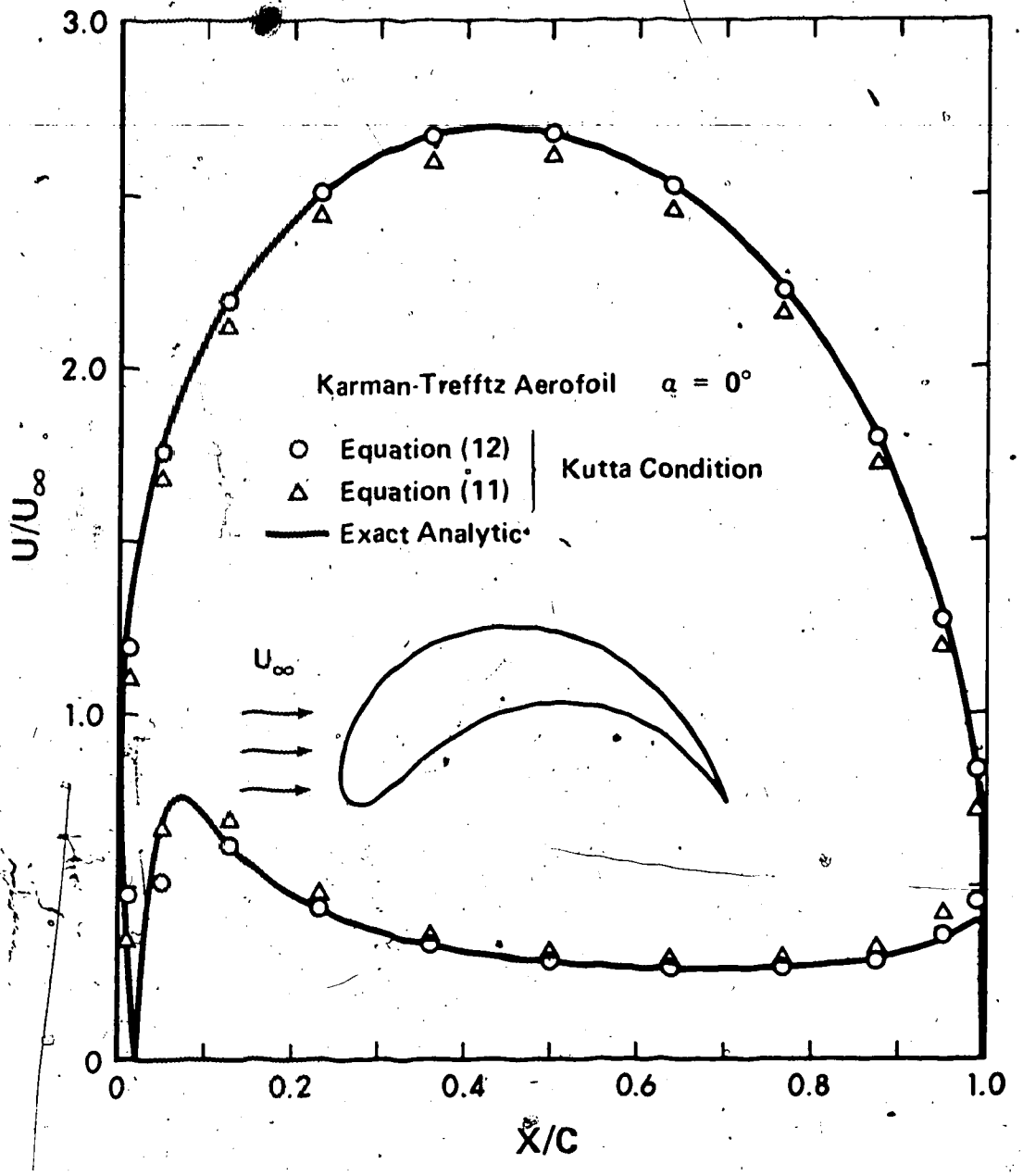

FIGURE 6 - COMPARISON OF RESULTS USING TWO KUTTA CONDITIONS

This results in errors in the velocity distribution in the nose region, as can be seen in the two points close to the stagnation point in Figure 6.

In every case tried, use of (12) provided the most accurate solution. The improvement is most noticeable, as expected, near the trailing edge. In calculating the lift coefficient of an airfoil section the errors involved in using (11) accumulate and result in an estimate of lift coefficient which is too low. Using equation (12) in preference to (11) involves some additional calculation but the greatly improved accuracy fully justifies this extra work.

For a more dense distribution of elements the results are improved as one would expect. This can be seen in Figure 7 where 40 elements are used compared to 22 elements in Figure 6. The improvement is most marked at the nose where the extra elements allow this highly curved area to be modelled with greater accuracy.

The results presented so far have been found using the basic approximation of straight line elements with constant vortex density distributed on each element. The effects of including the higher order terms due to surface curvature and a linearly varying vortex density on each element are shown in Figure 8. Here equation (12) is used as the Kutta condition. It is clear that the extra terms make only small changes to the results. In general the inclusion of element curvature raises the velocities while including the linear vortex density decreases the velocities. Both of these terms are of the same magnitude and when combined they tend to cancel.

There are two major similarities between the results of this higher order technique and that used by Hess [11]. Both methods show that the element curvature effect and the effect of linearly varying

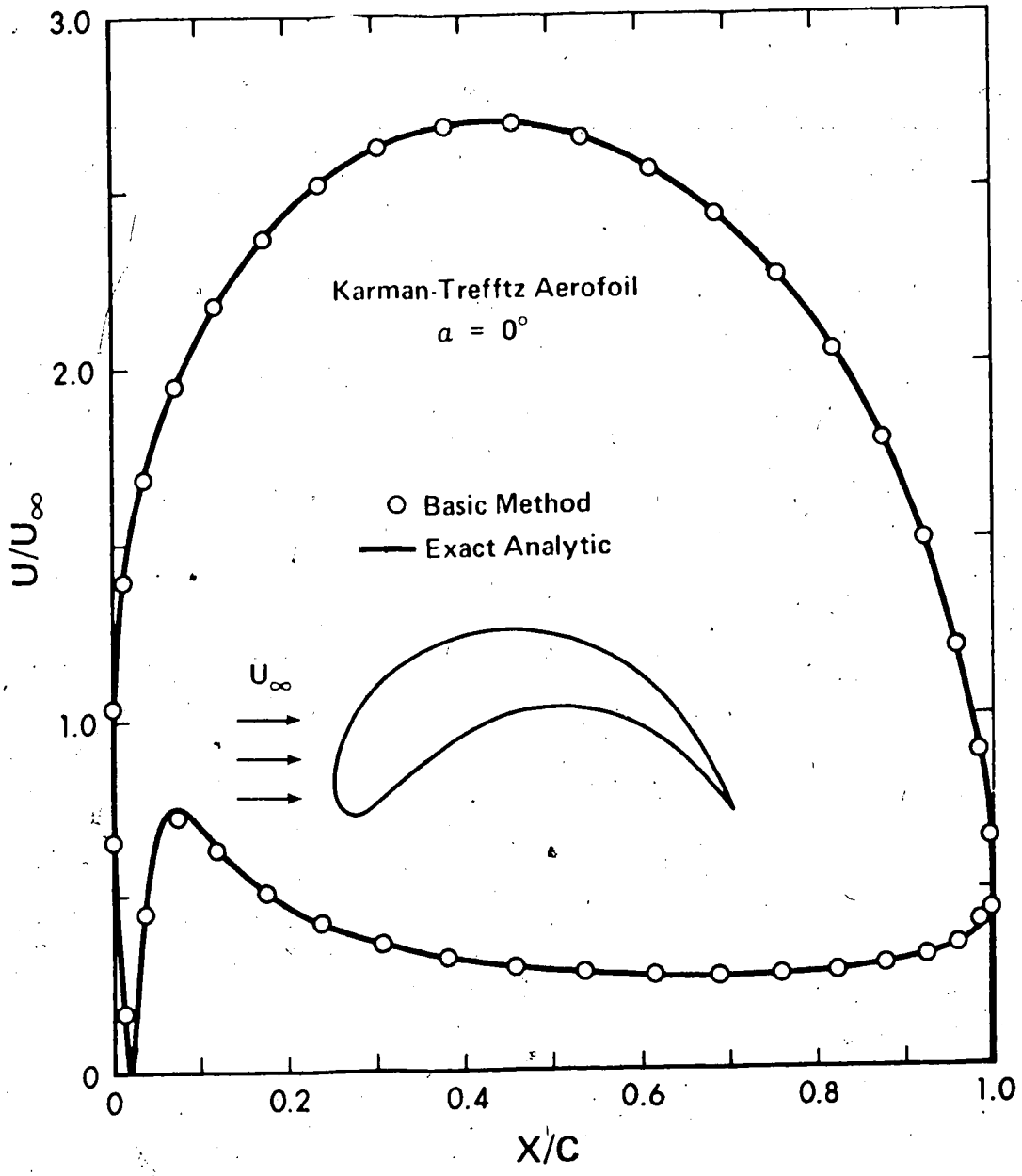

FIGURE 7 - RESULTS USING 40 SURFACE ELEMENTS

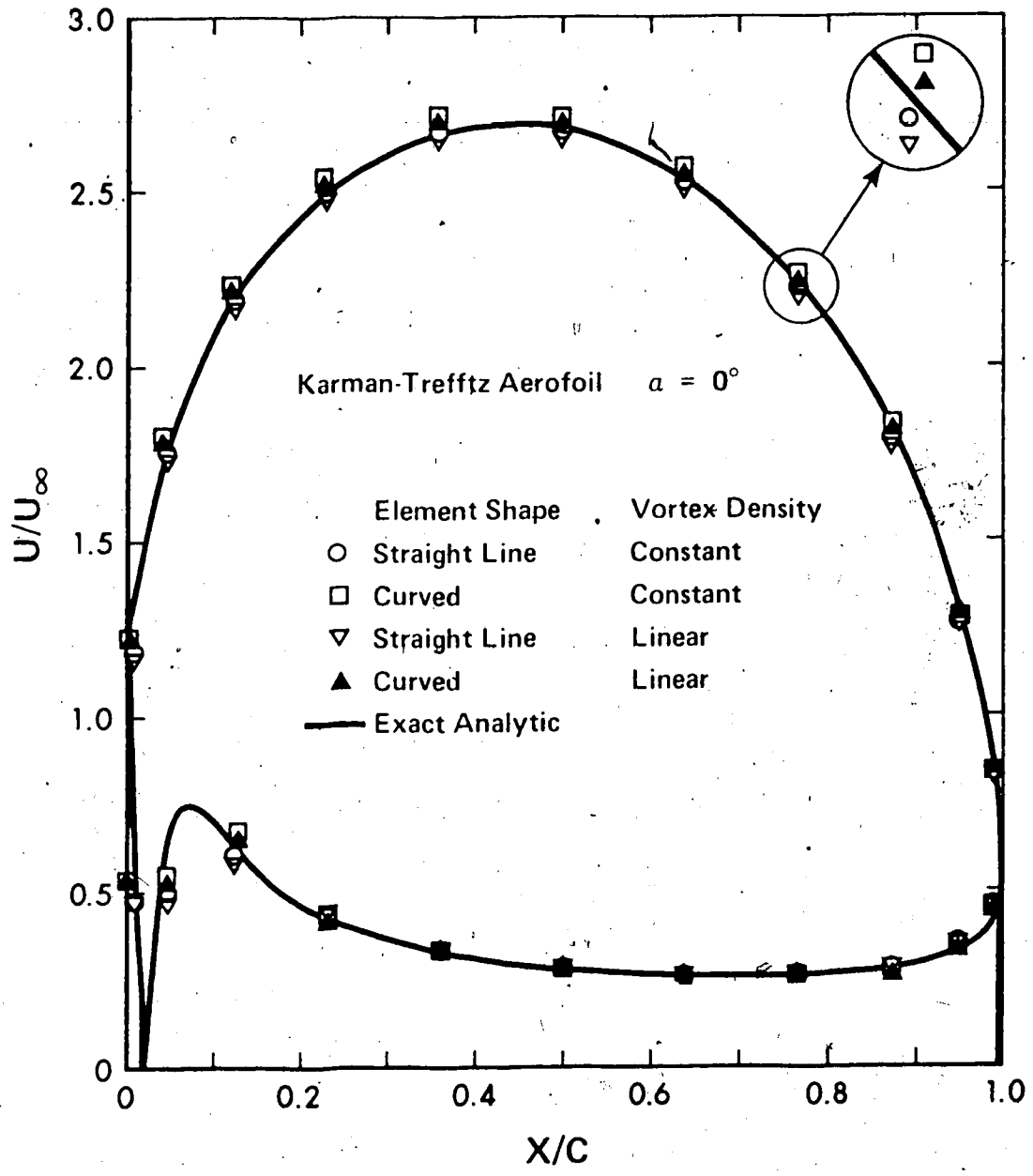

FIGURE 8 - COMPARISON OF HIGHER ORDER METHODS

singularities are of the same order of magnitude. The inclusion of one of the above effects alone cannot therefore be justified. Hess also concluded that higher order solutions give only a small change to the basic solution as was seen to be the case here.

In the data presented by Hess [11] the effects of higher order terms accumulate, each additional term giving a more accurate solution. In the present method the additional terms tend to cancel, and there is even less worth in keeping these higher order terms than there was for Hess. It is therefore recommended that only the basic method with straight line elements and constant vortex density be used.

The basic method with equation (12) as a Kutta condition gives accurate results for most airfoils. An example of a section with a fairly sharp peak in the velocity distribution is given in Figure 9. This is a Joukowski airfoil with a cusped trailing edge as opposed to the wedge shaped trailing edge of the general Karman - Trefftz airfoil section. Here 40 elements are used to describe the section and there is excellent agreement with the exact solution.

This singularity method will break down for an airfoil of zero thickness, where the upper and lower surfaces are coincident. It is therefore important to determine how thin an airfoil can be analysed by this method. A 1% thick, 30% camber Karman - Trefftz airfoil section with 40 elements provides results with accuracy similar to that shown in Figure 9. A Joukowski airfoil section with the same thickness and camber required a larger number of elements to provide such accuracy. The thinner tail on the cusped Joukowski section explains the loss of accuracy in this case.

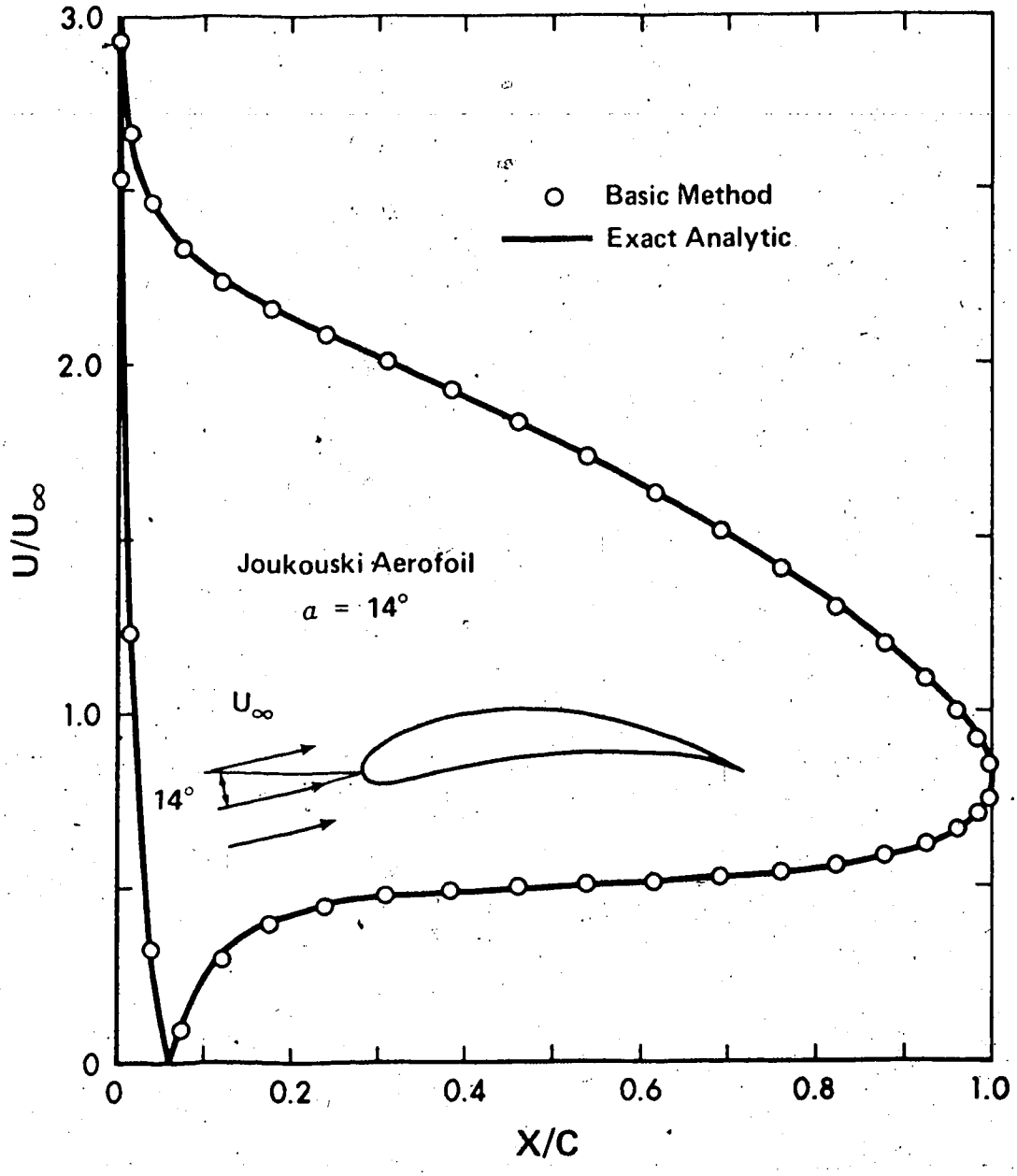

FIGURE 9 - VELOCITY DISTRIBUTION FOR A JOUKOWSKI AIRFOIL

From the results obtained from many practical airfoil sections it has been determined that, using the point distribution equation (13) one need not use more than 40 elements to obtain an accurate velocity distribution. In fact if the airfoil does not have a very highly curved surface and no sharp velocity peaks then 30 elements will suffice.

The performance of this calculation method for multi-component airfoil sections was tested against the exact test case solutions given by Williams [17]. The exact pressure coefficients given by Williams and those calculated by the basic method using Kutta condition (12) are shown in Figure 10. This is for Williams "Configuration B" with a 10^{o} flap deflection at 0^{o} angle of attack. A total of 60 surface elements are used to describe the airfoil section, 34 on the main section and 26 on the flap. As can be seen there is good agreement between the present method and the exact values of Williams.

The effect of using the equal velocity Kutta condition (11) in the two component case is similar to that experienced for a one component airfoil. The changes are most pronounced on the main section where velocities on the upper surface are lowered and those on the lower surface are raised. When using 60 elements this Kutta condition gave an error of about 3% in calculation of the lift coefficient.

In general the upstream components of multi-component airfoil sections show large velocity differences between upper and lower surfaces near the trailing edge. The trailing point Kutta condition handles this well with a relatively small number of elements, while any method using the equal velocity Kutta condition must resort to many elements closely packed at the trailing edge to achieve similar accuracy.

From the examples examined here it can be seen that this present

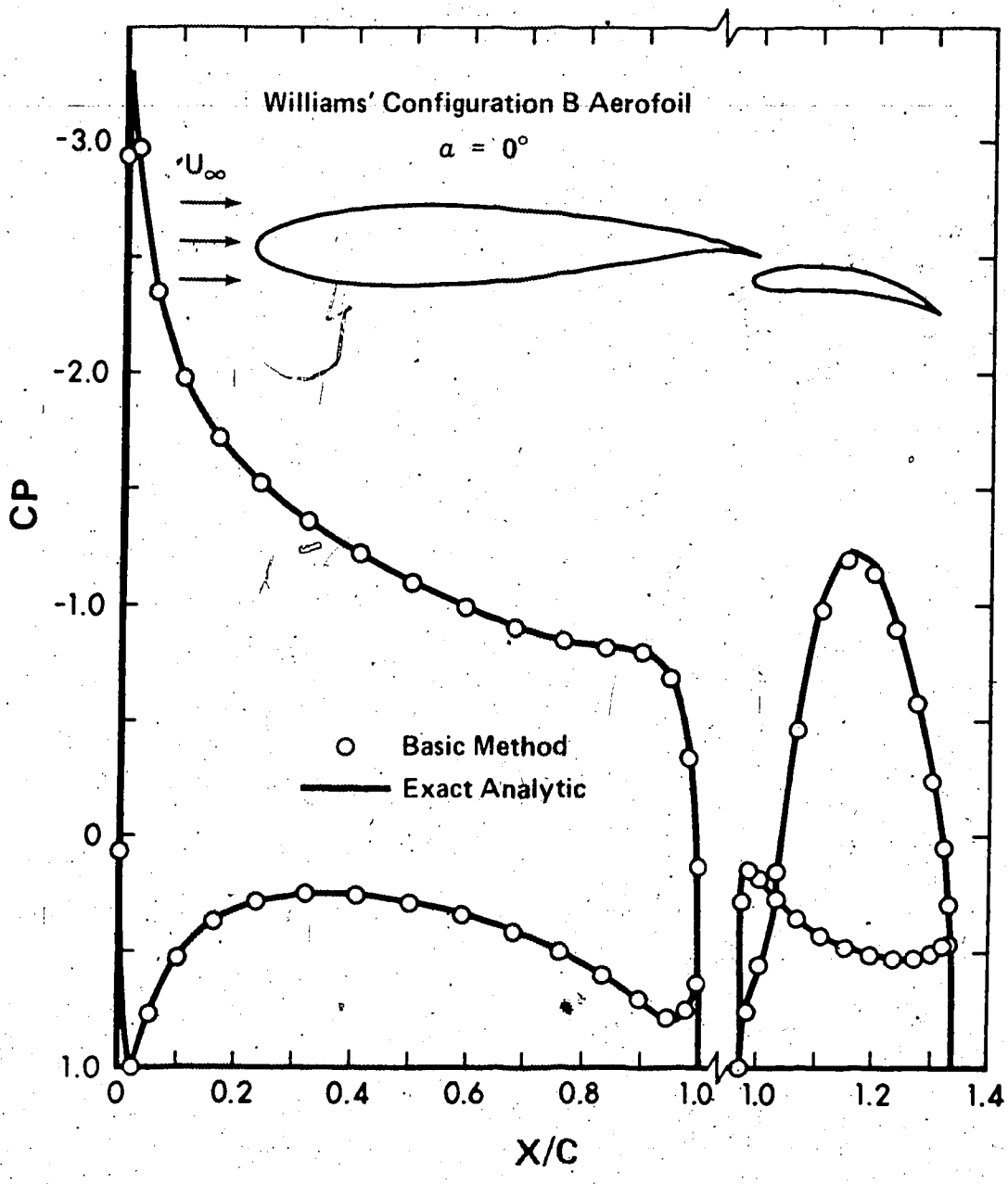

FIGURE 10 - PRESSURE DISTRIBUTION ON A TWO COMPONENT AIRFOIL

method gives excellent agreement with exact solutions for both single and multi-component airfoil sections. It is worthwhile to compare this method with other surface singularity methods of airfoil analysis. Results using the Hess and Smith method are given by Williams along with the exact solution for the two component airfoils which he developed. Seebohm and Newman [14] have applied their surface vortex method to one of Williams test cases as has Mavriplis [19]. A summary of results are shown for comparison in Table 1.

TABLE 1

Lift Coefficients of Williams' Airfoil Sections

Airfoil	Configuration B		Configuration A	
Angle of Attack	0^o	10^o	0^o	10^o
Exact	2.0290	3.5448	3.7386	5.1404
Present method (60 elements)	2.0296	3.5437	3.7440	5.1441
Hess and Smith (180 elements)	2.0092	3.5259	3.7029	5.1065
Mavriplis (140 elements)			3.7154	5.1158
Seebohm and Newman			3.64	

The present method is clearly the most accurate for the cases examined. Both the present method and that of Mavriplis use the constant stream function boundary condition. As is pointed out by Chen [3] and again by Mavriplis [9], the stream function boundary condition provides a more accurate matrix equation than do methods using normal or tangential velocity boundary conditions. These latter methods use the slope of the airfoil surface as part of the boundary conditions and small error in calculating surface slope result in relatively large

errors in resulting velocities.

The lift coefficient which an airfoil section develops is determined by the circulation around the section. It is the application of the Kutta condition which determines the circulation on the section. Of the four methods tabulated only the present method used a trailing point Kutta condition, while the others used the equal velocity Kutta condition. As was mentioned previously this latter condition underestimates the lift coefficient and this can be seen in Table 1. The high accuracy of the present method can therefore be attributed mainly to the use of the trailing point Kutta condition.

In the comparison shown in Table 1, the Hess and Smith method used 180 elements, Mavriplis [19] used 140 while the present method required only 60, for better accuracy than was achieved by the other methods. The larger number of elements are needed when using the equal velocity Kutta condition in order to make the size of elements near the trailing edge small enough that the error associated with this condition become negligible.

A reduction in the required number of elements by a factor of three in the present method reduces computer execution time by a factor of at least ten. Using 60 elements the computations take slightly less than 1 second on an Amdahl 470 V/6 computer. The small number of surface elements required reduces the storage requirements of the computer being used. Using this method single and even two components airfoil sections may now be analysed accurately using the latest generation of desk top computers.

2.6. Conclusions

The method of analysis of multi-component airfoil sections presented here is attractive because of its relative simplicity among other surface singularity methods. One need not determine components of velocity either normal or tangential to the airfoil surface, with the attendant problem of determining these directions accurately. The terms in the matrix equation can therefore be easily and accurately calculated. The resulting solution of the matrix equation provides the surface velocities directly.

A Kutta condition requiring that the streamline along the airfoil surface pass through a point close to the trailing edge is proposed. This Kutta condition is shown to be superior to the conventional Kutta condition of equal velocities on upper and lower surfaces near the trailing edge.

A higher order model which accounts for surface curvature and linearly varying vortex density was examined. The effects of the above terms were found to be small and when combined they tend to cancel. The basic method of straight line surface elements with constant vortex density is therefore recommended for practical use.

The basic method handles both cusped and wedge shaped trailing edges and airfoils as thin as 1 percent of chord. Multi-component sections are easily handled and provide accurate solutions when using the trailing point Kutta condition. Results for some exact test cases show that the present method predicts lift coefficient more accurately than three other surface singularity methods and that this accuracy is achieved with fewer surface elements.

The trailing point Kutta condition is the key to good accuracy with a small number of surface elements. By greatly reducing the number of elements required for an accurate solution this method makes analysis of multi-component airfoil sections a practical possibility for small computers.

CHAPTER III

POTENTIAL FLOW DESIGN

3.1 Introduction

By combining experience with sound aerodynamic principles airfoil designers can develop surface velocity distributions which will give an airfoil section a desired set of aerodynamic characteristics. The optimization methods of Liebeck and Ormsbee [1] and Chen [3], for examples, provide specific surface velocity distributions optimized for maximum lift coefficient, and the application of this design technique to the design of a section with a high lift coefficient will be described in Chapter V. The purpose of the design technique is to calculate the geometry of the airfoil section which will, to some accuracy, give this required velocity distribution.

To date the only practical, analytical methods of multicomponent airfoil section design are based on surface singularity techniques. While some exact transformation methods have been developed for single component sections, no working methods are known for the multicomponent case. Surface singularity methods are also desirable because, as the design process is iterative, adjustments can be made to both the designed geometry and the required surface velocities at each iteration. This allows the designer to include many of the constraints which frequently occur in the design of modern airfoil sections.

Surface vortex methods of airfoil analysis can always be converted to give a design technique. A desired surface velocity distribution is specified, which is equivalent to specifying the strength of the singularity in a surface vortex method. This cannot be done for surface source methods and for this reason they are not employed directly

in the design process.

The first use of a surface vortex design method is that of Goldstein and Jerison [7] who developed a technique of airfoil and cascade design. This technique sought to find the location of the vortices of known strength such that each lay on the same streamline. This streamline is then the airfoil section. The properties of this section were then determined by a conformal mapping technique as surface singularity analysis techniques were not then available. With the advent of such analysis methods Wilkinson [6] developed a technique in which the suction side velocities are specified and the camber of a specified thickness section is adjusted to satisfy the requirements. The convergence on the required solution is checked at each iteration by the analysis method. Two major limitations with this technique are that the velocities can be specified on only one side of the section and the thickness distribution of the section must be known in advance.

Both Chen [3] and Mavriplis [9] have developed similar design techniques based on improved analysis methods. These methods do not have the limitations that are inherent in Wilkinson's technique and are consequently much more powerful. In both these methods the design process follows naturally from the analysis method and the equations of the design method are developed from those found in the analysis. Recently Beatty and Narramore [20] have combined an accurate surface source analysis method with Wilkinson's design technique in order to achieve better accuracy.

The analysis method developed in Chapter II has been shown to be exceptionally accurate when tested against various exact solutions. It is also very efficient as it requires fewer points around the section

than other methods. As it is a surface vorticity method similar to those of Chen [3] and Mavriplis [9] the design method follows naturally from the analysis method. The use of this method introduces some new aspects to the design of airfoil sections. This, together with the efficiency of the method, provides a fast, accurate design technique. The simplicity and efficiency of the method make it ideal for those with limited computing facilities.

3.2 Theory

In the analysis method of Chapter II the geometry of the airfoil section was specified and the surface velocities were calculated. In the design problem the surface velocities are given as requirements and it is the geometry of the section which must be determined. At present there does not appear to be any way to do this in one direct step. An iterative procedure, in which a basic section is gradually modified until it yields a section with the desired velocity distribution is therefore used.

The equation (8) can be written as:

$$y_i \cos\alpha - x_i \sin\alpha = \sum_{j=1}^{N} K_{ij}\,\gamma_j + \psi_k, \quad i=1,2..N. \qquad (18)$$

This equation provides a means of systematically modifying the basic airfoil section. Assuming that the K_{ij} are approximately the same for the basic and the modified section, and given the required $\psi_k^{(r)}$ and $\gamma_j^{(r)}$ and α, (18) gives a relation between the x_i and y_i on the modified section. Another set of equations in x_i and y_i are then required to determine these co-ordinates. This set of equations contain the ideas on how the modifications are to take place. Generally one wishes the chord length, C, to remain constant and the thickness and the camber of the section are

considered as variables. For airfoil sections whose chord lines are located approximately along the x axis the x_i can be constant and variations in the y_i provide the modifications to the section. The scheme is adequate when designing single component sections or multi-component sections where the flaps have small deflection angles, up to 30^0. An alternative is to adjust each component along lines perpendicular to the chord of that component. This will be practical when such lines are not parallel, or approximately parallel to the free stream direction. As most design requirements are made at small flap deflections and small angles of attack the simple scheme of maintaining the x_i constant is employed here. The y co-ordinate of the control point C_i at the d^{th} iteration in the design procedure is then given by,

$$y_i^{(d)} = \frac{1}{\cos \alpha} \left[x_i \sin \alpha + \psi_k^{(r)} + \sum_{j=1}^{N} K_{ij}^{(d-1)} \gamma_j^{(r)} \right], i=1,2...N. \quad (19)$$

Whether this technique will converge on a solution will depend largely on the manner in which the influence coefficients vary between iterations. The elements of the coefficient matrix K_{ij} are generally small, the size depending on both airfoil section and the number of elements N being used. In general the diagonal terms, the self-influence coefficients, are the largest. These terms are functions only of Δ_j, the half-length of the j^{th} element. In progressing from design to design the lengths of elements should change only very slowly. Hence the terms which are generally the largest in the summation in equation (19) change slowly. This acts to stabilize the design procedure.

The Kutta condition, equation (12), can also be written into the design method as:

$$y_{tp}^{(d)} = \frac{1}{\cos \alpha} \left[x_{tp} \sin \alpha + \psi_k^{(r)} + \sum_{j=1}^{N} K_{tp,j}^{(d-1)} \gamma_j^{(r)} \right], \quad k=1,\ldots M. \tag{20}$$

The location of the trailing point is so close to the trailing edge that it can be assumed that $y_{tp}^{(d)}$ is the designed location of the trailing edge. This point together with the control point locations obtained from equation (19) define the airfoil section.

From equations (19) and (20) the role of the $\psi_k^{(r)}$ can be readily appreciated. The $\psi_k^{(r)}$, being constant on any one component, have the effect of raising or lowering that component by a constant amount. In a single component airfoil section this is of little consequence, and any value can be chosen for $\psi_1^{(r)}$. In the case of multi-component airfoil sections each component has its own separate $\psi_k^{(r)}$ and hence each component is raised vertically by a different amount. The difference between the $\psi_k^{(r)}$ on any two components represents the quantity of air which flows between these components. These differences control the slot widths between components while the value of one of the $\psi_k^{(r)}$ will, as in the single component case, determine the vertical location of the whole section.

3.3 Method of Solution

The approach taken by this method is that, starting from a basic airfoil section, the y co-ordinates of the surface are systematically altered to give a new airfoil section. This new section will have a surface velocity distribution closer to the required distribution than that on the basic section. The process is iterative and the newly designed section can be analyzed after each iteration to determine if a suitable section has been designed. This iterative approach allows one

to alter both the required solution and the designed geometry at each iteration. This allows the designer great flexibility in choosing the required velocities and also allows specific geometric constraints such as minimum thickness, leading edge radius to be incorporated in the technique. A flow chart of the solution procedure is given in Figure 11.

There are five necessary steps in the procedure. These are labeled 1-5 in Figure 11. In the fifth step the designer may be satisfied if a specific number of iterations have been performed or if the requirements were met to within some accuracy. There are three optional steps in the procedure. These are labeled a, b, c in Figure 11 and may or may not be used as the designer wishes.

The first and second necessary steps are performed exactly as in the analysis method of Chapter II. The airfoil surface elements have their end points located in a cosine distribution. The mid-point of the straight line joining the end points is the control point. The trailing control point lies a short distance behind the trailing edge. The influence coefficients, K_{ij}, of the j^{th} element on the i^{th} control point is calculated using Equation (9) where the distances a, b, r_1 and r_2 are defined in Figure 2. The left hand sides of the system of Equations (8) and the Kutta conditions (12) are then combined to form the coefficient matrix. At this point one can take the first optional step and use this matrix to solve for the velocity distribution around this section. This solution can then be compared with the required solution.

The third necessary step is the application of Equations (19) and (20) by the multiplication of the coefficient matrix by the vector of required velocities and stream functions. For a single component section these equations can be written as,

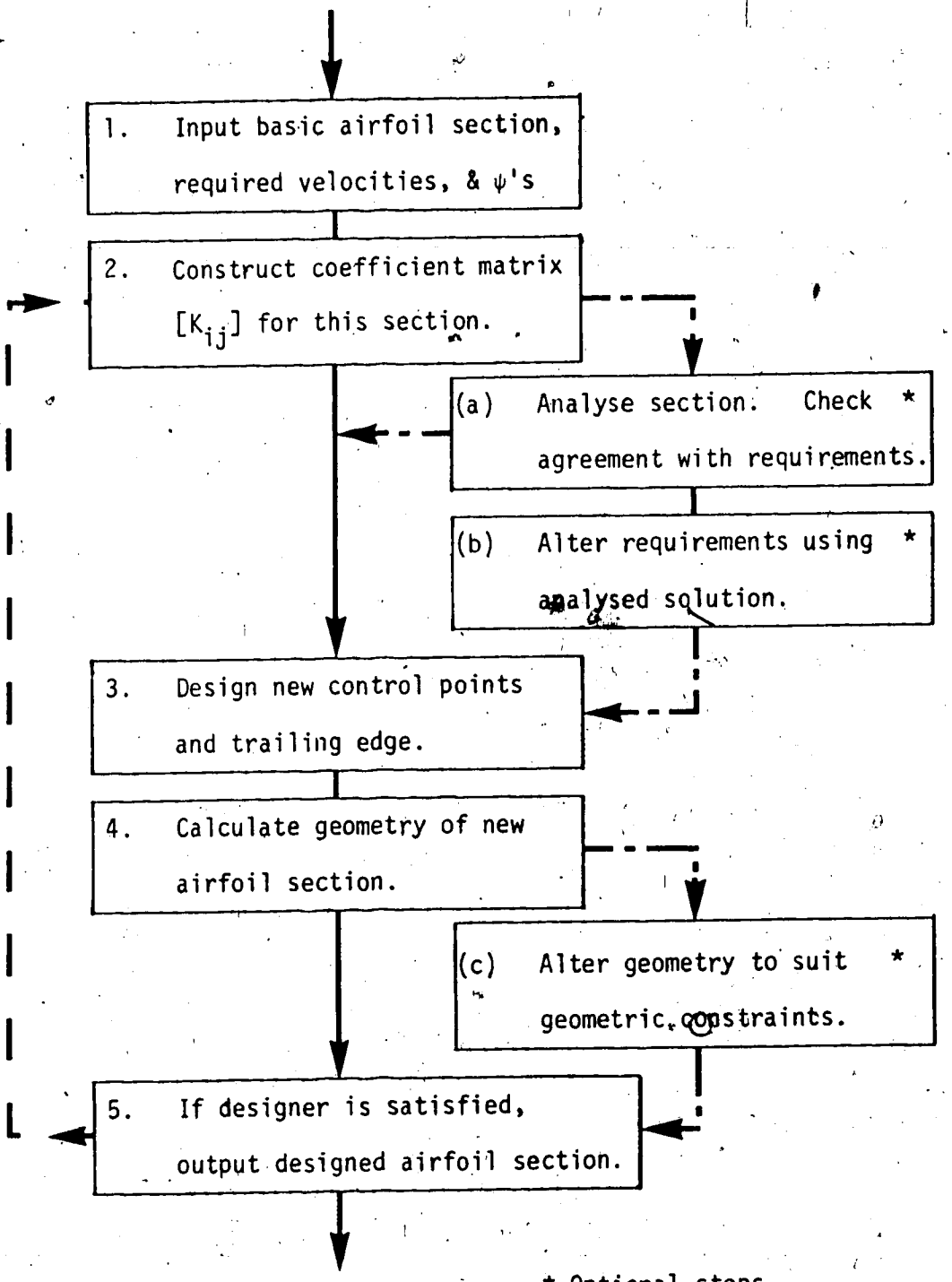

FIGURE 11 - FLOW CHART OF DESIGN PROCEDURE

$$\begin{matrix} i=1 \\ \\ \\ \\ i=N \\ i=N+1 \end{matrix} \begin{bmatrix} y_1 \\ \cdot \\ \cdot \\ \cdot \\ y_N \\ y_{tp} \end{bmatrix}^{(d)} = \frac{1}{\cos\alpha} \left\{ \sin\alpha \begin{bmatrix} x_1 \\ \cdot \\ \cdot \\ \cdot \\ x_N \\ x_{tp} \end{bmatrix} + \begin{bmatrix} K_{1,1} & \cdots & K_{1,N} & 1 \\ \cdot & & \cdot & \cdot \\ \cdot & & \cdot & \cdot \\ \cdot & & \cdot & \cdot \\ K_{N,1} & & K_{N,N} & 1 \\ K_{tp,1} & \cdots & K_{N,tp} & 1 \end{bmatrix}^{(d-1)} \begin{bmatrix} \gamma_1 \\ \cdot \\ \cdot \\ \cdot \\ \gamma_N \\ \psi_1 \end{bmatrix}^{(r)} \right\} \tag{21}$$

It frequently occurs that specific velocities are required at certain locations on the section but the velocities at other locations are not specified and no particular demands are made of them. In this case the vector of required velocities is not fully known. The values which are unknown can be replaced by the corresponding values of the surface velocities calculated in the analysis step. This is the second optional step and it requires, of course, that the analysis be done. The streamfunctions, $\psi_k^{(r)}$, can also be replaced by the values obtained from the analysis. In multi-component sections this procedure must be used with caution because of the important role played by the streamfunctions in controlling the slot widths between components.

The fourth necessary step is to obtain the co-ordinates of the airfoil section from the set of designed control points obtained from equation (21). The trailing edge location is taken to be that of the designed trailing point. Because the trailing edge and trailing point are very close the error in this assumption is very small. The detailed design of the trailing edge of an airfoil section can have a significant effect on the performance of the section. Only by this method can suitably accurate trailing edge shapes be designed.

Two methods are considered for determining the remaining airfoil co-ordinates, which are the end points of the surface elements. The first method uses the fact that, given one end point of an element and the mid-point, i.e. the control point, the other end of the straight line element can be found. The key to successful use of this principle lies in the accurate prediction of the trailing edge. This point is the only end point designed and it is an end point for elements on both upper and lower surfaces. Starting from the trailing edge the end points are found in turn up to the leading edge using the designed control points. This is done for both upper and lower surfaces. Ideally the location of the leading edge calculated from both upper and lower surfaces is identical. Typically the two locations are less than 0.05% of chord apart in which case the mean of the two values is taken as the leading edge location. The most distinct advantage of this method is that the designed airfoil section will have its control points located at exactly the designed locations, except perhaps for the two control points adjacent to the leading edge. One drawback is that if one end point goes astray subsequently calculated end points on that surface will suffer accordingly. This can result in rough, saw toothed surfaces on the designed section which cannot be tolerated.

To alleviate the problems of rough surfaces a second method was developed. This consists of fitting a smooth curve through the designed control points and interpolating on that curve to determine the end point locations. A cubic spline function was used for this purpose to ensure as smooth an airfoil surface as possible. The drawback to this is that for any element the two end points and the designed control point all lie on the same smooth curve. In analyzing the airfoil later the

same two end points. This tends to reduce the curvature of the surface which can have a serious effect near the leading edge of the component as can be seen in Figure 12.

The distance between control points adjacent to the leading edge is termed the nose thickness here. From Figure 12 it can be seen that the effect of smoothing is to produce an implied nose thickness smaller than the designed nose thickness. In general the nose of an airfoil section is a sensitive area and the designed nose thickness should be restored by some means. The upper surface co-ordinates are therefore raised and the lower surface co-ordinates lowered by an amount that varies linearly from the leading to trailing edge. . The amount of adjustment is such that the new implied nose thickness is equal to the designed nose thickness and there is no alteration to the trailing edge. This is equivalent to driving a wedge down the centerline of the airfoil component. Doubtless other schemes are available to determine an airfoil section co-ordinates from the control point locations but the above methods are fairly simple and in general provide suitable results.

The third optional step can be taken once a new airfoil section is designed. A check can be made to see if this section geometry is reasonable or even physically possible. If the design is not completely satisfactory alterations can be made to the geometry to meet specific requirements. Some of these requirements could be to retain a specific nose radius or trailing edge angle or to limit the maximum or minimum thickness to specific values. With such geometry changes the velocity distribution on the designed section will not necessarily be the one specified. However this method provides sufficient flexibility for the designer to come to a suitable compromise between geometrical constraints and the desired velocity distribution.

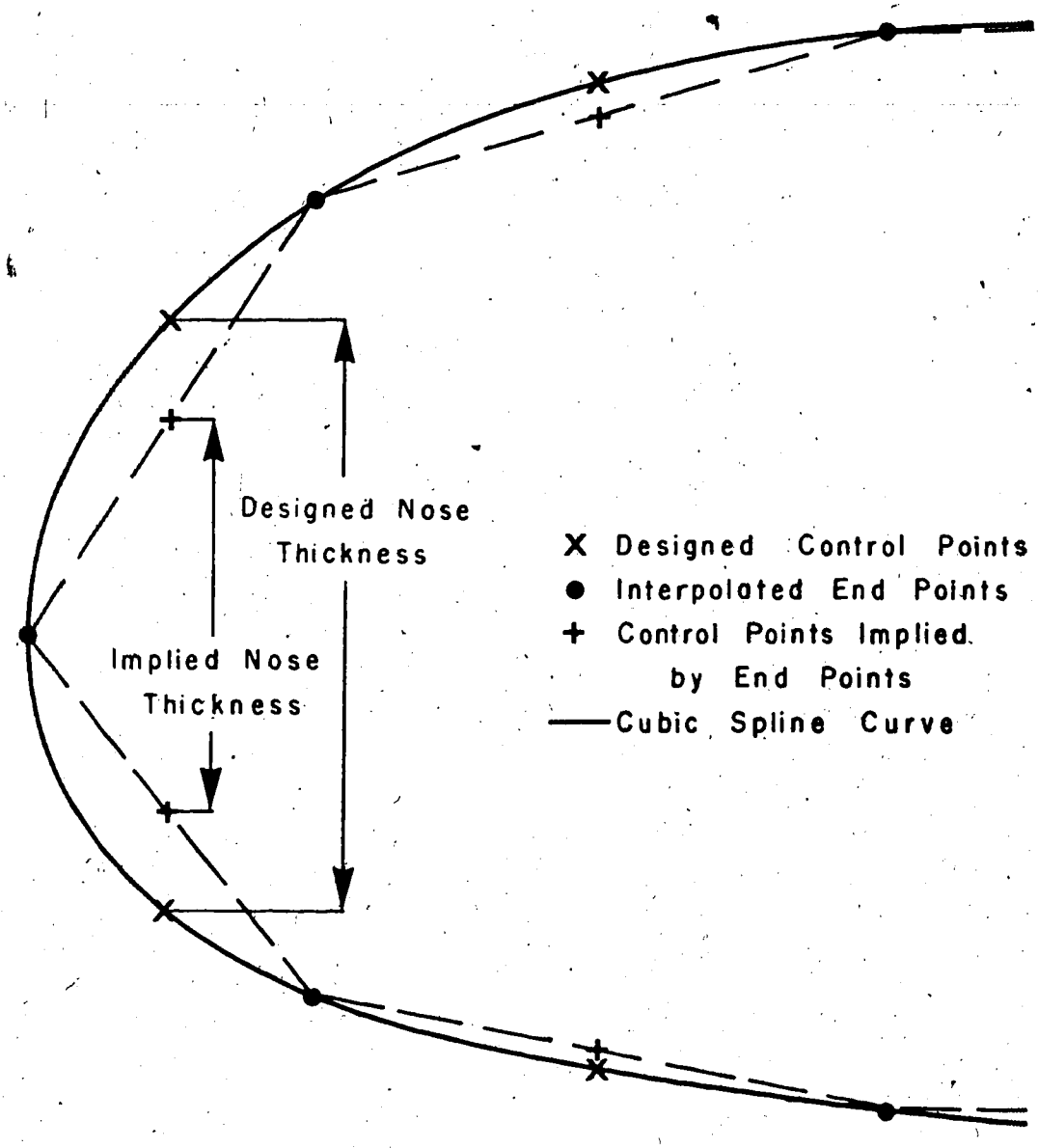

FIGURE 12 - DESIGN OF NOSE AREA WHEN SMOOTHED

In the set up described here two such modifications were used. If the thickness of the section fell below that of a 1% thick section then the thickness was increased to that of the 1% thick section. This was done because thinner sections are unrealistic from a practical point of view and also this represents the limit below which the analysis method becomes inaccurate. The second modification used allows any desired portion of the section to be kept unchanged from its original location. This feature is particularly useful when designing flaps to suit a main component whose geometry and location is fixed.

3.4 Results

The iterative design procedure should converge on an airfoil design which gives exactly the required velocity distribution. As the technique is numerical and iterative the results will not give exact agreement and it is first necessary to determine just how close this method will come to the required solution in practical cases. An example of a practical airfoil design is shown in Figure 13. As can be seen there is good, but not perfect, agreement between the designed and required velocity distributions. The velocity error at any control point is defined by,

$$E = \left| \frac{U - U^{(r)}}{U_\infty} \right| \qquad (22)$$

It is important to determine cause of these errors and how they vary with the number of iterations performed.

The major effect of the design procedure is to reduce the errors as the number of iterations increases. However, the errors introduced by the technique of determining the airfoil co-ordinates from the designed

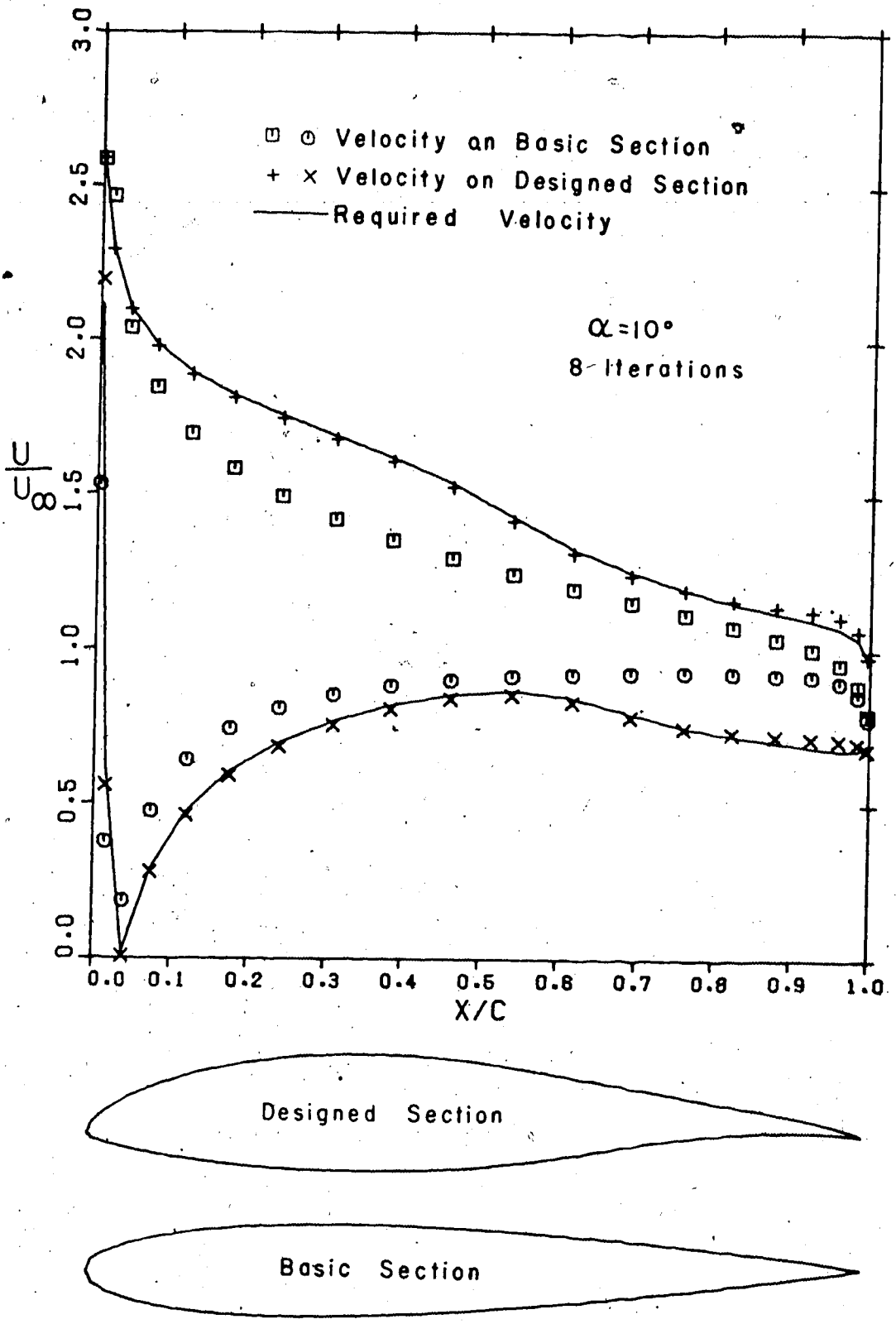

FIGURE 13 - SINGLE COMPONENT DESIGN

control points will tend to grow as the number of iterations increase. This will limit the method in its attempt to achieve the required velocity exactly. To some extent this can be examined by setting the required velocities identical to those on the initial basic airfoil. The airfoil should then continually design itself and in a perfect design technique the velocity errors E should always be zero.

Both techniques for determining the airfoil co-ordinates were tested, the flat element method and the cubic spline smoothing method. The basic airfoil was the Wortmann section FX-61-163 at 10^0 angle of attack using 40 surface elements. This has the required velocity distribution shown in Figure 13. The maximum and average velocity errors for both techniques are plotted in Figure 14. From this it is clear that, as expected, the flat element method is superior. The maximum errors in this method occur near the trailing edge where the approximation that the trailing point is the trailing edge is made. In the smoothing method the maximum errors occur at the nose where the effects of reducing the surface curvature are felt most accutely. The effects of not adjusting the airfoil to give the correct nose thickness was a 50% to 100% increase in the errors. Small geometric errors at the nose are greatly aggravated by the high angle of attack of the section, hence this is a severe test of the smoothing technique. The maximum errors, although they appear large, amount to less than 7% of the local velocity at the nose.

As a test of the design method a NACA 0012 section was designed to give the FX-61-163 distribution at 10^0 angle of attack. 40 surface elements are used as the analysis method of Chapter II has shown that this is adequate for highly accurate solutions from single component sections. The design method was applied 15 times with and without smoothing to

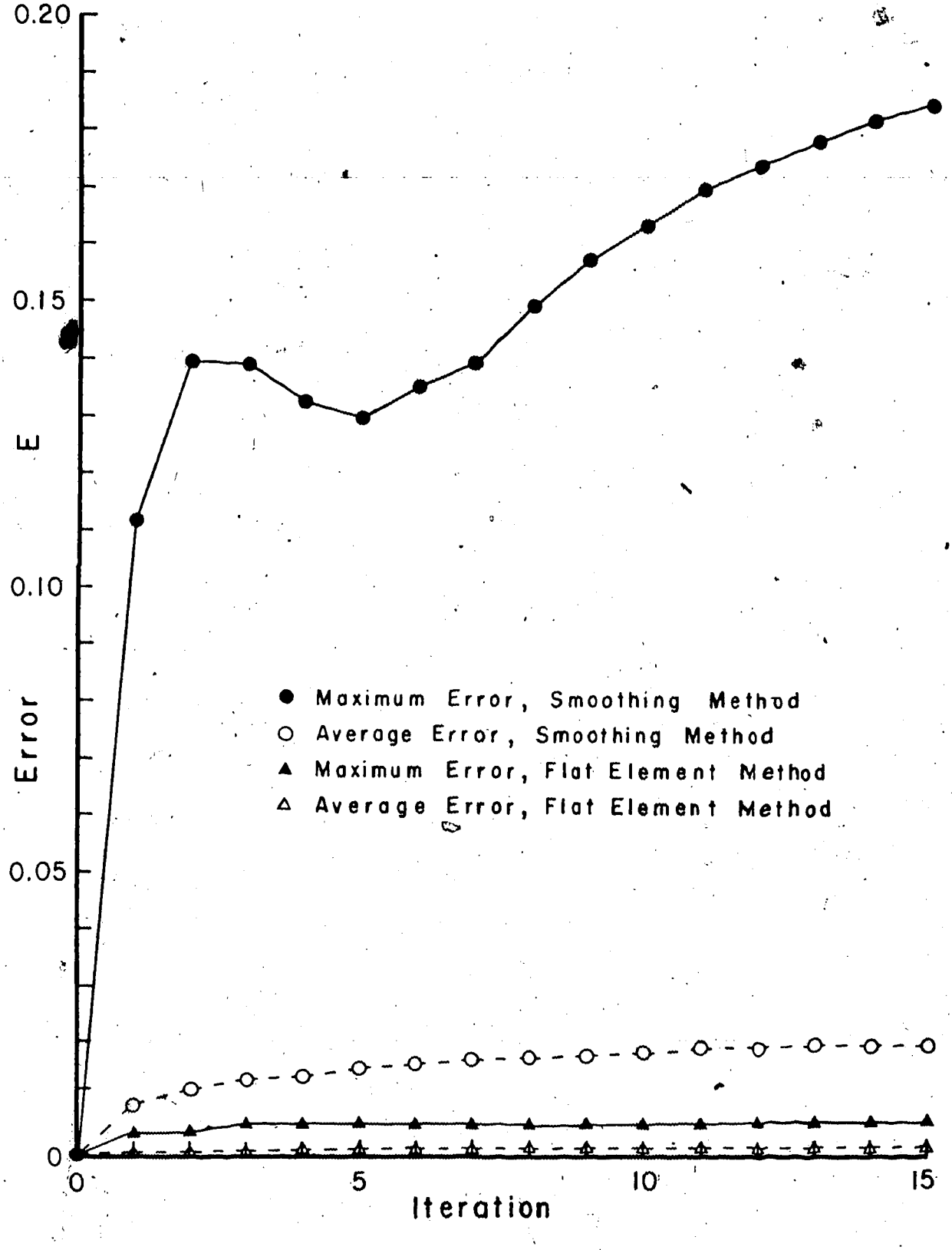

FIGURE 14 - ERROR GROWTH DUE TO METHOD

determine the relative rates of convergence. The average velocity errors at each iteration are plotted in Figure 15. The first few iterations provide the most rapid convergence and the rate of convergence gradually decreases from then on. The smoothing technique provides slower convergence than the flat element technique as could be expected.

Defining the term improvement as the difference between the average errors for any two consecutive iterations it is clear that the improvements decreases as more iterations are performed. There is therefore a point at which the design process should be terminated. The criterion used must provide a realistic balance between the need for accurate design and the cost of performing each iteration. In designing single component sections the criterion that the design process be terminated when the improvement becomes less than 1% of the original, average velocity error is used. In the cases shown in Figure 15 this occurs at the 8^{th} iteration for the flat element method and at the 6^{th} iteration for the smoothing method. The trends observed in Figure 15 are typical of those observed in the design of many single component sections with angles of attack ranging from -8^{o} to $+10^{o}$ and employing various numbers of elements on each section. Of these results the data presented in Figure 15 are representatives of the results obtained from difficult design test cases.

The results of the 8^{th} iteration of this test case using the flat element method were presented in Figure 13. This is a difficult test case as there is a high velocity peak at the nose and considerable loading in the rear 30% of the designed section. The designed section had substantially the same shape as the FX-61-163 profile but had a maximum thickness of 15.7% of chord compared to 16.3% of chord for the FX-61-163 section. The

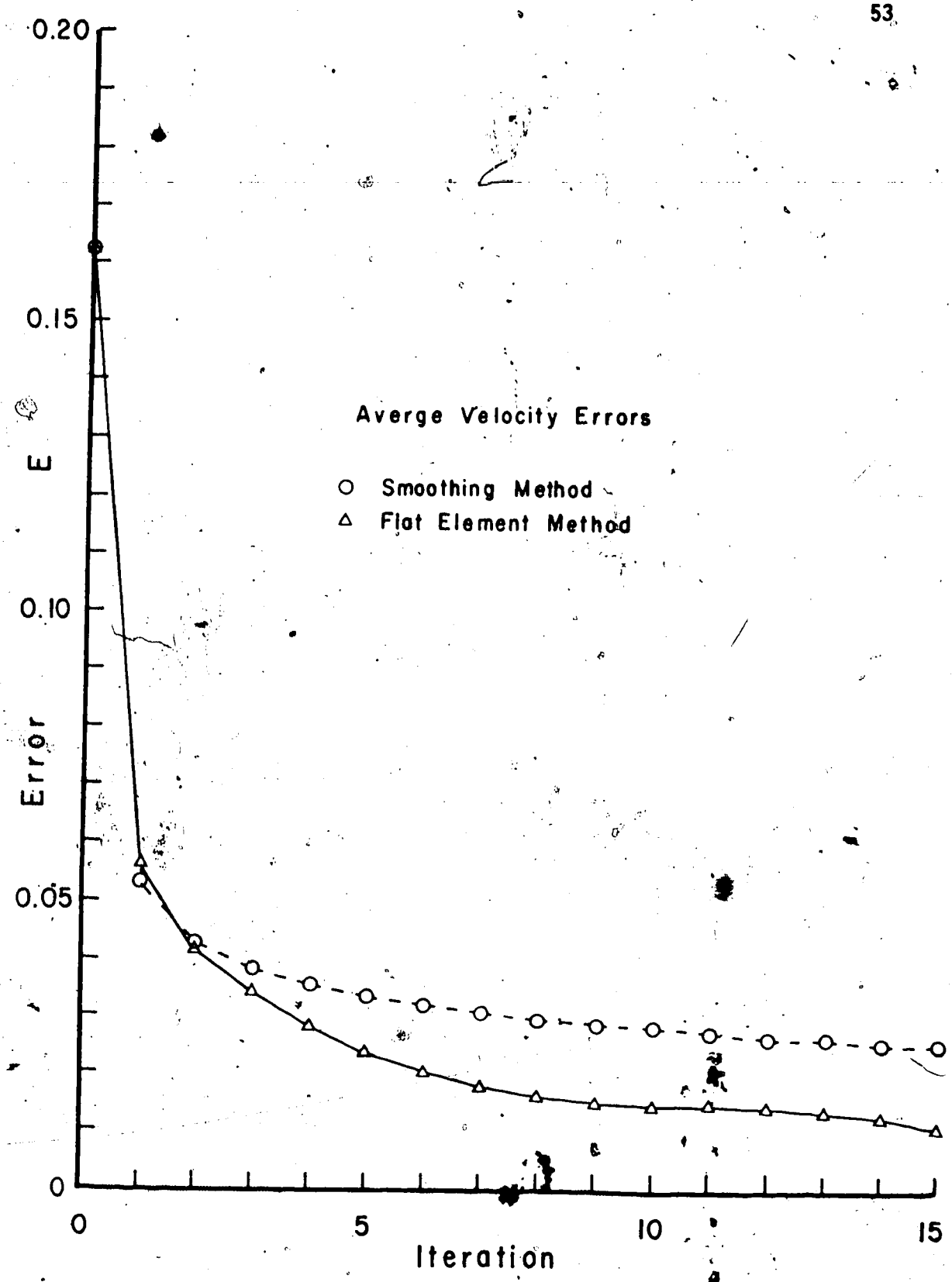

FIGURE 15 - CONVERGENCE OF SINGLE COMPONENT DESIGN

change in the thickness distribution is even more radical as the tail is designed from a thick, symmetric wedge shape to a thin, cambered, almost cusped shape. Considering these difficulties this design is considered to be quite adequate.

An example of a rather arbitrary design problem, based on a NACA 0012 section at 0^{o} angle of attack, is shown in Figure 16. The upper surface velocities are increased and the lower surface velocities decreased by an amount that varies linearly from leading edge to trailing edge. The results in this case after 8 iterations are exceptionally accurate. The required results are in fact those one would expect, according to the simple design rules of Abbott and Von Doenhoff [21] had one distributed the NACA 0012 thickness distribution around a NACA a=0 mean line at an angle of attack of 4.56^{o}. The designed section is inclined at an angle of approximately 5^{o} to the free stream and the thickness distribution has changed very little. The very accurate results which are achieved in this case are attributed mainly to the fact that there is so little change in the thickness distribution.

The viscous flow analysis of Chapter IV restricts this thesis to considering single component sections, however methods such as Stevens, Goradia and Braden's [15] are not so restricted and thus the performance of this design method on multi-component sections must be tested. A two component section was therefore designed to have a required velocity distribution obtained from a known two component section. The result of the design process after 12 iterations, when the convergence criterion was satisfied, is shown in Figure 17. The basic section was composed of two NACA 0012 sections each scaled to span the desired x co-ordinates. The required surface velocities on both components were supplied together with ψ_1 and ψ_2.

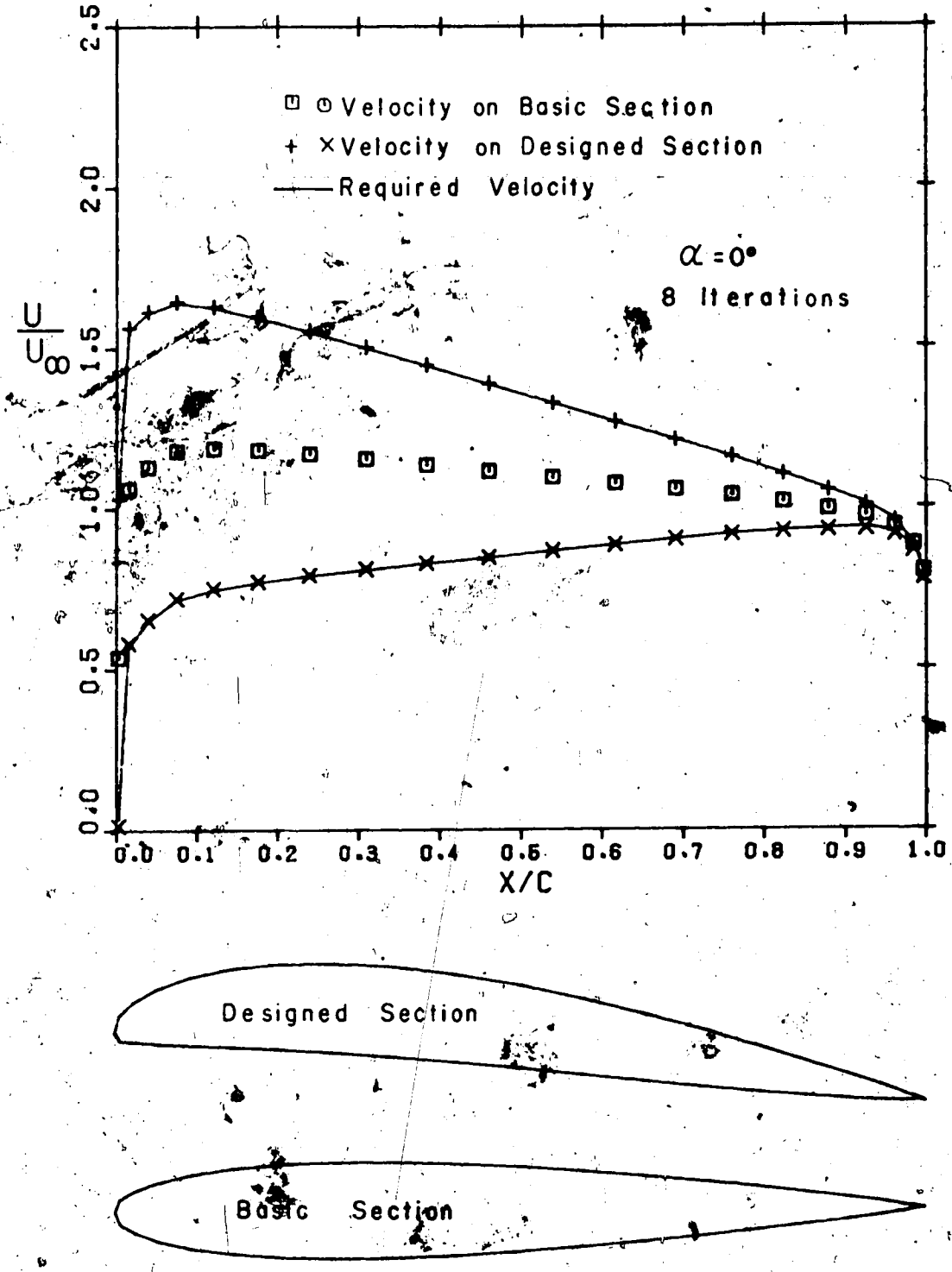

FIGURE 16 - ARBITRARY SINGLE COMPONENT DESIGN

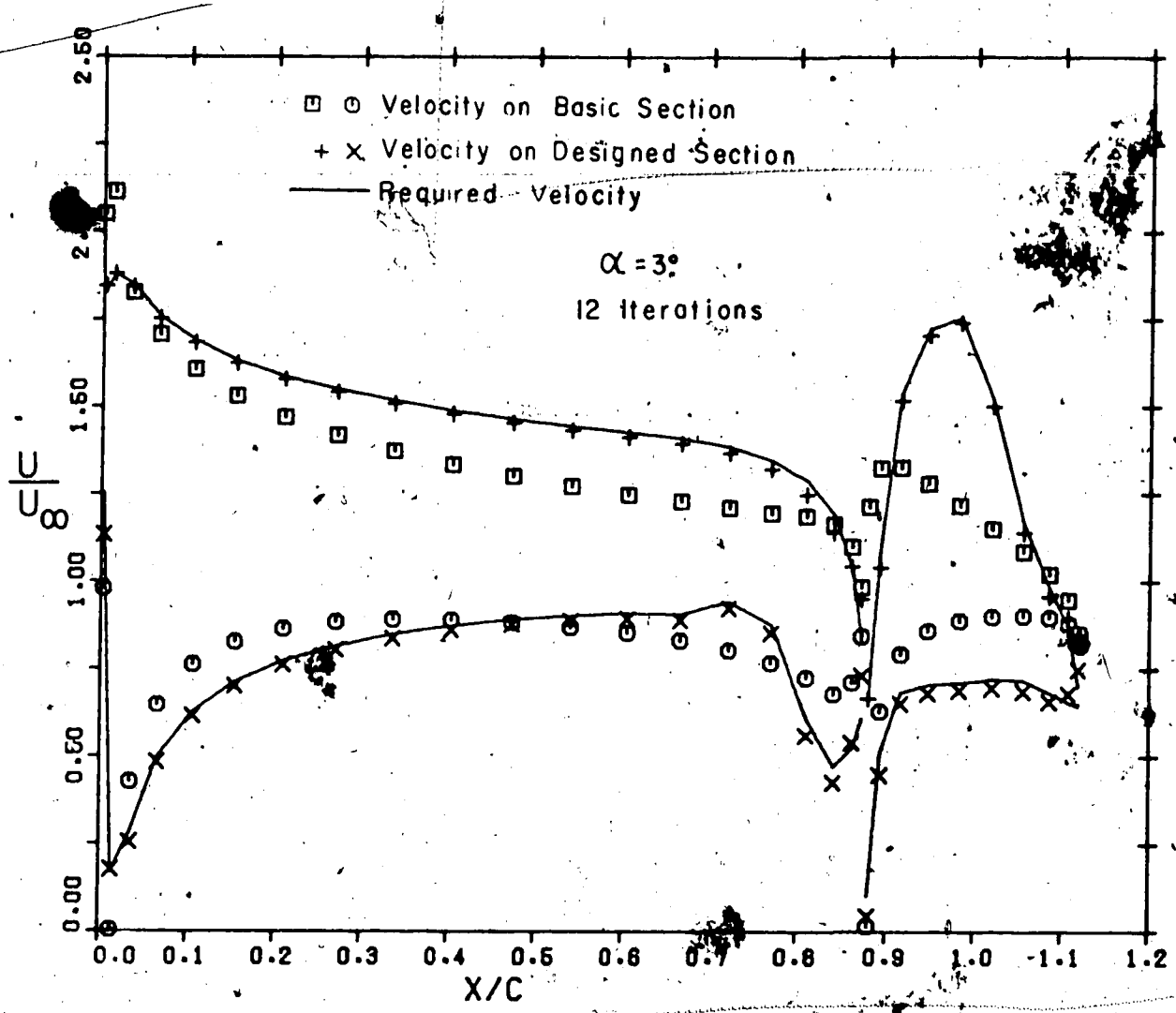

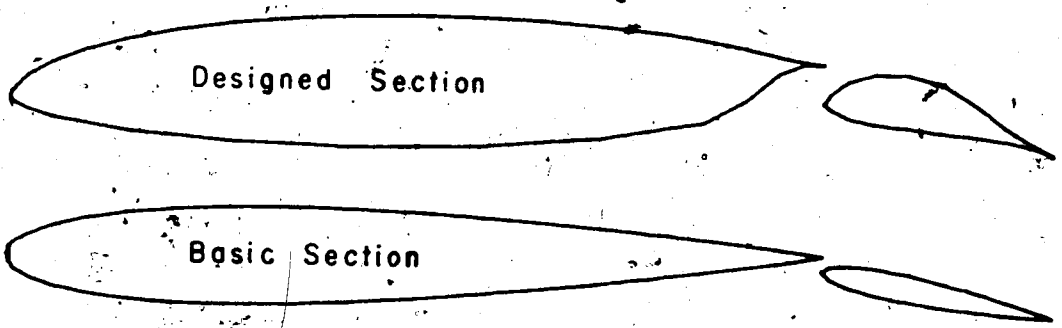

FIGURE 17 - TWO COMPONENT DESIGN

60 surface elements were used, 40 on the main component and 20 on the flap as the analysis method has shown that this is adequate for an accurate solution.

The results show good agreement between the desired and the designed velocity distributions. This is quite remarkable as, again, this case represents a difficult problem for the design method. Near the trailing edge of the main component there are quite drastic changes in thickness distribution and camber. On the flap the maximum thickness changes from 12% of chord to about 30% and the camber changes are quite large. The flat element method was used in this case and it is quite capable of handling the severe changes in slope which occur at the rear of the main component. At the same time it must be admitted that this is the region in which the largest velocity errors occur on the main component. The largest velocity errors on the flap occur on the under side. This is due to the inability of the flap to develop its full thickness in 12 iterations. This is caused largely by imputing such an unrealistically thin initial flap.

The method will therefore design a whole multi-component airfoil section starting from a fairly unrealistic basic airfoil section. This is however not a completely practical problem from the point of view of the airfoil design engineer. In general the main component, with the flap retracted, will have been previously designed as a single component section according to the requirements of high speed cruise. The main component is therefore already designed and cannot be altered as it was in the last example. The flap must be designed, under the influence of the main component, to suit the requirements of low speed and high lift.

To test the possibility of such a flap design technique a basic airfoil section with a fixed main component and a NACA 0012 flap was used. In general the velocities on the main component are not known and cannot be specified. The set of required velocities on this component are replaced by the values calculated in the previous analysis step. Fixing both the location and geometry of the main component makes the specification of ψ_1 redundant. Only the streamfunction on the flap, ψ_2, can be specified. The first choice of ψ_2 that was tested was the value from the known solution.

In this case the design process failed, after 12 iterations, to locate the flap correctly and the geometry became distorted as the method attempted to match the required flap velocity distribution. There was fair agreement between the designed and required velocity distributions but the errors were larger than those seen in Figure 17 and therefore not acceptable. The convergence of the velocities and streamfunction on the main section to the solution, which was known but not specified, was found to be very slow. In this regard it should be noted that there are many flap geometries, and corresponding locations, which provide approximately the correct velocity distribution over the flap. The configuration to which the method converges will depend to a large extent on the basic section used. Following the approach of Chen [3] and Mavriplis [9] and using the value of ψ_2 calculated in the previous iteration gave equally bad results unless the initial flap location was correctly chosen.

To surmount these problems one can, at each iteration force ψ_2 to remain a fixed amount, $\Delta\psi$, from the value of ψ_1 calculated in the previous analysis. In this manner the flap is raised or lowered to give the correct slot width between the main component and the flap. While

the $\Delta\psi$ used in this case is the exact $\psi_2 - \psi_1$ of the solution this will not, in general, be known in advance. It can however be estimated using the formula,

$$\Delta\psi = \text{Slot Width} \times \text{Average Velocity across the Slot.} \qquad (23)$$

The penalty to be paid in order to solve the flap design problem is that the slot width must be chosen. Leaving this parameter free results in poor solutions or excessively long calculations.

Using the $\Delta\psi$ in the design procedure gives the results shown in Figure 18 after 15 iterations. The velocity errors on the flap are comparable with those observed in Figure 17 and the velocities on the main section are in good agreement with those originally required of the two component section. Most important, using the constant $\Delta\psi$ technique, the flap is correctly located and its geometry is not distorted. The original velocity distribution around the basic airfoil section showed a large velocity peak at the nose of the flap which the design method removes. However, if one started from a more realistic flap geometry one could expect even better results.

A basic airfoil section with a NACA 0036 flap was employed and the results are shown in Figure 19. Here the results after 15 iterations are excellent. The velocity errors on the flap are very small and the velocity distribution on the main section agrees well with that required of the original two component design. The flap shape is marginally thicker than that in Figure 18, and comes closer to the expected value of approximately 30% of its chord. As with the single component cases the closer the basic section comes to the final thickness distribution the better the results. The reason for this is that while camber changes

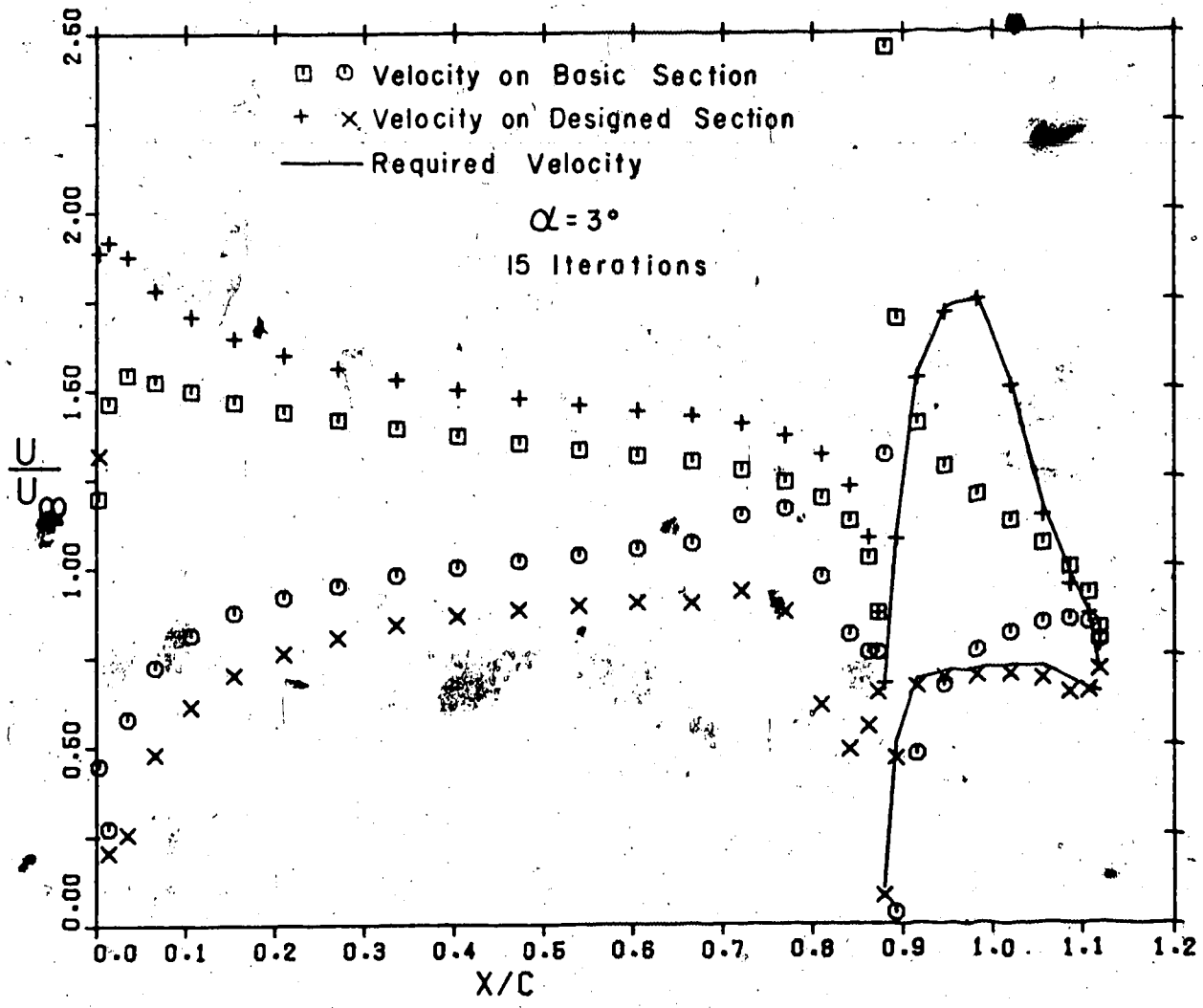

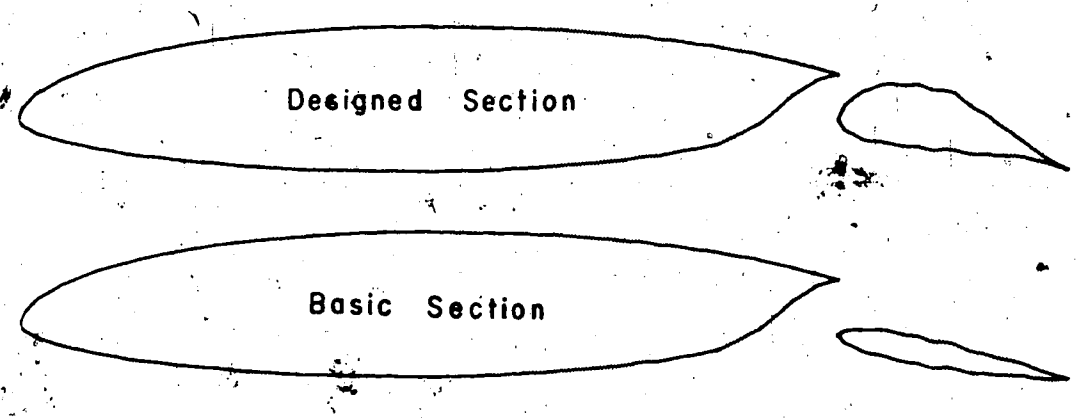

FIGURE 18 - FLAP DESIGN, NACA 0012 BASIC FLAP

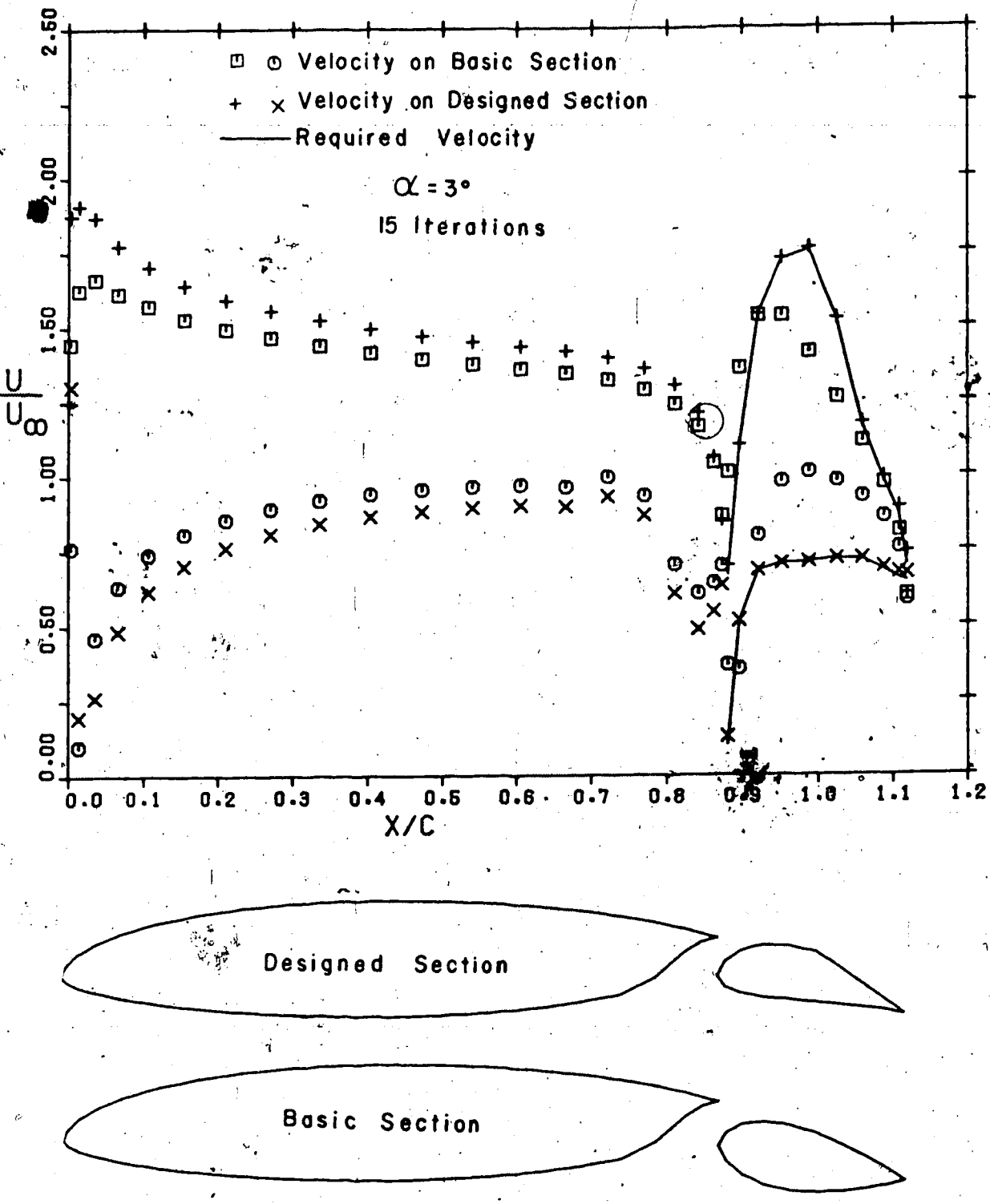

FIGURE 19 — FLAP DESIGN, NACA 0036 BASIC FLAP

are performed fairly rapidly alterations to the thickness are gradual and take many iterations.

The method of maintaining $\Delta\psi$ fixed at each iteration can be applied to the complete two component section designs also. This controls the slot width and specification of either ψ_1 or ψ_2 determines the location of the whole section. Clearly the slot width can be controlled in other ways than by the $\Delta\psi$ method. The method used by Beatty and Narramore [20] is to specify the distance between the leading edge of the flap and the trailing edge of the main component. Using such a method in this case would simply involve moving the designed flap vertically to meet this condition. In such cases the ψ_1 and ψ_2 can be arbitrary as their role in controlling vertical positioning has been replaced by actual physical positioning.

The convergence properties of the two component cases are slightly different from those seen in Figure 15 for single component cases. In Figure 20 the average velocity error at each iteration is plotted for three of the cases discussed here. In the complete design of the two component sections starting from two NACA 0012 sections the average error drops off more slowly than in the single component case. For this reason the convergence criterion of an improvement of less than 1% of the original error does not stop calculations until the 12^{th} iteration. This slower rate of convergence and a higher average velocity error are typical of two component sections when compared with single component cases. This is thought to be simply due to the general complexity of the geometry of multi-component sections with highly curved sections near the trailing edges of the forward components.

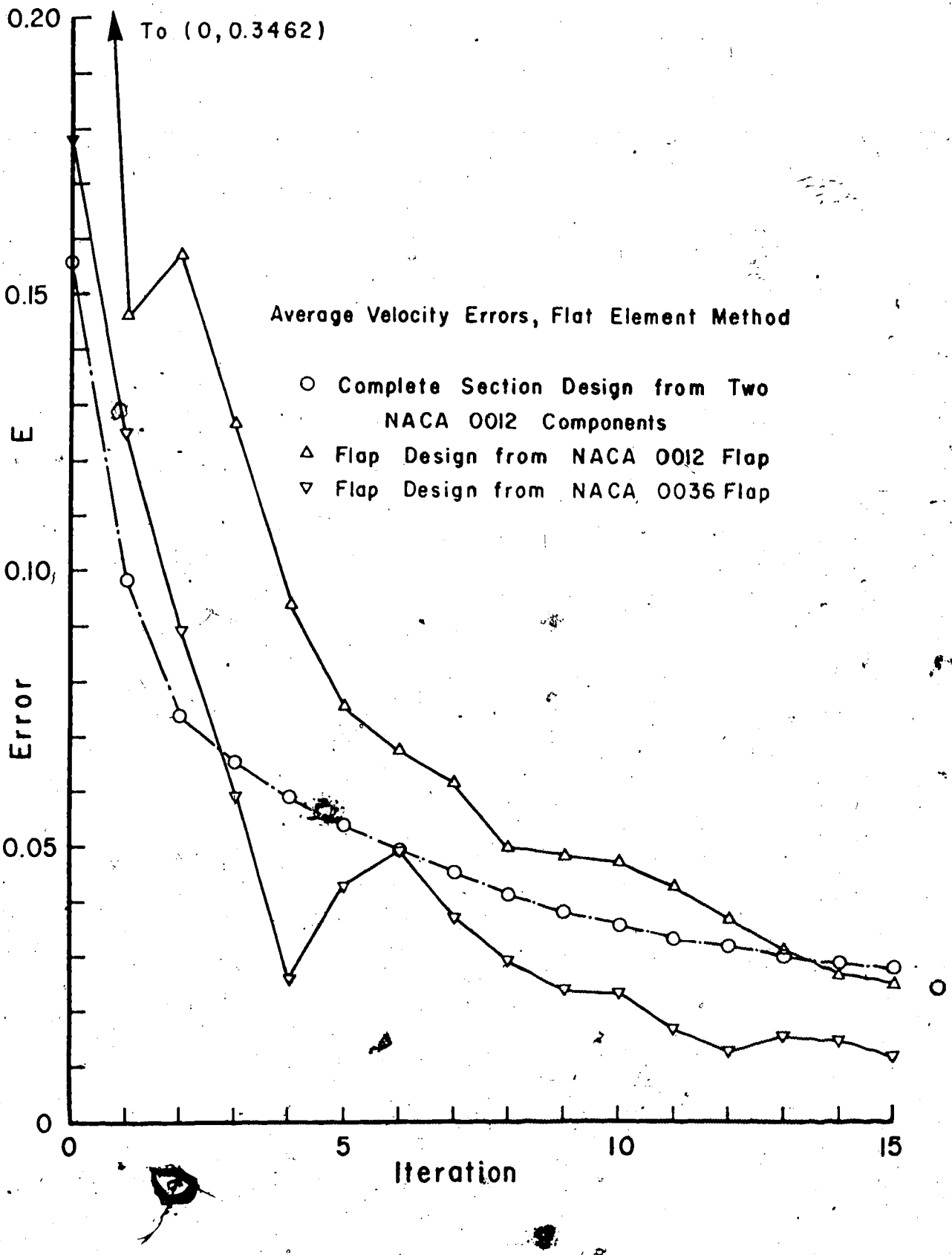

FIGURE 20 - CONVERGENCE OF TWO COMPONENT DESIGNS

In the case of the problems of designing the flap alone, using the $\Delta\psi$ method, the convergence is quite different. In these cases the average error is calculated for the flap alone. In the example starting from the NACA 0012 flap the convergence is fairly spasmodic. Using the NACA 0036 flap the convergence is very spasmodic showing divergence on some occasions. The divergence occurred on iterations where there were sudden changes in the calculated stream functions together with substantial velocity errors at locations near the nose of the flap. These errors die out rapidly in subsequent iterations. This erratic behaviour precludes the use of the previous convergence criterion and in its place a limit of 15 iterations is used. As can be seen, by comparison with Figure 13, the results using the more realistic flap shape give, after 15 iterations, accuracy similar to those of the single component design. The advantage of using this flap shape over the NACA 0012 section can be seen in Figure 20. The better shape gives approximately a 4 iteration advantage in achieving any given accuracy.

This design technique, being iterative, uses considerable amounts of computer time. The actual amount used depends on both the number of elements being used and the number of iterations performed. The times quoted below are for the CPU time used on an Amdahl 470 V/6 computer.

For a single component section using 40 elements and employing 8 or more iterations the time required is less than 0.34 sec. per iteration. This is for the complete program with all options shown in Figure 11. The analysis option (a) uses considerable time and when analysis is only performed on the final design the required time drops to less than 0.22 sec. per iteration. For two component sections using 60 elements, 40 on the main component and 20 on the flap, and employing 12 or more iterations

the required time is less than 0.90 sec. per iteration. Employing the analysis option only on the final design reduces the required time to less than 0.45 sec. per iteration. In the case where the flap alone is to be designed a saving of approximately 25% should be possible if one does not recalculate the influence coefficients linking elements and control points on the main section, and if the design of the main component is bypassed as this is redundant.

While the foregoing results may have made multi-component airfoil section design appear to be a relatively simple matter, there are some problems associated with this technique. The problem of choosing a velocity distribution which will yield a practical shape of airfoil must be examined. While this technique will be able to supply such answers on a trial and error basis the problems associated with the multi-element case seem to be quite large. In such cases the problem of the slot width, or effectively the $\Delta\psi$, which is to be chosen must be resolved. In this connection it must be noted that the highly curved portion of the main section is not, in general, a solid surface. It is usually the separation streamline leaving the underside of the main component, there being a large gap in the rear of this component to house the flap in its retracted position. As this is a free streamline its path can vary, according to the geometry of the flap, and thus the slot width will be altered.

For those who are interested in designing flaps at large flap angles the vertical movement of flap co-ordinates may not be desirable. The other alternatives mentioned in the theory may prove useful in this regard.

A frequently occurring problem in airfoil design is the need to remove a sharp velocity peak from the nose of the flap while retaining

the remainder of the velocity distribution and only altering the geometry of the flap in the nose region. Beatty and Narramore [20] have shown that, with their technique, it is not always possible to attain the required velocities with these local geometric alterations. This has been found to be the case with this method also and experience with this method indicates that the most successful designs are obtained when each component is designed as a complete unit. If a flap designed for a high lift configuration interferes with the cruise configuration then some compromise solution will have to be reached.

Because of its generality this design technique opens up a wide variety of possibilities depending on a users needs. The ability to alter the geometry of the designed section in any way will give rise to other problems. It has been found necessary to limit the thickness to greater than that of a 1% thick airfoil as this represents the limit of accuracy of the analysis technique. This precludes the possibilities of upper and lower surfaces crossing which was found to lead to very poor results. A scheme which arbitrarily alters the designed section can result in slower convergence or to a solution with large velocity errors. Each scheme used would have its own properties and these would have to be examined individually.

Occasionally a specific velocity distribution is required of the section upper surface but not of the lower surface. This is handled by using the lower surface velocities calculated from the analysis in the design calculations. This freedom of choice of velocities on the lower surface gives the result that in the final design the lower surface velocities depend largely on the basic airfoil section used. Cases where this option is used generally require more iterations.

Practical examples of airfoil design frequently involve trying many required velocity distributions before a suitable design is found. A graphics display terminal is used in this case to display the designed section geometry and the actual and required velocity distributions as soon as they are calculated. This allows for the rapid assessment of the designed section. Without this facility airfoil design progresses quite slowly.

3.5 Conclusions

A method of designing multi-component airfoil sections in potential flow has been developed. This method is based on an accurate, efficient analysis method from which the design equations are derived. Each component of an arbitrary basic airfoil is modified in both thickness and camber to give a new section which has the required surface velocity distribution. This is done in an iterative manner which allows the designed geometry and the required velocity distribution to be altered at will at each iteration. It was shown that this freedom results in a very powerful design tool which can be fitted to suit many of the constraints which occur in the design of modern airfoil sections.

The design method determines the location of the control points on the new section. The application of a Kutta condition in the design process gives the location of the trailing edge. From these points the airfoil co-ordinates are determined and two techniques of doing this were considered. A flat element technique was found to result in less error than a smoothing technique which had a tendency to reduce the surface curvatures. The flat element method converges on a solution considerably faster than the smoothing method. It is therefore recommended for use

except where it results in rough surfaces, in which case smoothing is called for.

The design method provides suitably accurate solutions for both single and two component sections. Generally the method will converge to an accurate solution in 8 iterations for the single component case and 12 iterations for a two component case. The method is flexible enough to handle the design of flaps under the influence of fixed main components. For this case it was shown that the difference between the stream functions on the components, or effectively the slot width between them, is an important parameter which should be kept constant throughout the design procedure. This applies to all multi-component designs.

The method can be started from any reasonable basic section, however alterations to the thickness of the section are performed more slowly than alterations to the camber line. Faster convergence can therefore be expected if the basic section chosen has a thickness distribution similar to the final design.

The power of this method as a design tool lies in its flexibility. Because of this many variations on this method are possible. The performance of each such variation will have to be examined individually.

CHAPTER IV

VISCOUS FLOW ANALYSIS

4.1 Introduction

In order to determine the performance of an airfoil section in a real fluid the effects of viscosity must be accounted for. The potential flow analysis of Chapter II does not account for these effects as it is applicable only to inviscid, incompressible flow. However, attempting to solve the full viscous flow equations for the flow about an airfoil section is too large a task to be handled here. Fortunately airfoils are designed such that the effects of viscosity are confined to a thin region near the surface, the boundary layer, and to the wake which leaves the airfoil trailing edge. A practical method of solving this problem is therefore to attempt to match the outer, potential flow, solution with the boundary layer solution next to the airfoil surface.

The effect of the boundary layer is to displace the streamlines just outside this layer by a distance equal to the local displacement thickness. The flow outside the boundary layer is then approximated by the potential flow over this displacement surface. Powell [22] has shown that, using experimentally obtained displacement thicknesses, this procedure provides adequate agreement with experimental results for airfoils. Powell's approach was to consider the displacement thickness effects as altering the thickness, the camber line and angle of attack of the section. The thickness changes were carried through to a wake which extends to infinity and it was shown that the detailed development of the wake had little effect on the results.

Stevens, Goradia and Braden [15] have developed a method for analyzing multi-component sections in viscous flow. This method used the thickness and camber changes to define what is termed an equivalent airfoil. This is the airfoil which, in potential flow, produces the pressure distribution of the section in viscous flow. The equivalent airfoil had both thickness and camber changes relative to the actual section. Of these the camber modification is the most important and for multi-component sections thickness effects are neglected. The displacement thicknesses were calculated from a boundary layer analysis based on velocities calculated from a potential flow analysis. The potential flow and viscous flow results are matched by an iterative process which converges on the equivalent airfoil section which should yield the experimental pressure distribution.

A similar iterative process has been used by Seebohm and Newmann [18]. The boundary layer calculations in this followed the method of Cebeci and Smith [23] which utilizes Thwaites' [24] method for calculating the laminar boundary layer and Head's [25] method in the turbulent boundary layer. The ability of the boundary layer calculations to predict the displacement thickness correctly is crucial to all such matching procedures. While differential methods are generally regarded as the most accurate for boundary layer calculations they consume large amounts of computing time. For economic reasons integral methods of boundary layer analysis are generally used.

In the case of multi-component sections the wakes from upstream components can merge with the boundary layers on downstream components. Although the method of Stevens, Goradia and Braden [15] can handle this confluent boundary layer problem, it is not simple to apply. This

confluence can have a considerable effect on the airfoil performance and ignoring it restricts the validity of a viscous flow method to single component sections or to those with separated components.

The viscous flow of primary concern here is that for a single component section and confluent boundary layer methods will not be used. Recent developments in boundary layer analysis permit the accurate calculation of the characteristics of the boundary layers on airfoil sections. When combined with the reliable potential flow analysis of Chapter II an accurate viscous flow analysis method should result.

4.2 Boundary Layer Analysis

In steady, two dimensional, incompressible, isothermal flow the boundary layer equations reduce to.

$$\frac{\partial u}{\partial x} + \frac{\partial v}{\partial y} = 0 \tag{23}$$

$$u \frac{\partial u}{\partial x} + v \frac{\partial u}{\partial y} = U \frac{dU}{dx} + \frac{1}{\rho} \frac{d\tau}{\partial y} \tag{24}$$

The boundary conditions on these equations are,

$$u(x,o) = v(x,o) = 0, \quad u(x,\infty) = U(x)$$

Differential methods could be used to solve these equations for the boundary layer velocity profiles at each x station on the airfoil surface. The use of integral methods removes the need to calculate these profiles and consequently they involve much less work. As integral methods have also been proven to be fairly accurate it was decided to use one in this analysis. The particular method must be able to predict accurately the boundary layer parameters in both laminar and turbulent flow.

The turbulent region provides the most stringent test of this criterion and Kline [26] provides a rating of various methods in turbulent flow. There is little difference between the best methods and consequently a method which blends easily with the laminar calculations can be chosen. A method which is readily programable and has been successful in predicting airfoil boundary layers is also desirable.

The boundary layer analysis methods chosen were those of Eppler [27] in the laminar region and Felsch, Geropp and Walz [28] in the turbulent region. This scheme has been used by Miley [29] and has proven accurate in tests on airfoil sections. These methods involve the integration of both the momentum integral equation and the mechanical energy integral equation.

To arrive at these equations the displacement thickness, δ^*, momentum thickness, θ, and energy thickness, δ^{**}, are defined as,

$$\delta^* = \int_0^\infty \left(1 - \frac{u}{U}\right) dy$$

$$\theta = \int_0^\infty \frac{u}{U}\left(1 - \frac{u}{U}\right) dy \qquad (25)$$

$$\delta^{**} = \int_0^\infty \frac{u}{U}\left(1 - \left(\frac{u}{U}\right)^2\right) dy$$

The skin friction coefficient, c_f, and dissipation integral C_d are defined by,

$$C_f = \frac{\left(2\tau\right)}{\rho U^2}_{y=0}$$

$$C_d = \frac{2\int_0^\infty \tau \frac{\partial u}{\partial y}\, dy}{\rho U^3} \qquad (26)$$

The shape factor H and H* are defined by,

$$H = \frac{\delta^*}{\theta}$$

$$H^* = \frac{\delta^{**}}{\theta} \qquad (27)$$

By manipulating the boundary layer equations (23) and (24) and employing the definitions (25) to (27) the integral equations of the boundary layer are obtained as,

$$\frac{d\theta}{dx} = \frac{C_f}{2} - (2 + H) \frac{\theta}{U} \frac{dU}{dx} \qquad (28)$$

and

$$\frac{d\delta^{**}}{dx} = C_d - \frac{3\delta^{**}}{U} \frac{dU}{dx} \qquad (29)$$

Using the assumption that the laminar boundary layer velocity profiles form a one parameter family Eppler [27] provides the correlations for H, C_f, C_d in terms of H* and Re_θ, the Reynolds number based on the momentum thickness. These are provided in an analytic form which allows for easy computation.

While Eppler provided his own turbulent boundary layer analysis this has been superseded by that of Felsch, Geropp and Walz [28]. This method uses the shape factor correlation of Nicoll and Escudier [30] the skin friction correlation of Felsch [31] and the dissipation integral correlation of Felsch [31]. This last correlation, which was originally given graphically, was expressed as a series of equations by Felsch, Geropp and Walz [28] which makes it suitable for computers. This dissipation integral correlation takes into account the past history of the

boundary layer. The shear stress distribution therefore depends not only on the mean velocity distribution but also on upstream effects. It is this property which allows this method to rank among the best available.

The differential equations (28) and (29) are integrated simultaneously by second order Runge-Kutta techniques and for this procedure Eppler [27] has supplied stability criteria. If these criteria are not met the stepsize, Δx, is cut in half and the integration repeated. It has been found that, for the airfoil sections tested, the largest stepsize which provides sufficiently accurate results is 0.5% of chord.

The scheme is ideal for computers as the correlations are written analytically and the same equations are solved by the same technique in both laminar and turbulent flow. The method has been well documented by Miley [29], however there are some unfortunate typing errors in both Miley [29] and Felsch, Geropp and Walz [28]. Before applying the method it was necessary to return to the source of the correlations to determine the correct formulas.

The boundary layers develop from the stagnation point near the leading edge of the airfoil section. The initial values for (28) and (29), from the stagnation point flow velocity distributions [34], are

$$\theta_o = 0.292 \left(Re \frac{dU}{dx}\right)^{-\frac{1}{2}} \tag{30}$$

and

$$\delta_o^{**} = \sqrt{0.475} \left(Re \frac{dU}{dx}\right)^{-\frac{1}{2}} \tag{31}$$

The laminar flow analysis can proceed from that point to the point of transition to turbulent flow.

Several criteria exist for predicting this transition point. Michels method [32] employs an empirical relation between Re_θ and Re_x at transition. Smith [32] shows that stability theory explains the correlation and approximated this with the formula,

$$Re_\theta = 1.174 \; Re_x^{0.46} \tag{32}$$

Cebeci, Mosinskis and Smith [33] later updated this formula to,

$$Re_\theta = 1.174 \left(1 + \frac{22{,}400}{Re_x}\right) Re_x^{0.46} \tag{33}$$

to improve the correlation at lower Reynolds numbers. In this region (33) agrees well with the formula of White [34]

$$Re_\theta \quad Re_x^{0.4} \tag{34}$$

Miley [29] has shown that Michels criterion is not distinguishable from the Schlichting, Ulrich, Granville [35] criterion used by Stevens, Goradia and Braden [15]. As Miley points out, Michels data was obtained in wind tunnel experiments. Eppler's [27] criterion, which was based on free flight data, yields later transition than other methods. In practice it was found, for the test cases examined, that differences in transition location were negligable and equation (34) was used.

The above methods were concerned with transition due to the growth of instabilities in the attached laminar boundary layer. Another mechanism which can lead to transition in airfoil boundary layers is that of laminar separation. This phenomenon can lead to complete breakdown of the flow over the section if the boundary layer fails to reattach to the surface. Laminar separation is therefore a very important parameter.

In the light of several exact solutions Curle and Skan [36] modified the laminar separation criterion of Thwaites to read,

$$\sigma = \frac{-\theta^2}{\nu} \frac{dU}{dx} = .090 \qquad (35)$$

at separation. By plotting the values of H and σ at separation from various exact solutions Liu and Sandborn [37] showed that such a unique value is inadequate. The values of H and σ at separation for the exact solutions given by Tani [38] and Liu and Sandborn [37] are replotted on Figure 21. These solutions can be correlated approximately by

$$H = 3.2\, e^{-17.5\,\sigma} + 3.1 \; ; \; 0.07 < \sigma < 0.36. \qquad (36)$$

This expression is used as the criterion for laminar separation. As Epplers' [24] correlations are derived from a one parameter family of profile, the boundary layer calculations have their own unique separation criterion. This happens to be that of Hartrees' profile which has an H of 4.03 at separation. This value is used for $\sigma < 0.07$.

After separation the flow may reattach as a turbulent boundary layer. If the reattachment point is far downstream of the separation point the long bubble that forms can have a considerable effect on the pressure distribution around the section. Owen and Klanfer [39] show that there is a critical Reynolds number, Re_{δ^*}, at separation below which the transition and hence the reattachment process is considerably delayed giving long bubbles. They suggest that the critical value of Re_{δ^*} at separation is in the region 400-500. The present analysis uses 450. Gaster [40] shows that the pressure gradient over the length of the bubble also influences the structure of the bubble. However there

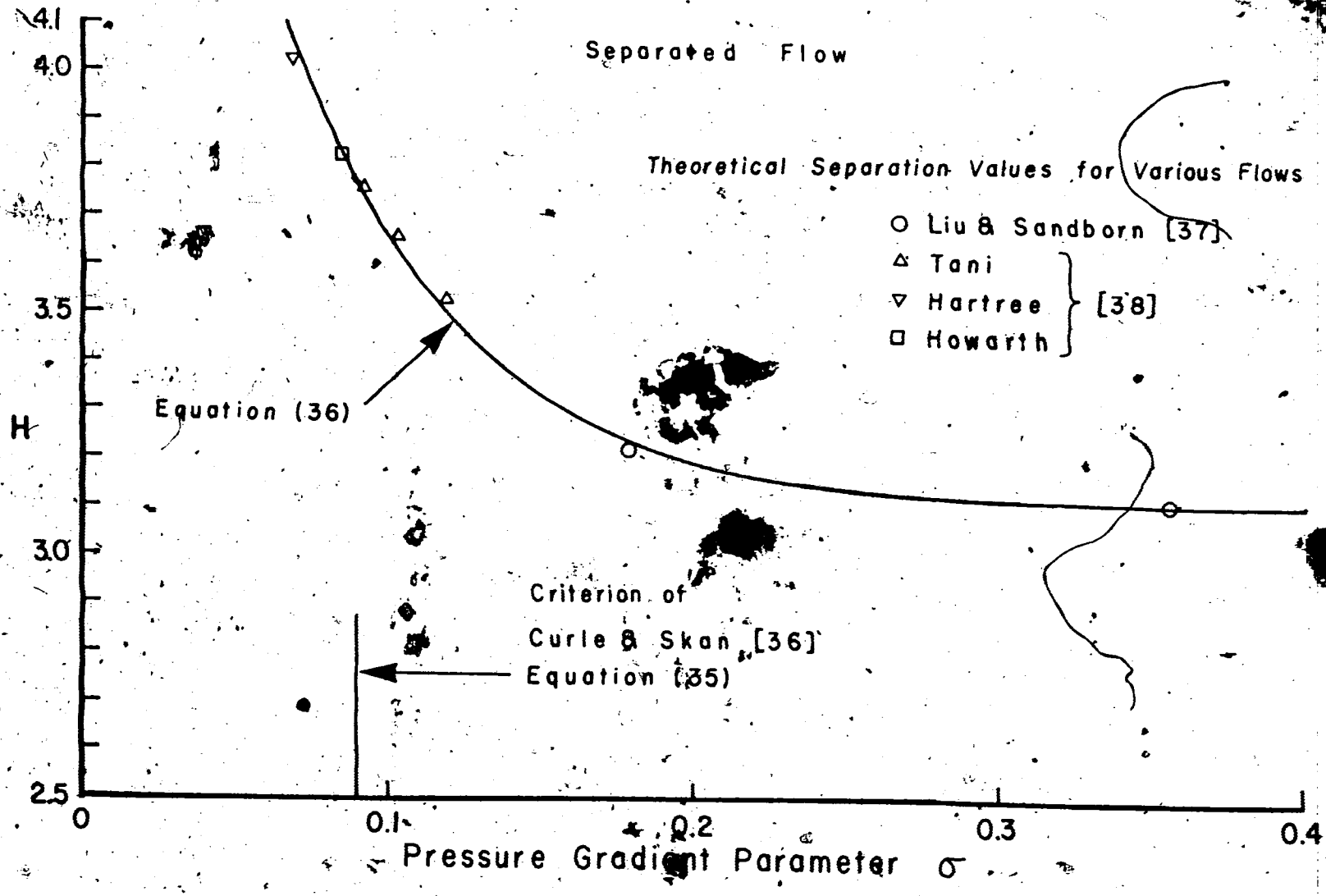

FIGURE 21 - LAMINAR SEPARATION CRITERION

still remains the problem of determining the bubble length. Horton [41] provides some assistance in calculating the lengths of bubbles however, agreement between theory and experiment is not good enough for airfoil analysis.

Regardless of the type of bubble predicted, long or short, the effect is presumed to be the same in each case. Transition to turbulent flow is assumed to occur at the separation point. When very long bubbles are predicted the boundary layer calculations should rightfully be terminated. This is not done as long bubbles in one analysis may become short due to changes in the pressure distribution caused by the viscous corrections. At transition it is assumed that there is continuity in both θ and δ^{**}. This differs from Miley's approach of maintaining θ and δ^* constant. The method used here is simple and reflects the fact that δ^* drops considerably at transition.

The turbulent boundary layer analysis can proceed up to the trailing edge of the section, or to the point of turbulent separation. Many criteria have been proposed for turbulent separation and frequently separation is predicted for a particular value of H. Chang [42] has reviewed many of these techniques and notes that the theoretical values of H at separation range from 1.8 to 2.8. As turbulent analysis methods do not generally agree exactly on the boundary layer parameters the criteria used depends to some extent on the analysis method.

Ideally the separation occurs where the skin friction becomes zero. Such a criterion gives rise to numerical problems and the criterion used here is

$$C_f = 0.0003 \tag{37}$$

at turbulent separation. For airfoil flows at a Reynolds number of 10^6 this results in separation when H is approximately 2.4. This is within the range of values suggested by Chang and also represents, approximately, the limit of applicability of Felsch's skin friction correlation.

A separation criterion frequently used in airfoil analysis is that of Stratford [43]. On some test cases this simplified method gave separation at values of H ranging from 1.7 to 1.8. Such values are thought to be too low. Sandborn and Liu [44] have shown that there exists a region of intermittent separation prior to complete turbulent separation. In their investigations no profiles with shape factors as low as 1.8 were encountered at separation. They further conclude that the minimum value of H at the start of intermittent separation is 2.0.

The drag coefficient of the section is calculated from the semi-empirical relation of Squire & Young [35]. The drag coefficient due to one surface is given by

$$C_D = 2\,\theta_{te}\,U_{te}^{(H_{te}+5)/2} \qquad (38)$$

This has been shown by Cebeci and Smith [23] to be adequate for most airfoil sections. Smith and Cebeci [45] have considered the use of other, similar relations but conclude that equation (38) is as good as any other and simpler to apply. In calculating the drag coefficient when the flow separates from the surface ahead of the trailing edge the values of θ, U and H at separation are used. The total drag coefficient of the section is the sum of the components from each surface.

4.3 The Equivalent Airfoil Technique

The equivalent airfoil section was obtained from the actual section and the calculated boundary layer displacement thicknesses. The thickness distribution on the equivalent section was assumed to be the same as that on the actual section. Small changes in thickness cause small changes in the potential flow velocity distribution. The camber line was however adjusted as shown in Figure 22 such that it lay midway between the calculated displacement surfaces. The airfoil surfaces were therefore moved vertically by a distance

$$(\delta_u^* - \delta_\ell^*)/2.$$

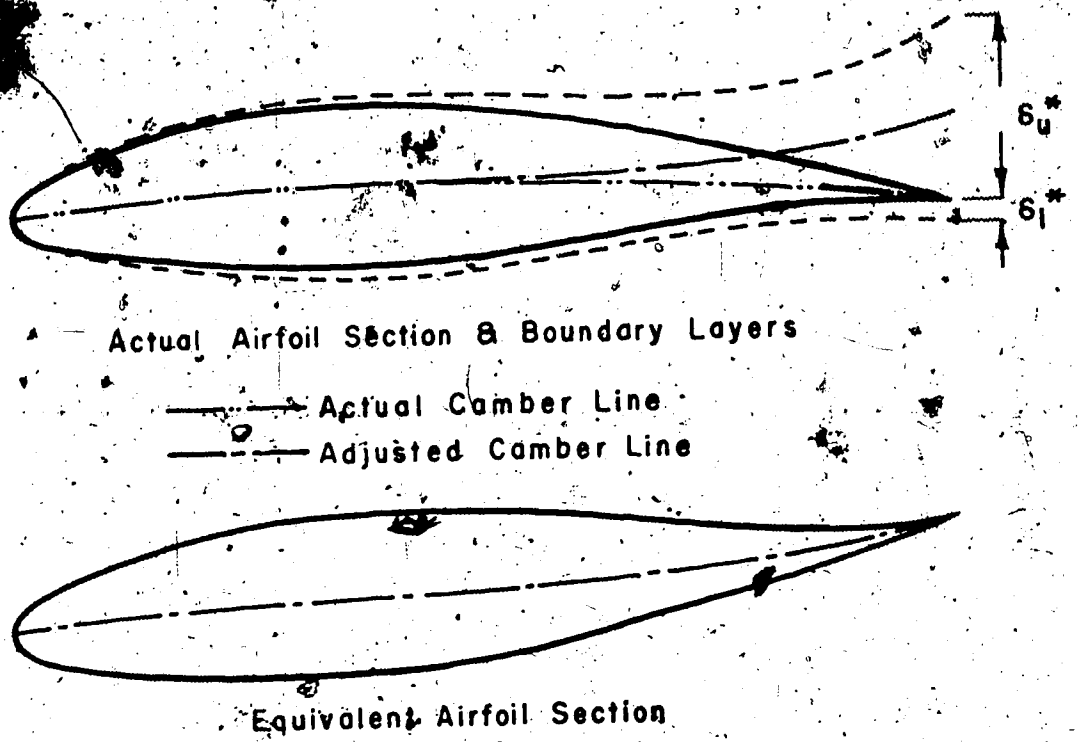

FIGURE 22 - AIRFOIL GEOMETRY MODIFICATION DUE TO BOUNDARY LAYERS

The equivalent airfoil technique relied therefore on the prediction of the displacement thicknesses. In a region of turbulent separated flow no adequate method for calculating the displacement thicknesses exists. The displacement thickness was therefore assumed to grow linearly from the separation point at the rate at which it was growing at that point. This is an approximate method and can only be expected to be sufficiently accurate when the separation point is close to the trailing edge.

Calculated values of δ^* show some irregularities especially at transition. These irregularities could cause changes in the calculated pressure distribution which would have been smoothed over in the real flow. The calculated surface displacements were therefore smoothed to provide a realistic equivalent airfoil section.

The iterative procedure which was performed to converge on the equivalent airfoil section is illustrated in Figure 23. The criterion for convergence on an equivalent airfoil section was that the lift coefficient has converged to within 0.005 and the drag coefficient to within 0.0001. The use of smoothing had the effect that it stabilizes the iterative procedure. Convergence on a solution was generally obtained within 5 iterations.

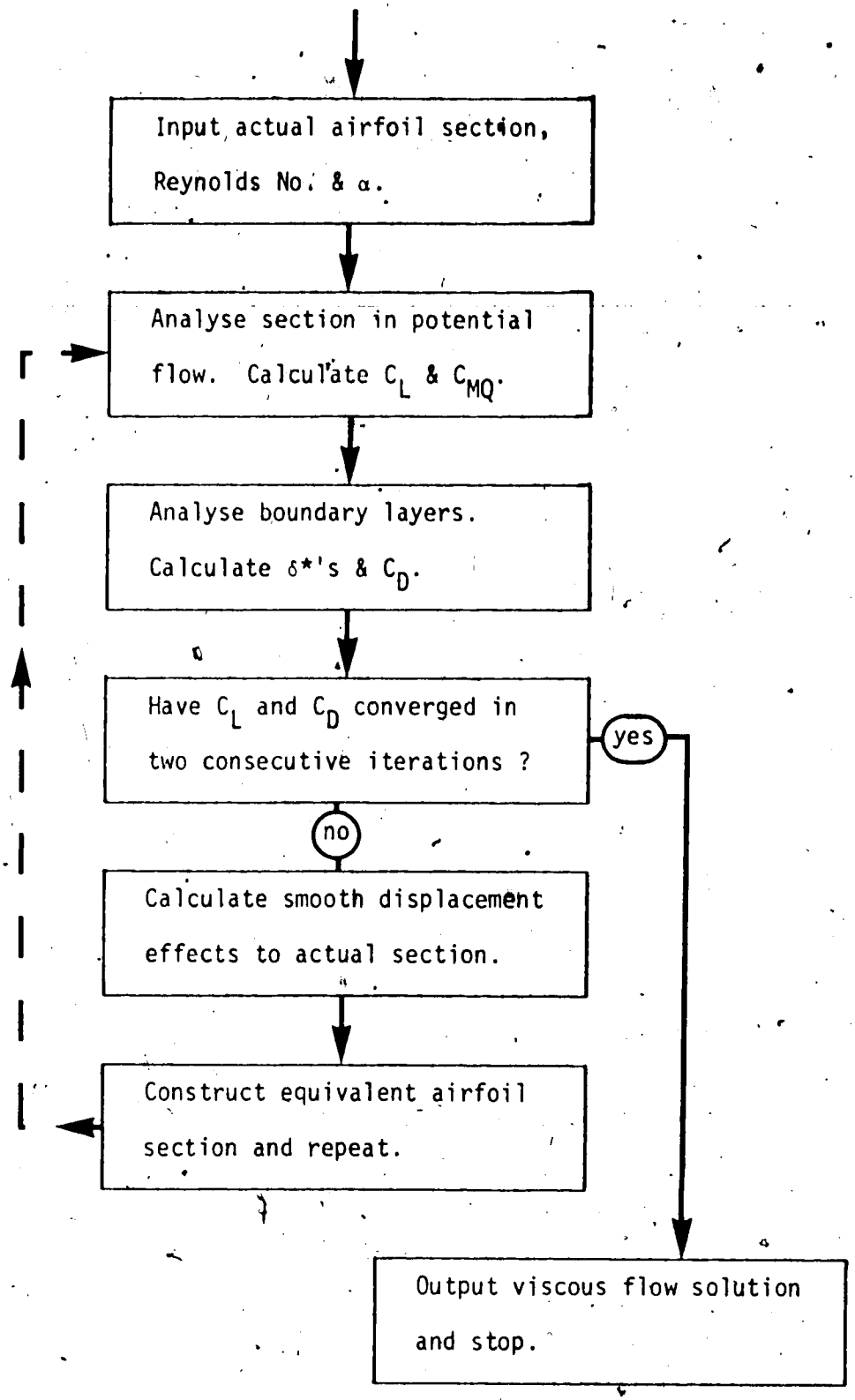

FIGURE 23 - FLOWCHART OF VISCOUS FLOW PROCEDURE

4.4 Results

The capabilities of the boundary layer analysis method were assessed by application to test cases where the boundary layer characteristics were available in the literature. Tests of this integral method on the flow over a circular cylinder gave good agreement with Schoenauer's numerical solution of the differential, laminar boundary layer equations as reported by Schlichting [35]. The laminar separation criterion (36) predicted separation at 105^{0} which compares well with Schoenauer's prediction of 104.5^{0}. The "Newman Airfoil Flow" given by Kline [26] was used to test the turbulent flow computations. Again there was good agreement with the experimental values. Since the detailed boundary layer calculations were reliable the viscous flow analysis method was tested on some known airfoil sections.

The data of Raspet and Gyorgyfalvy [46] on the "Phoenix" wing section provide an excellent test of this calculation method. The data were obtained in free flight tests of the Phoenix sailplane and consequently the Reynolds number, based on test section chord, varied with the lift coefficient according to the formula

$$Re_{c} = 1.19 \times 10^{6} (C_{L})^{-\frac{1}{2}}. \qquad (39)$$

The input data to the analysis was the given set of airfoil coordinates and equation (39), the lift coefficient being the value from the potential flow calculation. No angle of attack information was given by Raspet and Gyorgyfalvy so angles from -7^{0} to 8^{0} were tested at approximately one degree intervals. The resulting profile drag polar is given in Figure 24 together with the experimental results. In the low drag range the agreement between theory and experiment is excellent

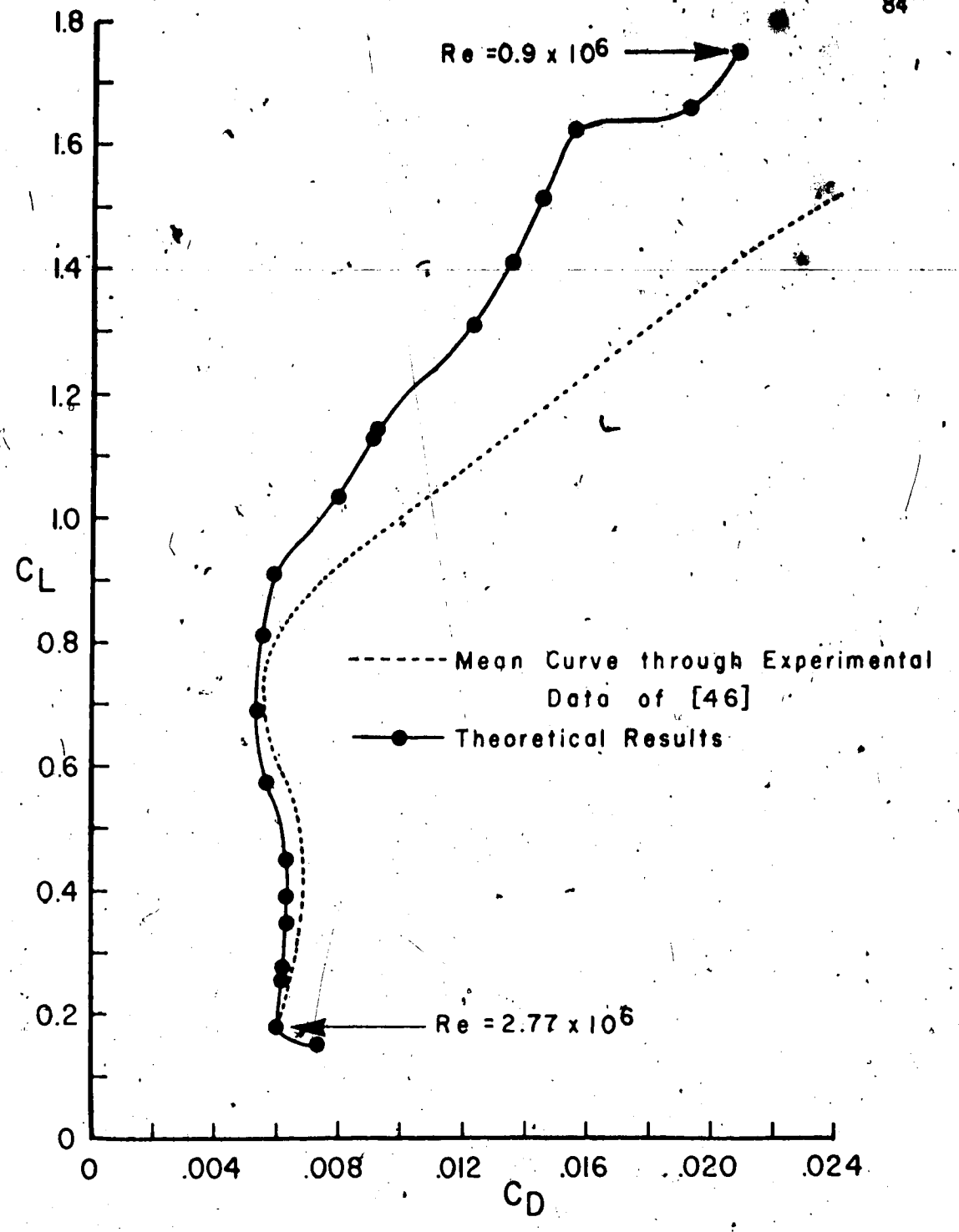

FIGURE 24 - PHOENIX WING, PROFILE DRAG POLAR

showing the two low drag regions found in the experiments. At higher lift coefficients the theoretical drag coefficient is up to 40% lower than the experimental results. The reason for this discrepancy can be seen in Figure 25.

Here the locations of laminar separation, transition and turbulent separation are shown. According to the experimental data, at lift coefficients greater than 1.2 separation occurs ahead of 90% of chord. At these lift coefficients the theoretical results predict separation at approximately 95% of chord. At higher angles at attack the theoretical results cannot be expected to yield accurate solutions due to the approximate modelling of the separated region.

The position of transition is predicted well by the viscous flow analysis. In general transition was brought about theoretically by short laminar separation bubbles. In the experiments only a small section of the upper surface, between lift coefficients of 0.17 and 0.6, is specifically mentioned as having a laminar separation bubble. The experimental results were obtained from boundary layer profiles taken at approximately 10% of chord intervals and from flow visualisations using tufts. Such methods could have detected the transition but perhaps not the short bubble which caused it.

Some details of boundary layer measurements at specific lift coefficients were also provided by Raspet and Gyorgyfalvy [46]. Comparisons between the theoretical and experimental results for two lift coefficients are provided in Figure 26. The measured values of momentum thickness agree well with the theory for all cases. The agreement for the shape factor H is good in the turbulent region but less satisfactory in the laminar region. The difficulties of measuring the

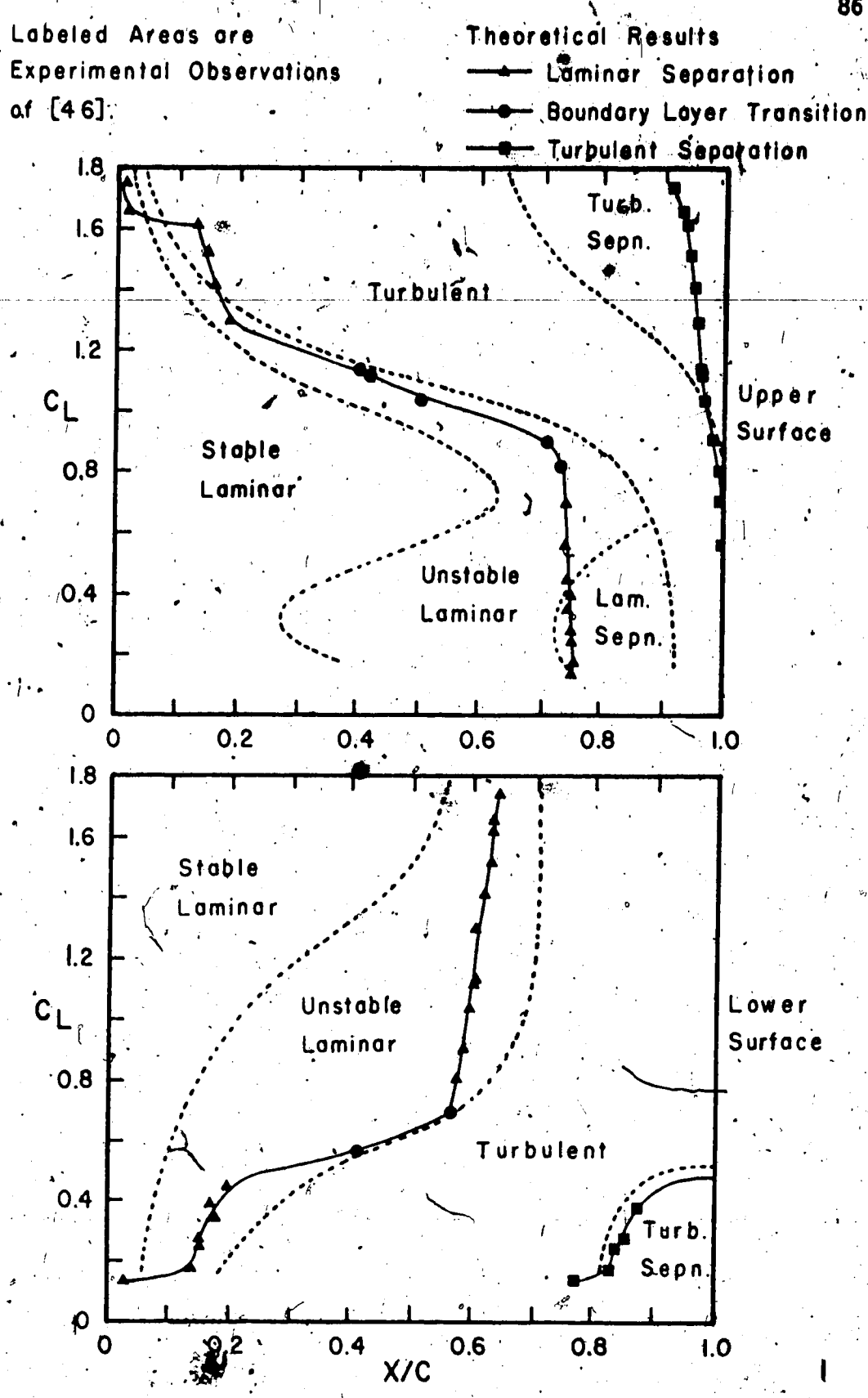

FIGURE 25 - PHOENIX WING, BOUNDARY LAYER DEVELOPMENT

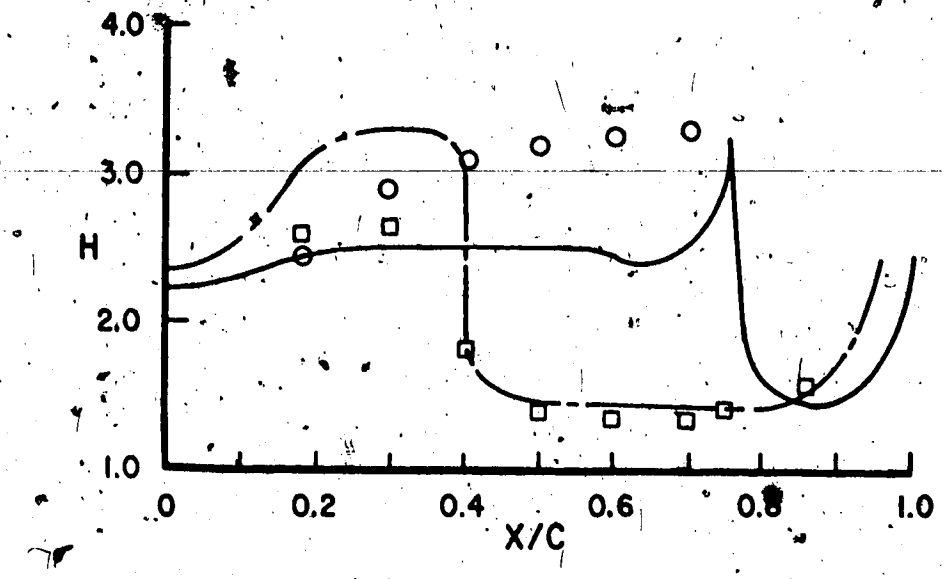

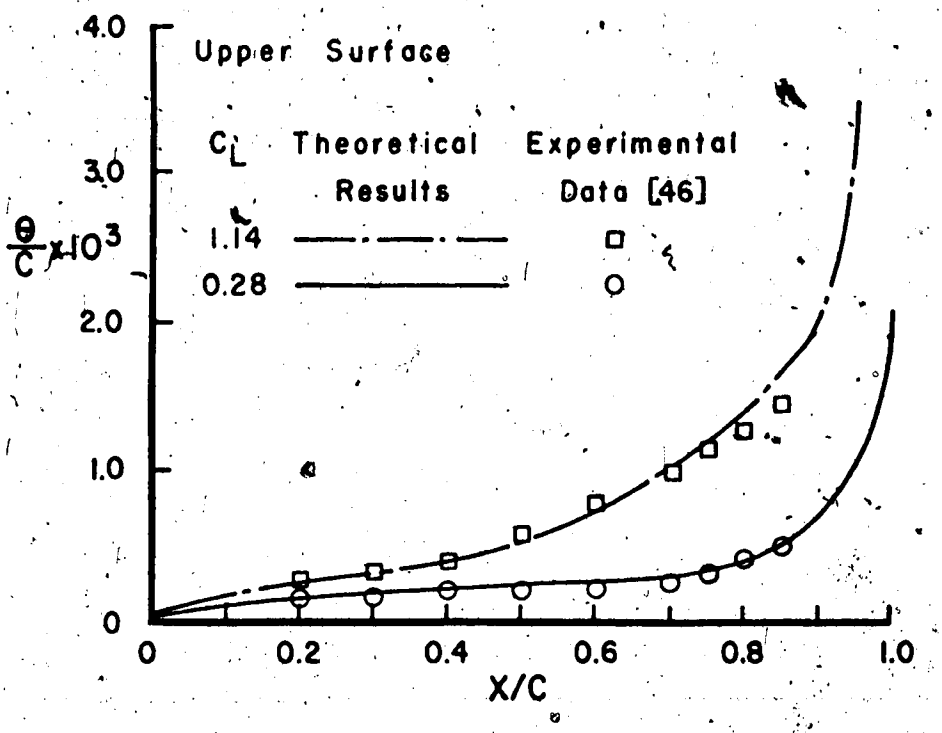

FIGURE 26 (a) - PHOENIX WING, BOUNDARY LAYER PARAMETERS

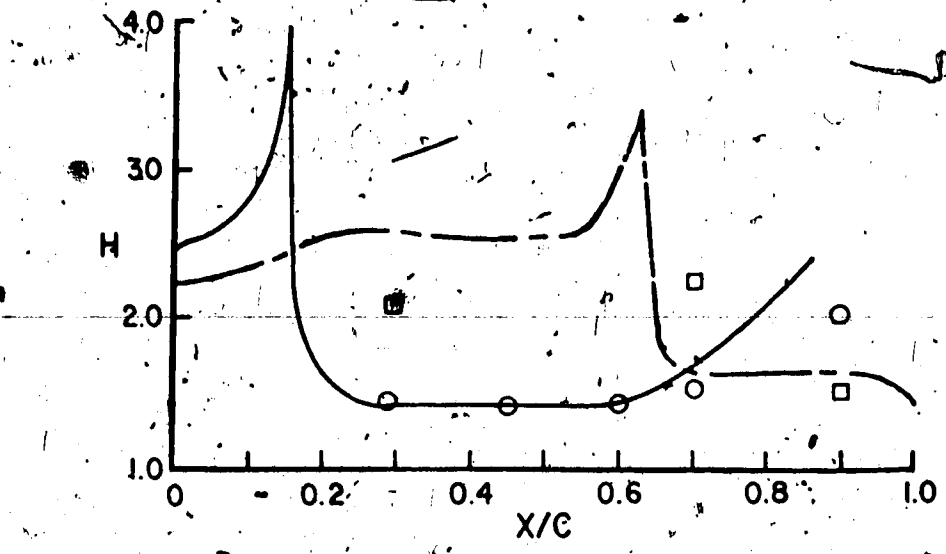

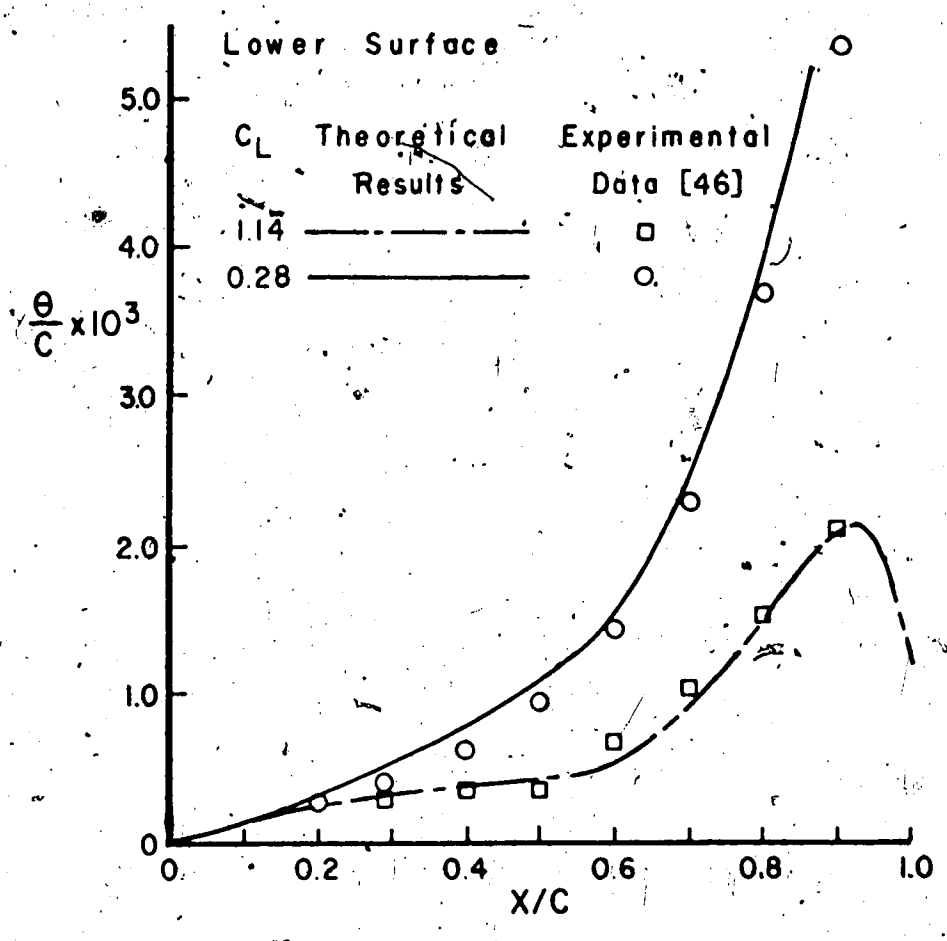

FIGURE 26 (b) - CONCLUDED

thin laminar boundary layers could cause large errors in determining H. This is supported by the fact that the experimental data on the upper surface at C_L = 0.28 shows values of H greater than 3. This is a region of favourable pressure gradient and by boundary layer theory, shape factors of greater than 2.6 would not be expected. In regions where δ^* ($=H\theta$) is large it has a correspondingly large effect on the equivalent airfoil section. The boundary layer calculations therefore provide the most accurate values when they are required the most.

The above case provided a detailed test of the boundary-layer calculations on a section at a given lift coefficient. However the data did not provide a test of the ability of the equivalent airfoil technique to correctly predict the lift coefficient at any given angle of attack. To test this the data obtained by Loftin and Smith [47] on some NACA airfoil sections was used. Comparisons between theoretical and experimental lift coefficients for a NACA 64_1 - 012 section at Reynolds numbers of 9×10^6 and 0.7×10^6 are given in Figure 27. The theoretical results shown are those for which turbulent separation is confined to the final 10% of chord.

The theoretical results agree well with the experimental values and show clearly the effects of the fluid viscosity on lift. The agreement is certainly better at the higher Reynolds number where the viscous effects are weaker. The thicker boundary layers which develop at lower Reynolds numbers cause larger viscous corrections. This affects the calculation method as the computations converged slower at the lower Reynolds numbers due to the larger changes which must be made to the equivalent airfoil section. Typically 4 iterations were required at the higher Reynolds number and 6 at the lower.

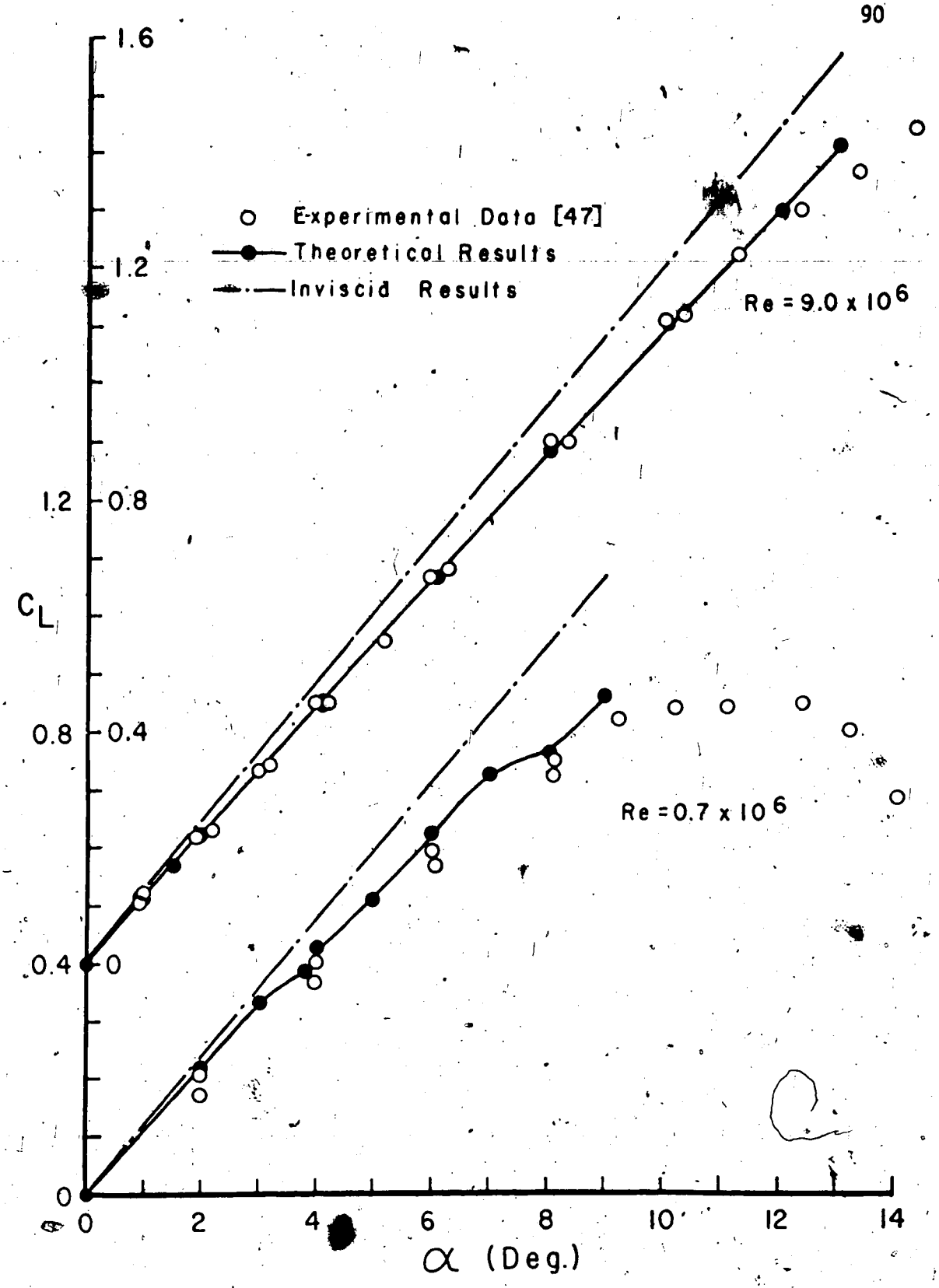

FIGURE 27 - NACA 64_1 -012 SECTION LIFT CHARACTERISTICS

Theoretical and experimental drag coefficients are compared in Figure 28. The agreement at the higher Reynolds number is remarkable as, at high lift coefficients, up to 10% of the section experienced turbulent separation. At the lower Reynolds number the drag is predicted well at the lower angles of attack. Also the position of the edge of the laminar bucket at a lift coefficient of 0.4 is predicted exactly. At this angle of attack the transition point moves from 46% to 3% of chord due to the formation of a laminar separation bubble at the leading edge. At higher angles of attack the drag prediction gets gradually worse. Clearly the formation of a leading edge bubble results in a turbulent boundary layer whose characteristics are not adequately modelled by this method.

Recently some experimental results on a model of an FX-61-163 airfoil section were obtained by Mr. G. Kiss in the University of Alberta low turbulence wind tunnel. In trying to duplicate these results using the given co-ordinates very poor results were obtained, and on measuring the co-ordinates of the section it was found that there were errors in the profile shape. Near the trailing edge the model was too thick and did not have the correct camber line. The model co-ordinates were therefore used in a viscous analysis and a comparison between the theoretical and experimental results is given in Figure 29.

Using the correct co-ordinates there is good agreement between lift coefficients up to the stalling angle. In general the theoretical drag coefficients are lower than those found experimentally. In this case agreement is poorest at low drag coefficients although the accuracy of the results is quite adequate.

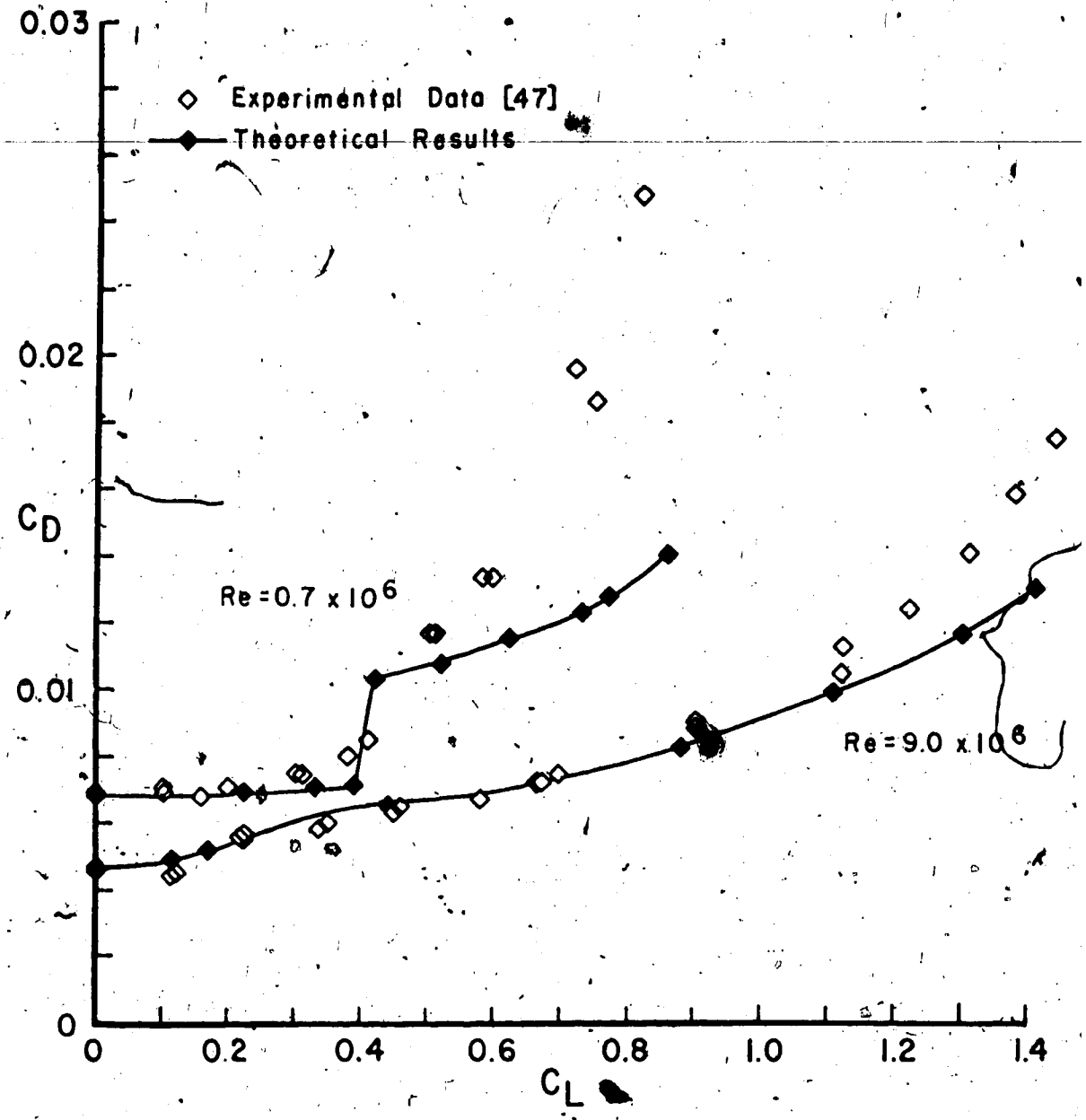

FIGURE 28 - NACA 64_1 -012 PROFILE DRAG POLAR

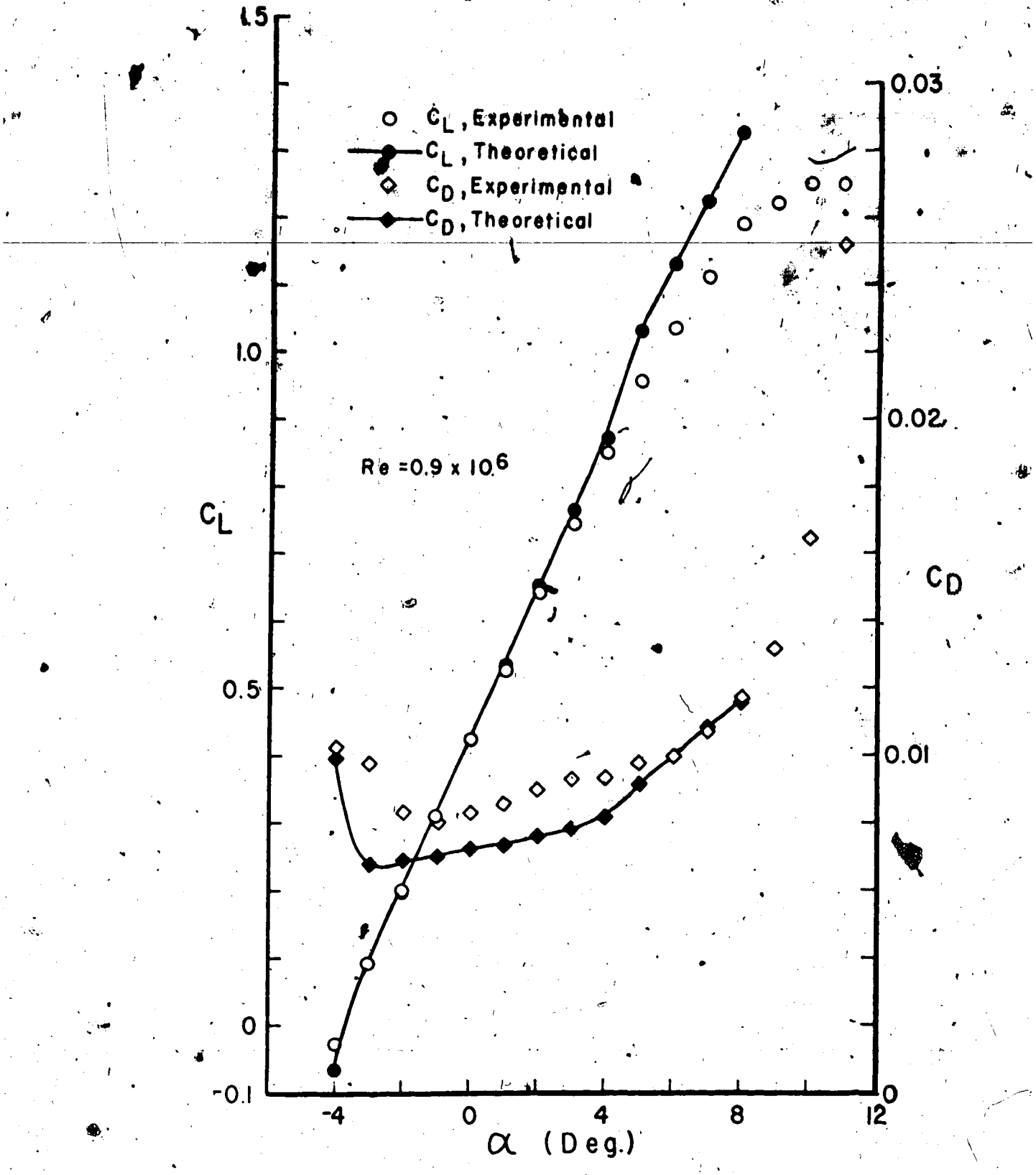

FIGURE 29 - FX-61-163 MODEL LIFT AND DRAG CHARACTERISTICS

The FX-61-163 section model exhibits laminar separation bubbles on both surfaces over most of its useful range at the test Reynolds number of 0.9×10^6. The bubbles are of varying length and their location is not fixed. This section therefore provides a good test of the laminar separation criterion. The location and lengths of these bubbles and the predicted location of laminar separation are presented in Figure 30. On the upper surface the predicted location of laminar separation is generally a short distance ahead of that found experimentally. The largest error in location was 10% of chord when the section angle of attack was 6^0. On the lower surface almost perfect agreement was found. No long bubbles were predicted and the experiments indicate that none were longer than 5% of chord. The influence of these bubbles on the pressure distribution is therefore expected to be small.

The calculations were terminated at 8^0 as further increases in angle of attack caused the turbulent separation point to move rapidly upstream. Turbulent separation is not easy to detect with the flow visualisation technique used. The results however indicate that the point of turbulent separation can be predicted, up to the stall, to within a few per cent of chord.

Presure distributions for this section were also taken and two theoretical and experimental distributions are given in Figure 31. These are for the 0^0 and 6^0 angle of attack cases. It is noticeable that, while there is in general good agreement, the differences between the theory and experiment are most pronounced on the upper surface near the laminar separation location. A possible explanation for this is that the laminar separation bubble could be affecting the pressure distribution in this area. As the displcement effects of bubbles are

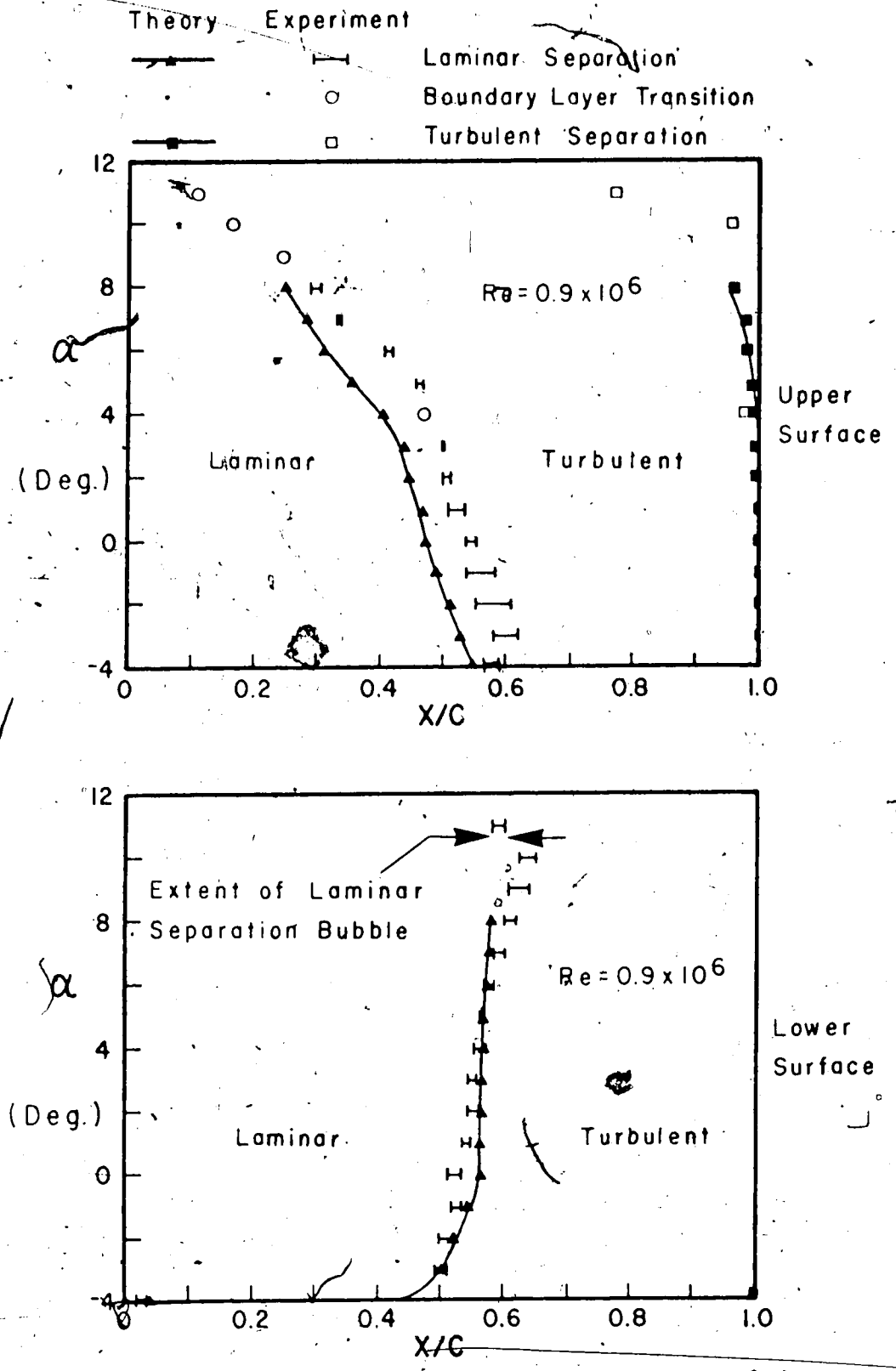

FIGURE 30 - FX-61-163 MODEL BOUNDARY LAYER DEVELOPMENT

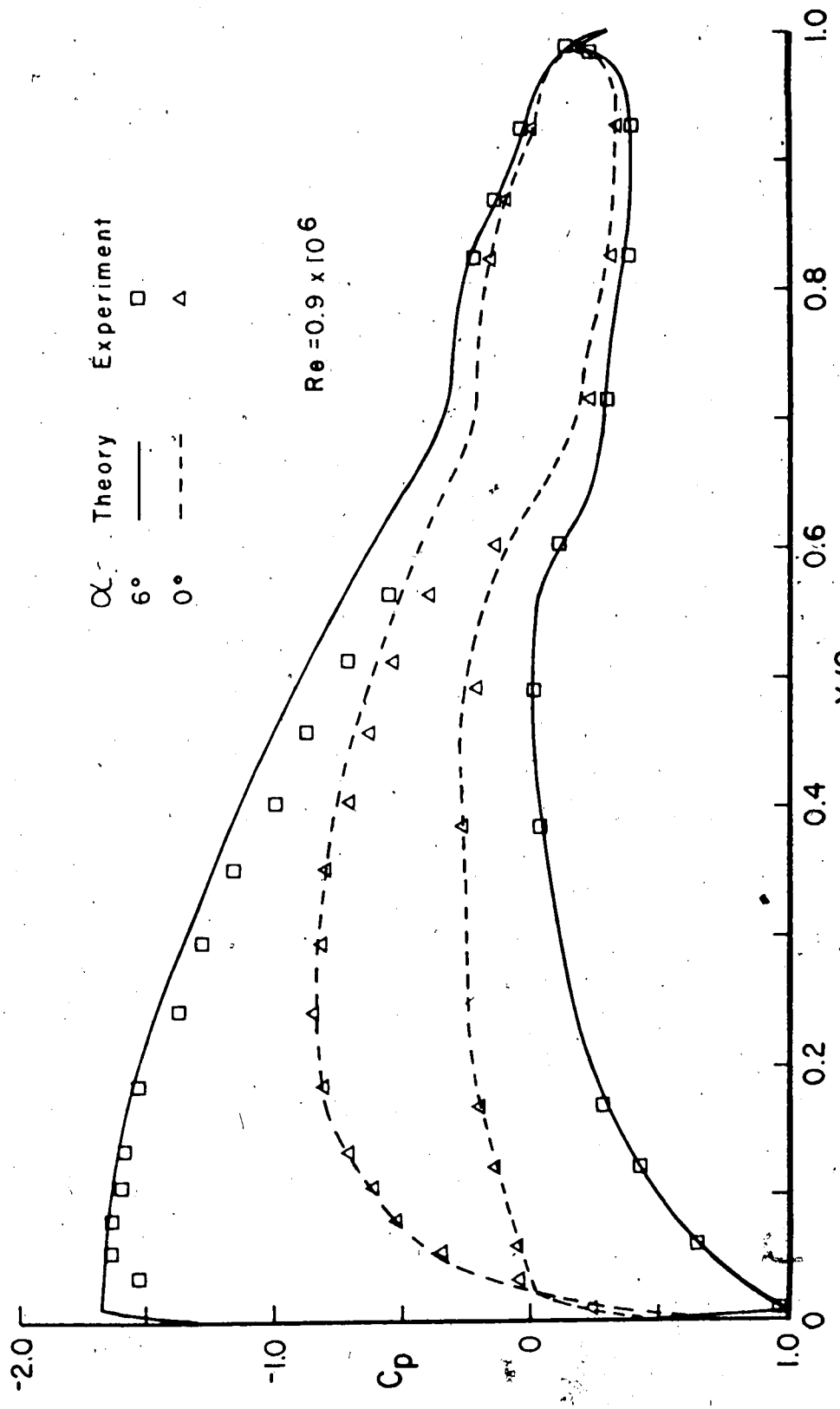

FIGURE 31 - FX-61-163 MODEL PRESSURE DISTRIBUTIONS

not known adequately this could not be modelled in the viscous flow analysis. Alternatively the model co-ordinates may not have been determined to an adequate accuracy. As the section was manufactured from two components, the shape of the model could be altered if these were not held firmly enough together. In either case the differences between the measured and theoretical pressure distributions are small.

4.5 Conclusion

The boundary layer analysis combing the laminar calculations of Eppler and the turbulent calculations of Felsch, Geropp and Walz agree well with experimental results for the cases tested. The locations of the points of transition, laminar separation and turbulent separation are adequately predicted by this method.

In applying the boundary layer results to the equivalent airfoil technique a method of viscous flow analysis was obtained. Using this, good agreement was achieved between theoretical results and experimental results on airfoil sections.

The theoretical results were found to be most reliable when less than 5% of the section showed turbulent separation. Beyond that point this equivalent airfoil technique is not valid. The results were found to agree best with experiments at high Reynolds number where the viscous effects are the smallest. While the drag coefficients could not be predicted as accurately as the lift coefficients, the accuracy is adequate for most airfoil analyses.

The viscous flow analysis can therefore be used to adequately predict the actual properties of an airfoil section in a real flow. Strictly one can only expect accurate prediction for airfoil sections of

the type tested and in the Reynolds number range tested. There must therefore always remain the possibility that airfoil sections of a radically different type may not give as accurate results as were observed in these test cases.

CHAPTER V

HIGH LIFT VELOCITY DISTRIBUTIONS

5.1 Introduction

It was demonstrated in Chapter III that an airfoil section can be designed when the surface velocity distribution about the section is given. This velocity distribution determines the aerodynamic characteristics of the section. Therefore, to obtain a section which posesses specific characteristics the aerodynamicist has to determine the surface velocity distribution which will produce them. Whole families of velocity distributions can be systematically examined to determine which one yields a desired property in an airfoil section. The resulting distribution can then be used in the design of an airfoil section.

One property which may be of use in several different situations is large rear loading of the section. In such sections the velocities on the upper surface are substantially higher than those on the lower surface near the trailing edge. A comparison between sections with and without rear loading can be made from Figure 13. There the designed section showed considerable rear loading while the basic section did not.

Designers of high lift airfoils have not fully considered the use of large rear loadings. This is not completely surprising as all previous surface singularity design methods apply the equal velocity, no load, Kutta condition. Consequently sections were designed to satisfy this no load condition. With the introduction of the trailing point Kutta condition the designer is able to investigate the design of sections with large rear loadings.

The application of rear loading to airfoil sections is of interest mainly in the generation of high lift sections. Another area of use is in the development of high speed sections where a more equitable loading of the section permits a reduction in the maximum velocity over the section. This allows such sections to travel faster than current sections before encountering the problems of compressible flow. The analytical tools developed here and the experimental equipment available however limit this investigation to incompressible flow problems. Hence the investigation of velocity distributions which produce high lift coefficients.

The optimization of the velocity distribution on a single component section for maximum lift coefficient was investigated by Liebeck and Ormsbee [1]. This work was later expanded to two components by Chen [3]. In both cases it was known that increasing the upper surface velocity at the trailing edge would result in higher lift coefficients. The design technique used by Ormsbee and Liebeck [1] forced them to use a velocity of approximately 0.9 U_∞ and did not permit rear loading on the section. Chen [3] used the value U_∞ for convenience and did achieve some rear loading. The advantages of rear loading were called into question by Liebeck [48] when his section performed well in experimental tests while Chen's section failed to yield its designed lift coefficint [49]. Chen [49] however blamed this failure on separation of the wind tunnel wall boundary layer at the junction with the model.

Wortmann [50] has designed high lift sections for which the potential flow shows some rear loading. He has also developed a method of controlling the point of transition on the section thus permitting the design of sections which operate well in practice. By combining this

with the optimum solutions for maximum lift and the design technique of Chapter III a practical method of designing high lift sections can be developed. The sections so designed can then be analyzed using the viscous flow analysis of Chapter IV.

Smith [51] has shown that there are great gains in lift available from multi- component sections. This is due largely to the large rear loadings developed on forward components as can be seen in Figure 10. However, as the viscous flow analysis is not capable of accurate prediction of the properties of multi-component sections only single component sections will be considered here.

5.2 Generation of Possible Distributions

The optimum velocity distributions developed by Liebeck and Ormsbee [1] and Chen [3] are of the same type. On the upper surface there is a region of constant high velocity, the rooftop. This is followed by the Stratford [43], zero skin friction, pressure recovery distribution to the trailing edge velocity. On the lower surface there is assumed to be stagnation pressure. The condition of the boundary layer at the start of the adverse pressure gradient plays a large part in determining the pressure recovery distribution as thin boundary layers can withstand larger pressure gradients than thick ones.

Stratford's turbulent separation criterion [43] was used by both Liebeck and Ormsbee [1] and Chen [3] to calculate the pressure recovery distribution. However when used in the analysis of Chapter IV this criterion predicted separation at values of the shape factor H between 1.7 and 1.8. It is therefore quite conservative, as Liebeck [48] discovered when a section exceeded its optimum lift coefficient. The

method of Stratford was also found to be awkward to use.

An alternative approach to determining the velocity distribution in the pressure recovery region has been given by Wortmann [52]. He assumes a velocity distribution of the form:

$$\frac{U}{U_{pr}} = \left[1 + \frac{\beta}{\theta_{pr}}(x-x_{pr})\right]^{-m} \qquad (40)$$

Wortmann [52] has provided the correlations for β and m in terms of the Reynolds numbers of the flow which will produce a boundary layer of some constant value of H. These correlations were developed before the advent of Felsch, Geropp and Walz's turbulent flow analysis. They must therefore be re-examined in the light of this advance in boundary layer theory. From tests applied with this boundary layer technique it was found that the exponent m is adequately given by Wortmann's relation:

$$m = 0.33 - \frac{0.074}{6\beta\ Re^{0.2}} \qquad (41)$$

However the values of β which provide specific values of the shape factor H were no longer applicable. To give values of H of approximately 1.8 required $\beta = 9.2 \times 10^{-3}$ at $Re = 10^6$ and $\beta = 8.0 \times 10^{-3}$ at $Re = 5 \times 10^6$.

This latter value allows a comparison to be made between optimum velocity distribution obtained using Wortmann's distribution and the results of Smith [51] using the Stratford distribution. The comparison, assuming a completely laminar rooftop, is shown in Figure 32. The results are almost identical and this explains the conservative results obtained from Stratfords method. The shape factor H of approximately 1.8 will not yield zero skin friction and hence is not the optimum. The results of Sandborn and Liu [44], and those from the

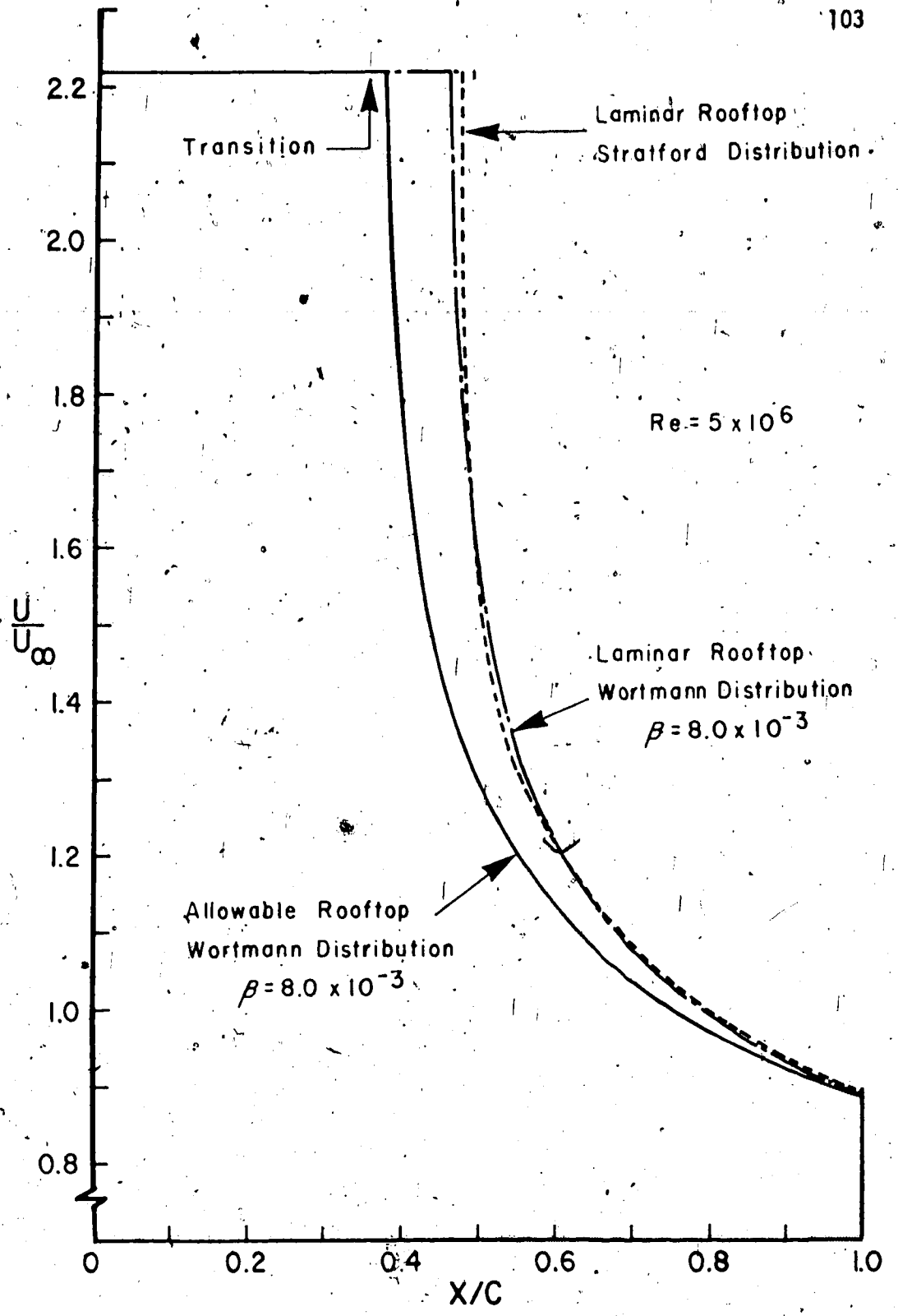

FIGURE 32 - COMPARISON OF THEORETICAL UPPER SURFACE VELOCITY DISTRIBUTIONS

boundary layer tests carried out in Chapter IV suggest that values of H up to 2.4 may be tolerable.

Because of the freedom of choice of H which Wortmann's method allows this method is to be preferred to Stratford's. This allows one to design pressure recovery regions with any desired factor of safety. A design value of 1.8 was chosen here as it provides a fairly large factor of safety.

Liebeck and Ormsbee [1], Chen [3] and Smith [51] all make the assumption that the rooftop is either completely turbulent or completely laminar with transition at the start of the pressure recovery region. The choice of fully turbulent flow leads to short rooftops due to the rapid growth of the boundary layer. The choice of the laminar flow rooftop gives longer rootops and higher lift coefficients but does not account for the very real possibility of transition prior to the pressure recovery region. This would lead to failure of the boundary to remain attached in the subsequent adverse pressure gradient. It is, however, not necessary to make this choice between extreme pessimism and extreme optimism if an adequate boundary layer analysis is available.

In the comparison in Figure 32 a completely laminar rooftop was assumed as in Smith's case. However this flow cannot be realised, according to the boundary layer calculations, as transition takes place at 35% of chord. The ensuing turbulent boundary layer results in rapidly increasing values of θ from this point downstream. The result of this is to increase the length required to make any specific pressure recovery. The allowable velocity distribution for this rooftop velocity is also plotted in Figure 32.. By comparison with the fully laminar rooftop case the possible case yields a lower lift coeficient.

The procedure adopted here in determining possible velocity distributions is to calculate the values of θ at locations along the chord assuming a 100% of chord rooftop distribution. This is done by the boundary layer calculation method of Chapter IV and includes the effects of transition. Using equation (40) the location of the Wortmann distribution which provides the specified pressure recovery, from rooftop to trailing edge, is easily determined. A design Reynolds number of 10^6 was taken and a value of β of 9.2×10^{-3}.

As Wortmann points out [50] the abrupt pressure rise at the start of the adverse pressure gradient could, if the boundary layer was laminar there, cause a long laminar separation bubble. Chen's airfoil section [49] shows this sharp discontinuity. Analysis of Chen's airfoil using the method of Chapter IV showed that at large angles of attack the turbulent boundary layer which began there immediately separated. This is thought to be the main reason for the failure of Chen's airfoil to produce its designed lift coefficient.

In the design of a practical airfoil section it is therefore necessary to introduce, as Wortmann did, an instability gradient between the rooftop and the turbulent pressure recovery region. The purpose of this gradient is to locate the transition point on the upper surface of the section. Transition could be made to occur due to the natural growth of instabilities or by the formation of short laminar separation bubbles. The latter was chosen here as test results show that the point of laminar separation can be predicted accurately by the boundary layer analysis.

From experience with short laminar separation bubbles at Reynolds numbers of approximately 10^6 it is clear that rarely are they

longer than 5% of chord. The instability region therefore was made to be 7% of chord long to provide some factor of safety. The velocity in this region decreased linearly from the rooftop value. The velocity gradient being that which produced laminar separation at about 2% of chord from the end of the rooftop. The gradient for this can be calculated approximately by using the laminar separation criterion of Curle and Skan [36]. The velocity distribution which results is not the optimum from the point of view of maximum lift coefficient but it does represent a more practical distribution.

From the designed velocity distribution the maximum possible lift coefficient can be calculated by integration assuming stagnation conditions on the lower surface. The minimum possible drag coefficient can be found by performing a boundary layer analysis on the upper surface velocity distribution. From these the maximum possible glide ratio and endurance ratio can be determined.

For each trailing edge velocity chosen there is a family of possible velocity distributions depending on the rooftop velocity chosen. Only one of these distributions is the optimum. For the case of a trailing edge velocity $U_{te} = 0.9\ U_\infty$ a family of possible distribution is given in Figure 33. As the rooftop velocity is increased the length of laminar flow decreases. The thinner boundary layers which then develop require steeper instability gradients to cause laminar separation.

The lift coefficients which were obtained from this family of distribution are plotted in Figure 34. The distribution which produces the maximum lift coefficient is obtained when the rooftop velocity is $1.866\ U_\infty$. There is however a fairly broad peak to the curve and increasing or decreasing the rooftop velocity by $0.1\ U_\infty$ causes less than a 1%

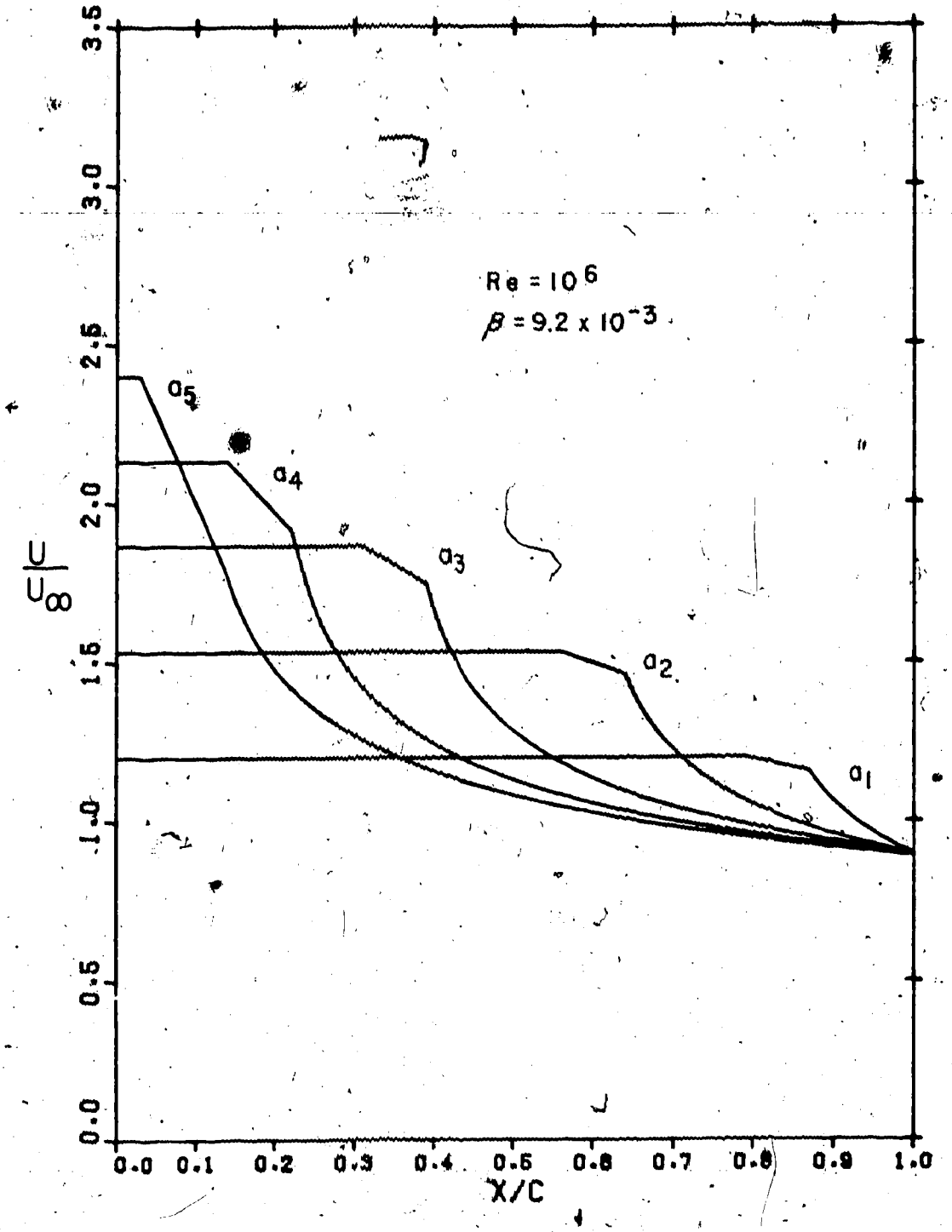

FIGURE 33 - POSSIBLE VELOCITY DISTRIBUTIONS, $U_{te} = 0.9U_{\infty}$

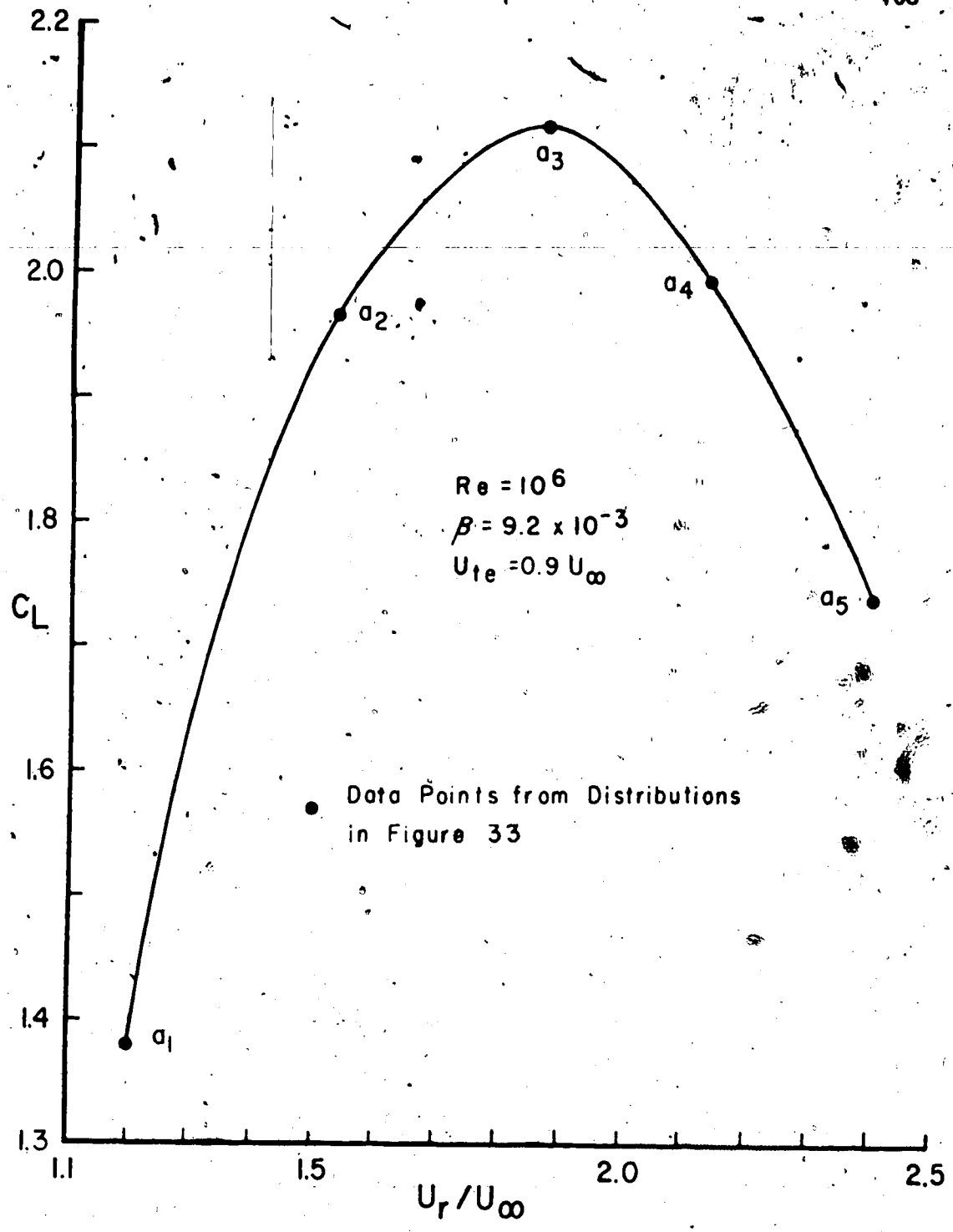

FIGURE 34 - LIFT COEFFICIENTS FROM A FAMILY OF POSSIBLE VELOCITY DISTRIBUTIONS

decrease in lift coefficient. The curve is typical of results obtained from analyzing cases with various trailing edge velocities.

The surface velocity distributions producing the maximum lift coefficients for various trailing edge velocities are plotted in Figure 35. In each case the optimum rooftop is approximately the same length and thus the distributions are approximately the same when plotted in the canonical form used by Smith [51]. The higher trailing edge velocities allow for higher rooftop velocities and consequently higher lift coefficients. The rooftop velocities and lift coefficients which are obtained from this analysis are presented in Figure 36. The rooftop velocity varies linearly with the trailing edge velocity while the lift coefficient curve rises even faster. This shows clearly that the effect of increasing the trailing edge velocity is to permit greatly increased lift coefficients. However these same higher trailing edge velocities do cause nonlinear increases in the drag coefficient.

5.3. Design of a High Lift Airfoil Section

The above calculated velocity distributions provide high lift coefficients in theory. However it is not known whether an airfoil section exists which can produce such velocity distributions. The high trailing edge velocities can be generated on an airfoil component by adding another properly designed component downstream of it. This has been demonstrated both theoretically and experimentally by Smith [51] who terms this the "dumping velocity" effect.

It is of interest to see if these high trailing edge velocities can also be achieved on a single component section. The design method of Chapter III was therefore applied with the requirements of the

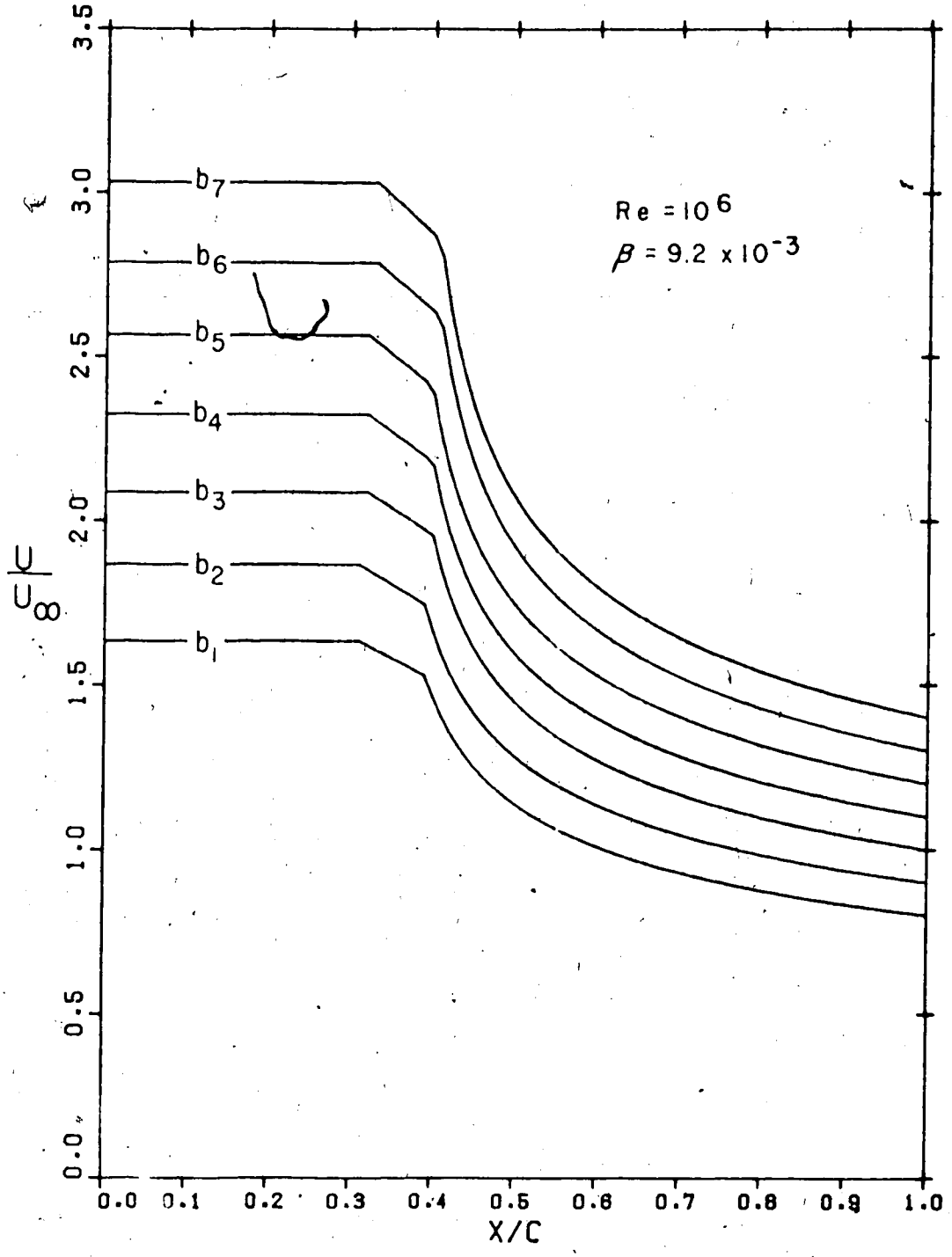

FIGURE 35 - SOME OPTIMUM VELOCITY DISTRIBUTIONS

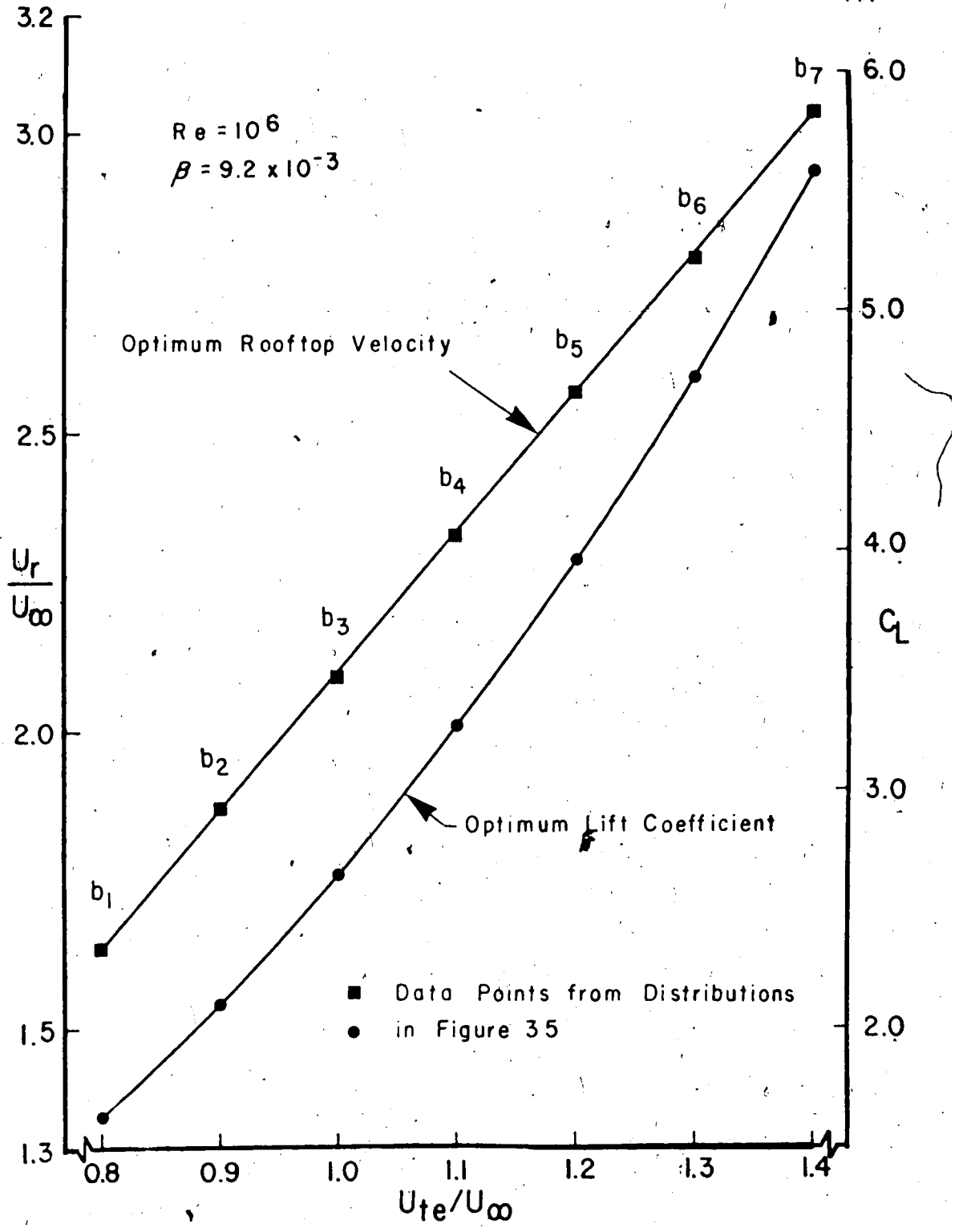

FIGURE 36 - EFFECTS OF VARYING TRAILING EDGE VELOCITY

optimum velocity distributions on the upper surface and no requirements on the lower surface. The basic section used was the Wortmann airfoil, FX-61-163, as this showed some rear loading in potential flow. It was also hoped that the favourable characteristics of the lower surface of this section would be transferred to the designed section.

The design process proved to be no easy thing and to accomplish it took more than one step. The freedom of the undersurface to alter its velocity distribution at each iteration results in a profile whose lower surface depends to a large extent on the design angle of attack. The only practical geometry of section was achieved when designed at a low angle of attack. This had the result that the designed section chord was inclined to the horizontal axis. This was overcome by rotating the designed section until its chord line was approximately horizontal. The design process was then completed using this as the basic section.

In designing the sections it was found that, for a trailing edge velocity of 1.2, the velocities near the trailing edge were sensitive to the number of surface elements used. There was however little difference between results using 80 and 100 surface elements. These results suggest that the potential flow method is approaching the limits of accuracy on such a section. This section was therefore considered in detail.

The designed section and its potential flow velocity distribution are shown in Figure 37 at an angle of attack of 15^{o}. The coordinates of the section are given in Table 2. The upper surface velocity distribution is almost indistinquishable from the design requirements except near the leading edge and instability gradient. There the

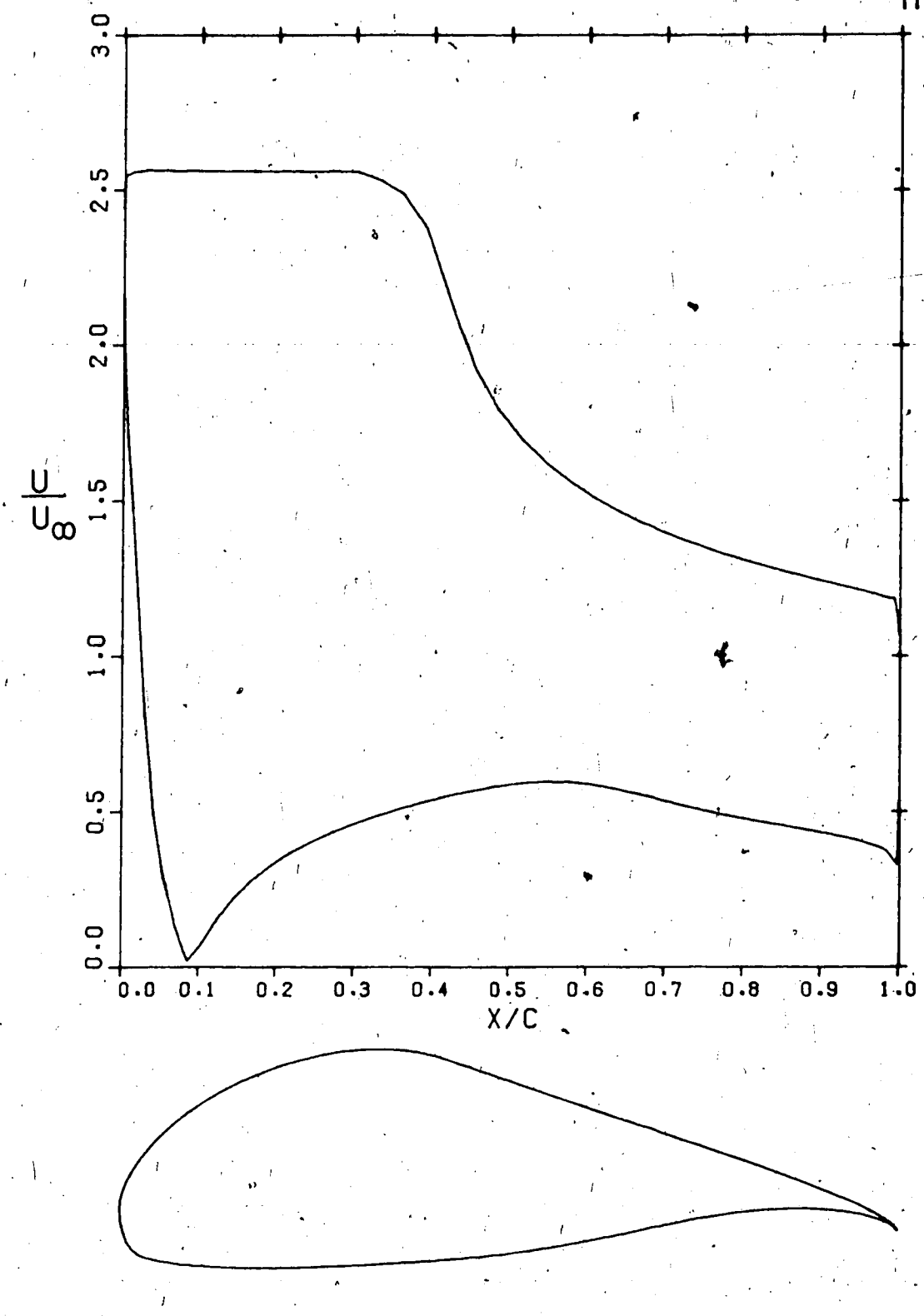

FIGURE 37 - DESIGNED SECTION AND POTENTIAL FLOW VELOCITY DISTRIBUTION

TABLE 2

COORDINATES OF DESIGNED SECTION

X	Y UPPER	Y LOWER	X	Y UPPER	Y LOWER
0.0	0.08916	0.08916	0.50000	0.25439	0.02949
0.00099	0.09922	0.07532	0.53140	0.24346	0.03352
0.00394	0.11173	0.06076	0.56267	0.23263	0.03825
0.00886	0.12433	0.04720	0.59369	0.22194	0.04367
0.01571	0.13737	0.03712	0.62434	0.21144	0.04970
0.02447	0.15090	0.03025	0.65451	0.20116	0.05608
0.03511	0.16463	0.02603	0.68406	0.19111	0.06249
0.04759	0.17843	0.02291	0.71289	0.18131	0.06856
0.06185	0.19214	0.02034	0.74088	0.17178	0.07400
0.07784	0.20561	0.01808	0.76791	0.16251	0.07862
0.09549	0.21869	0.01620	0.79389	0.15351	0.08232
0.11474	0.23123	0.01473	0.81871	0.14480	0.08508
0.13552	0.24311	0.01364	0.84227	0.13638	0.08691
0.15773	0.25417	0.01291	0.86448	0.12825	0.08785
0.18129	0.26427	0.01256	0.88526	0.12043	0.08793
0.20611	0.27328	0.01258	0.90451	0.11291	0.08721
0.23209	0.28102	0.01296	0.92216	0.10571	0.08580
0.25912	0.28732	0.01364	0.93815	0.09884	0.08380
0.28711	0.29195	0.01461	0.95241	0.09232	0.08125
0.31594	0.29456	0.01583	0.96489	0.08618	0.07824
0.34549	0.29468	0.01728	0.97553	0.08045	0.07491
0.37565	0.29216	0.01897	0.98429	0.07516	0.07145
0.40631	0.28575	0.02095	0.99114	0.07048	0.06807
0.43733	0.27595	0.02330	0.99606	0.06618	0.06477
0.46860	0.26530	0.02611	0.99901	0.06254	0.06211
0.50000	0.25439	0.02949	1.00000	0.05992	0.05992

discontinuities in slope are smoothed out. There is also a sharp drop in velocity in the viscinity of the trailing edge which will cause separation of the boundary layer there. Such velocity drops occur on most sections when examined in this detail and it is not thought to be a practical problem in the real flow. The high velocities on the upper surface force the lower surface velocities to unusually low values thus giving the large rear loading that was desired. Stagnation pressure cannot be obtained over the length of the lower surface as the optimum condition required. The general form of the lower surface velocity distribution owes much to the FX-61-163 basic section used in the design process. Other basic sections would have produced different distributions. Although there is the possibility that these could give greater lift coefficients, the possible gains are small.

The designed section was fully tested with the viscous flow analysis method of Chapter IV to determine how it would perform in a real flow. At the design condition of 15^{o} angle of attack and a Reynolds number of 10^{6} the lift coefficient was 3.72 and the drag coefficient was 0.028. The upper surface velocity distribution showed a short laminar separation bubble at 35% of chord. The subsequent turbulent boundary layer had a value of H of 1.84 over most of its length. However in the last 10% of chord H rose rapidly and the turbulent boundary layer was predicted to separate at 99.5% of chord. On the lower surface the boundary layer experienced laminar separation at 63.5% of chord and turbulent separation at 98% of chord.

As the angle of attack was lowered from the design value the point of laminar separation remained fairly constant and the turbulent boundary layer shape factor, H, gradually decreased. Little change was

observed on the lower surface down to 3^{o}.

Tests were carried out at various Reynolds numbers at the design angle of attack. Results showed that while the point of laminar separation remained fairly constant the shape factor in the turbulent layer decreased rapidly with Reynolds number. At Reynolds numbers greater than 10^{6} the section appeared to be even farther from the stall. At lower Reynolds numbers the point of turbulent separation moved upstream from the trailing edge. At a Reynolds number of 0.5×10^{6} the calculations predicted turbulent separation at 98.5% of chord.

The present viscous flow analysis therefore suggests that the designed section will perform adequately at the design condition. There also appear to be no formidable barriers to overcome to reach this condition either in increasing the angle of attack or in increasing the Reynolds number.

CHAPTER VI

EXPERIMENTAL TESTS

6.1 The Airfoil Section

A model of the section designed in Chapter V was built for testing in the University of Alberta low turbulence wind tunnel. The model chord was chosen as 1 metre as this allows for a Reynolds number of 2×10^6 in the tunnel. Also such a large model makes accurate construction of the section possible.

The model was constructed from a series of sheets of "Styrofoam S.M." insulating material bonded together. The section profile was cut out using a heated wire. Grooves were cut in the surface of the section for the plastic tubing used to connect the pressure taps to the pressure transducer. The skin of the section, 0.020 inch thick Aluminium sheet, was wrapped around the foam section and bonded to it. The skin was kept in place and under uniform pressure by enclosing the wing in a plastic bag which was evacuated using an industrial vacuum cleaner. This process resulted in some crushing of the foam giving a non uniform profile across the span of the model.

Hollows in the section were filled with a body filler until the profile at the centre span conformed closely to accurate templates. The final wing model had a constant section over the centre 50% of span, the outer areas of non-uniformity being faired in as best as possible. The non-uniformity amounted to less than 3 mm at any chordal position. This was thought to be aceptable to produce two dimensional flow in the central section.

The static pressure taps were located on the mid-span line.

They were manufactured by drilling through the skin and pulling the 1/16 inch diameter plastic tubing through the skin. These tubes were cemented in place and sheared off flush with the airfoil surface.

After construction the co-ordinates of the section at the mid-span location were measured. This was accomplished using vernier height gauges and a surface table. It is estimated that the measurements were accurate to 0.1 mm. The measured co-ordinates are given in Table 3. The measurements show that the upper surface of the model was never more than 0.5 mm from the desired section. The lower surface showed deviations of up to 3 mm near the leading edge and up to 2 mm near the trailing edge.

The actual profile was then analyzed in both potential and viscous flow. The pressure distribution at the design angle of attack of 15^{o} in potential flow is given in Figure 38. Also given there is the desired pressure distribution from the optimisation in Chapter V. The upper surface pressure distribution is very close to that desired with the rooftop pressure coefficient exhibiting some fluctuations. Considering the accuracy to which the model was manufactured this demonstrates how sensitive this area is to geometric variations. In the adverse pressure gradient region there is good agreement and no fluctuations in the pressures except aft of 98% of chord where there is a drop in pressure coefficient followed by a rise towards the trailing edge.

Employing the viscous flow technique of Chapter IV gave little alteration to the potential flow pressure distribution shown in Figure 38. The boundary layers on both surfaces were calculated to be thick near the section trailing edge. On the upper surface the displacement thickness is approximately 15 mm and on the lower surface it is 8 mm at

TABLE 3

MEASURED COORDINATES OF MODEL

X	Y UPPER	Y LOWER	X	Y UPPER	Y LOWER
0.0	0.0873	0.0873	0.5000	0.2549	0.0297
0.0010	0.0977	0.0731	0.5314	0.2439	0.0338
0.0039	0.1107	0.0596	0.5627	0.2329	0.0388
0.0089	0.1250	0.0470	0.5937	0.2219	0.0440
0.0157	0.1379	0.0375	0.6243	0.2112	0.0497
0.0245	0.1519	0.0293	0.6545	0.2010	0.0556
0.0351	0.1654	0.0238	0.6841	0.1908	0.0621
0.0476	0.1793	0.0200	0.7129	0.1809	0.0682
0.0619	0.1924	0.0173	0.7409	0.1715	0.0738
0.0778	0.2060	0.0155	0.7679	0.1621	0.0780
0.0955	0.2188	0.0143	0.7939	0.1529	0.0816
0.1147	0.2312	0.0132	0.8187	0.1444	0.0845
0.1355	0.2427	0.0123	0.8423	0.1360	0.0864
0.1577	0.2539	0.0119	0.8645	0.1280	0.0871
0.1813	0.2638	0.0119	0.8853	0.1199	0.0871
0.2061	0.2733	0.0122	0.9045	0.1126	0.0865
0.2321	0.2807	0.0129	0.9222	0.1050	0.0850
0.2591	0.2867	0.0137	0.9381	0.0985	0.0826
0.2871	0.2915	0.0146	0.9524	0.0919	0.0800
0.3159	0.2943	0.0158	0.9649	0.0861	0.0774
0.3455	0.2945	0.0173	0.9755	0.0802	0.0741
0.3756	0.2919	0.0191	0.9843	0.0752	0.0702
0.4063	0.2855	0.0210	0.9911	0.0703	0.0669
0.4373	0.2764	0.0234	0.9961	0.0654	0.0634
0.4686	0.2660	0.0263	0.9990	0.0615	0.0603
0.5000	0.2549	0.0297	1.0000	0.0594	0.0594

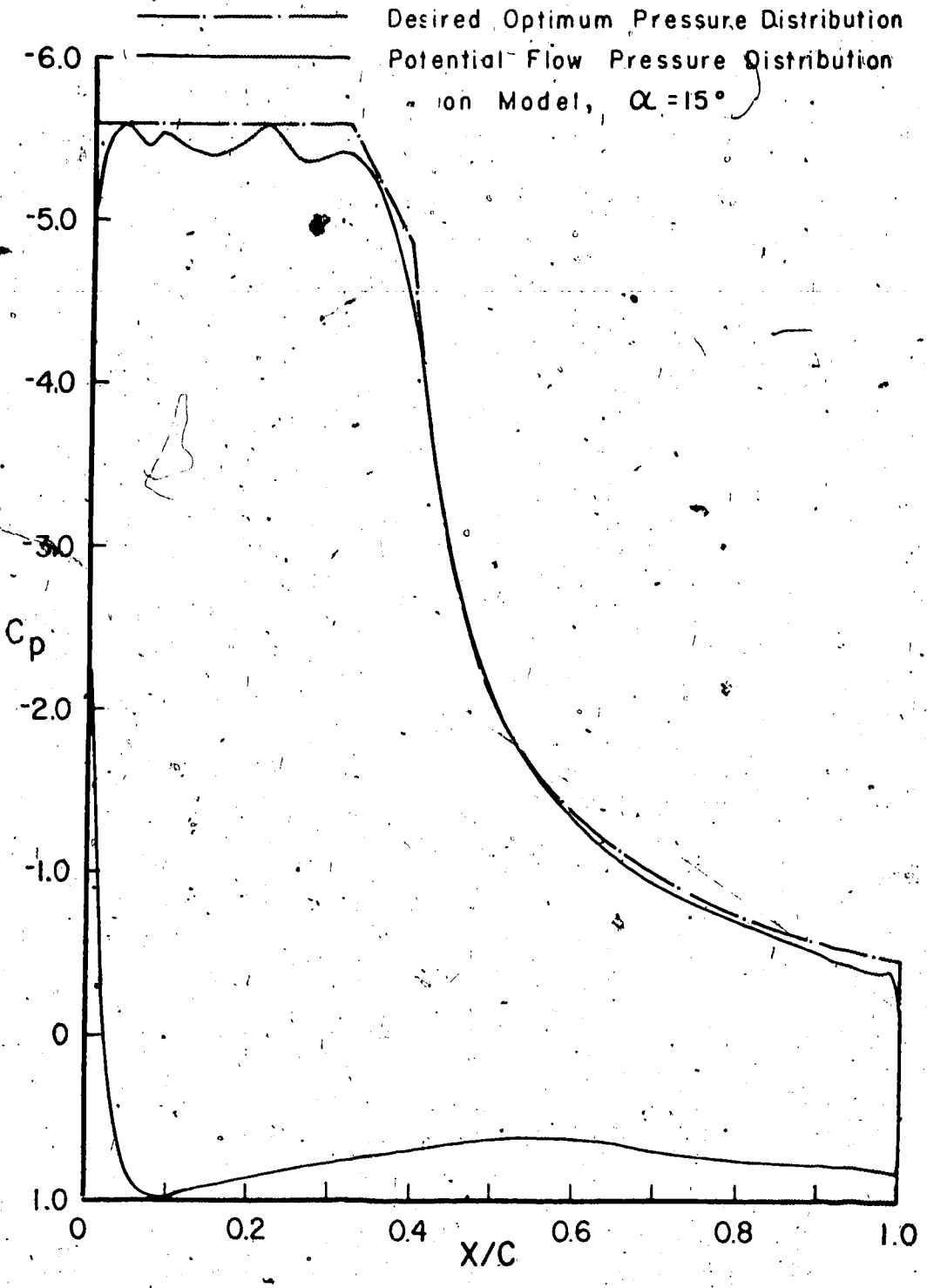

FIGURE 38 - POTENTIAL FLOW PRESSURE DISTRIBUTION ON MODEL SECTION

98% of chord. After this point the upper surface experiences a favourable pressure gradient and then separates in the subsequent adverse gradient. The viscous analysis converged on a solution with a lift coefficient of 3.71, a drag coefficient of 0.0284 and a pitching moment coefficient of 0.411. The prediction of turbulent separation near the trailing edge of the section was not thought to be a problem. The separated area is very small and the pressure fluctuations which cause it may be smoothed out by the thick boundary layer there.

6.2 The Wind Tunnel and Instrumentation

The University of Alberta low turbulence wind tunnel test section is 2.44 m broad and 1.18 m high. The model was mounted vertically on the tunnel centreline as shown in Figure 39. The model was held between circular end plates which permit it to be rotated to any desired angle of attack. The end plates have boundary layer control suction holes in them. These are a series of 1/8 inch diameter holes drilled through the end plates at 1/4 inch intervals at the junction of the model and the end plates. This is only necessary in areas where adverse pressure gradients will be encountered on the model. The purpose of the holes is to remove parts of the boundary layer which builds up on the floor and ceiling of the tunnel. If this was not done these thick boundary layers may separate under the influence of the large adverse pressure gradients generated by the wing sections. This would result in large disturbances to the flow field which would interfere with the two-dimensional nature of the flow. The other side of the suction holes are connected via plenum chambers to a large air suction pump. The pressure in the chambers was approximately 0.6 p.s.i. below atmospheric.

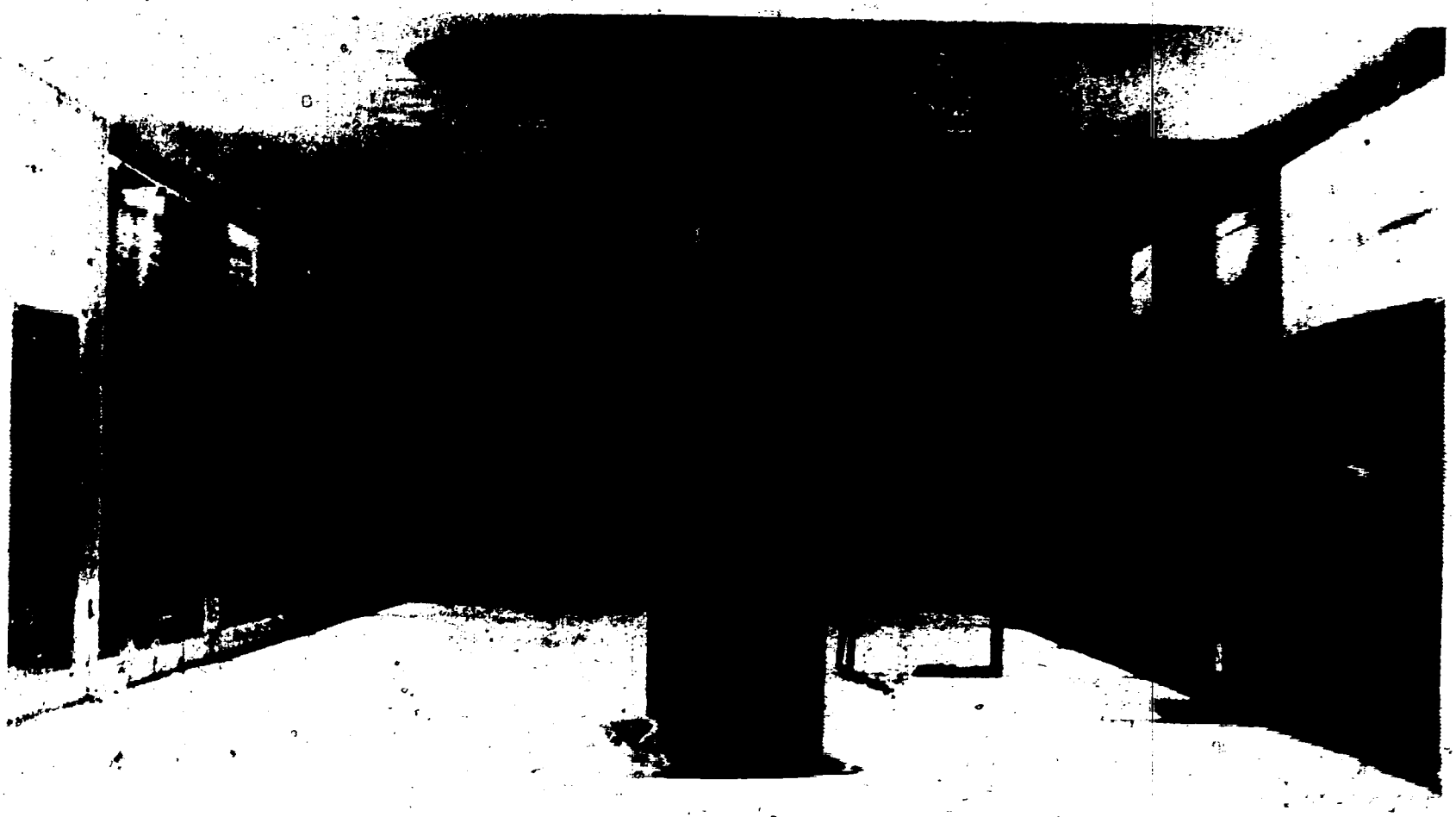

FIGURE 39 - MODEL MOUNTED IN WIND TUNNEL

The tunnel airspeed was measured by a pressure transducer connected to a total pressure tap and a test section static pressure tap. The static pressure tap is located 1.5m upstream of the model where it will not be affected by the presence of the model. The lift coefficient and pitching moment coefficient can be calculated from the static pressures on the airfoil section. The static pressures at every tap on the section were measured sequentially around the airfoil. Each tap was connected in turn, via a "Scanivalve" switching unit, to a pressure transducer. The drag coefficient of the section can be calculated from the loss of total pressure in the wake. A pitot tube on a traversing mechanism was therefore used in the model wake. The difference between total pressure inside and outside the wake was measured on a pressure transducer. The distance travelled being measured on a potentiometer connected to the traversing mechanism.

All readings from the pressure transducers were fed to a data acquisition system which was able to process the results to some extent. Using this system the Reynolds number could be monitored and the sensitivity of the wind tunnel controls permitted the Reynolds numbers to be held constant to within 2%. The measured section static pressures were converted to pressure coefficient form and integrated by the trapezoidal rule over the length and thickness of the section. This provided both the lift and pitching moment coefficients. The results from the wake survey were also integrated by the trapezoidal rule to provide the drag coefficient. When taking the wake traverse the transducer output was plotted continuously. This allowed the experimenter to adjust the traverse speed to suit the wake being measured.

The pressure transducers were calibrated to determine their sensitivity before and after the tests. An accurate inclined tube manometer was used for this purpose. The maximum change in sensitivity was less than 0.' . As part of each experimental run the zeros of the pressure transducers were determined. This minimised the possibility of the results being affected by drift in the transducers.

6.3 Wind Tunnel Corrections

Because the tunnel walls affect the flow over the section all data must be corrected to give the results which would be expected had the tests been performed in free air. The wind tunnel wall corrections are a function of both the geometry of the test set up and of the uncorrected coefficients. The standard corrections have been developed over the years on a semi-empirical basis, and are well documented in Garner [53] and Pope and Harper [54].

The first correction applied is that for blockage. The model and its wake occupy a certain volume in the wind tunnel and the air must flow around this while being constrained by the tunnel walls. The resulting distortion in the streamline pattern from the free air pattern causes an increase in the local fluid velocities. This is accounted for by assuming that the effective airspeed at the model is faster than the measured velocity, U_∞, by an amount $U_\infty \varepsilon_b$. As the dynamic head, q, is correspondingly increased, all pressure coefficients are reduced from their uncorrected values.

The blockage correction has two components, that due to the solid wing and that due to the wake. For a 27.7% thick section, which is the model thickness, Pope and Harper [54] give a body shape factor of 0.5. Using the formula of Garner [53] this gives a solid blocking

factor of 0.016. The wake blockage depends on the drag coefficient and was calculated from Garner's formula to be 0.102 C_D. The total blockage is the sum of these two components,

$$\epsilon_b = 0.016 + 0.102\ C_D. \tag{42}$$

No adjustment was made to these values to account for the amount of air removed from the tunnel by the end plate boundary layer suction. Such an adjustment would reduce the corrections.

The second correction applied is for streamline curvature. A model which produces lift causes curvature in the streamlines of the flow about it. The presence of the tunnel walls interferes with the natural curvature expected in free air. The nature of these corrections is examined by comparing the theoretical solutions for the free air and tunnel wall boundary conditions. The potential flow analysis technique of Chapter II could be extended to handle this case. However considerable work would have to be done to accomplish these changes. The generalized corrections given by Garner [53] were therefore used.

The corrections depend on the ratio of airfoil chord to the tunnel width, as the model is mounted vertically, and the uncorrected coefficients. The presence of the walls induces an upwash at the mid-chord point. This gives an effective angle of attack increase, $\Delta\alpha$, at that point. The natural curvature of the free stream is straightened by the tunnel walls which makes the model appear more highly cambered relative to the straightened flow. This results in a distortion of the pressure distribution and consequently corrections must be applied to the lift and pitching moment coefficients. The corrections which must be added to the uncorrected values are given by Garner [53]. For this

model they can be written as:

$$\Delta\alpha = 0.3\ (C_L + 4\ C_{MQ}),$$

$$\Delta C_L = -\ 0.026\ C_L\ , \qquad (43)$$

$$\Delta C_{MQ} = 0.0067\ C_L\ .$$

No such corrections are applied to the drag coefficients as this is essentially an inviscid correction.

The streamline curvature corrections are necessary because the measured pressure distribution would not be observed in a free air test. At the corrected angle of attack in free air the pressure distribution would be such as to produce a reduced lift coefficient. This calls into question the assumption that the corrected maximum lift coefficient is the maximum lift coefficient obtainable from the section in free air. It is the characteristics of the pressure distribution which determine the point of maximum lift. The effectively higher camber of the wind tunnel test will introduce lower peak pressures and higher adverse pressure gradients than the free air condition. A free air test model would presumably not stall until approximately the same peak pressures and pressure gradients occurred on its surface. At such a point the two maximum lift coefficients would be approximately the same. The only way to check this theory is to carry out free air tests on the section. Until that time the conservative approach of assuming that the corrections apply to the maximum lift coefficient is used.

6.4 Experimental Results

Tests were carried out on the model at Reynolds numbers, based on the model chord, of 10^6, 1.5×10^6 and 2×10^6. These Reynolds numbers were maintained to within ± 2% by monitoring the tunnel temperature and freestream velocity. Measurements of lift and pitching moment coefficients were taken at every $\frac{1}{2}^o$ interval of angle of attack. Wake traverses for the drag coefficient measurements were taken at each degree interval of angle of attack. Except for a few readings at 2×10^6 Reynolds number at least two sets of readings were taken at each condition to test the repeatability of the results. This is particularly necessary at low Reynolds numbers where the pressure differences across the pressure transducers are small.

Drag traverses at all Reynolds numbers were taken at a location 0.5 m downstream of the trailing edge. As the stalling angle was approached the wakes became unsteady and grew wider than the 0.17 m that the traverse mechanism could span. For this reason drag values are not available up to the stalling angle. In order to estimate the effect of possible static pressure variations in the wake the apparatus was moved to 1.3 m downstream of the trailing edge. At this distance downstream the wake required two separate traverses to cover its width. Results at this station differed by less than 5% from those at the original station.

Downstream static pressure variations and those across the wake can cause errors in the measured drag coefficients depending on the calculation method used. In evaluating the drag the accurate formula of Jones [55] accounts for any static pressure variations which may occur.

The drag coefficient is calculated from the formula:

$$C_D = \frac{4}{\rho U_\infty^2} \int_w (P_{tw} - P_w)^{\frac{1}{2}} \left[(P_o - P_\infty)^{\frac{1}{2}} - (P_{tw} - P_\infty)^{\frac{1}{2}} \right] dy \quad (44)$$

This equation was used in this case with the modification that $P_w = P_\infty$, i.e. the static pressure in the wake is the freestream static pressure. The error in this assumption will arise from both downstream and cross-stream pressure gradients. These will depend on the model test configuration and no uniform correction can be applied to the data.

The corrections will be largest at the maximum drag conditions and at these conditions static pressure measurements were made across the wake at the traverse section. The maximum value of $P_w - P_\infty$ in the wake was 0.08q. The minimum value of $P_{tw} - P_\infty$ was approximately 0.75q. The maximum possible error due to static pressure variations will be:

$$\left[1 + \frac{P_\infty - P_w}{P_{tw} - P_\infty} \right]^{\frac{1}{2}} - 1$$

or approximately 5%. This is a tolerable error considering the errors due to the unsteady nature of the flow and the numerical integration technique.

Measured pressure distributions around the model are presented in Figure 40 for angles of attack of 4.2^o, 8.3^o, 12.4^o and 16.0^o at a Reynolds number of 10^6. Two sets of data are presented for each data point showing that the repeatability is better than 0.1 for C_p except in regions of very high pressure gradient. As the angle of attack is increased the largest changes in pressure coefficient occur near the leading edge. The lower surface pressures gradually increase while the

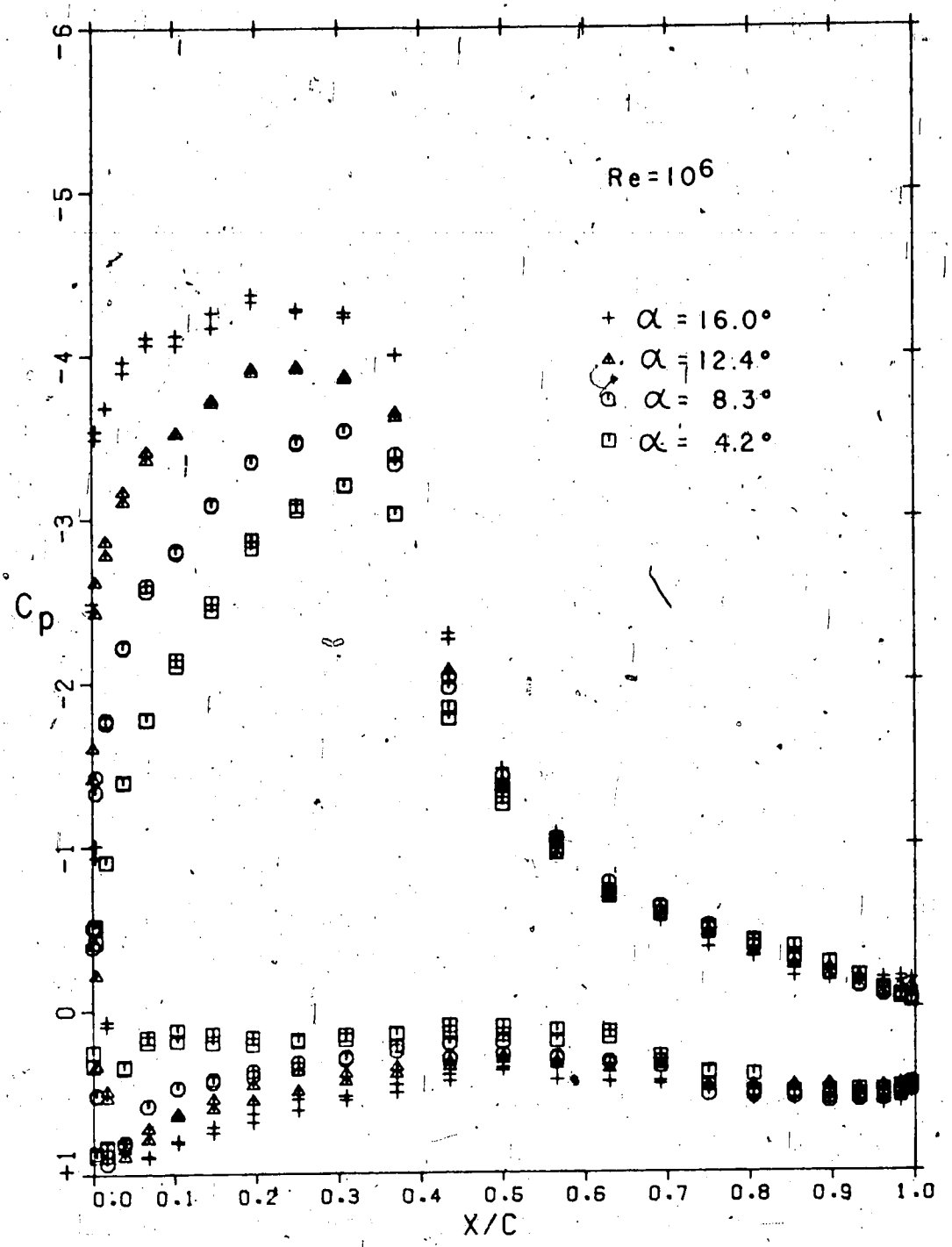

FIGURE 40 - EXPERIMENTAL PRESSURE DISTRIBUTIONS

upper surface pressures rapidly decrease. At 16^{o}, the angle of attack for maximum lift, the distribution approaches a rooftop distribution over the first 30% of chord. Downstream of mid-chord there is little variation in pressure distribution with angle of attack. However, at 16^{o} the pressure coefficients over the last 10% of chord are, to within experimental accuracy, constant. This is generally taken as an indication of a region of separated flow and any further increase in angle of attack led to complete breakdown of the flow.

The variations on the lower surface are characterised by a rearward movement of the stagnation point and a general increase in pressure coefficient as the angle of attack is increased. Over the rear 20% of the section the pressure coefficients change by less than 0.1. There is therefore almost constant loading near the trailing edge at these angles of attack. The loading at 99.6% of chord is, for each case, greater than 0.5q. On the upper surface the trailing edge velocity, U_{te}, lies between 1.02 U_{∞} and 1.08 U_{∞} whereas the design requirement was 1.2 U_{∞}. Although considerable rear loading was achieved the designed amount was not reached.

The angle of attack of 16^{o} gave the maximum lift coefficient at this Reynolds number. A comparison between the pressure distribution in this case and the calculated potential flow results of Figure 38 show that the design lift coefficient was not achieved. The largest discrepancy between theory and experiment is in the rooftop region where the measured pressure coefficients are approximately -4.25 compared to the theoretical value of approximately -5.5. The agreement improves towards the trailing edge where the error in pressure coefficient prediction is approximately 0.3. This applies to both upper and lower surfaces in this

location. The stagnation point in the experiment was located at 5% of chord at this angle while the theoretical location is at 8.5% of chord.

These differences between theory and experiment are consistent with a decrease in circulation about the section relative to the theoretical value. This is due to viscous effects and should have been predicted by the viscous flow analysis.

A series of flow visualisation experiments were therefore conducted on the model to determine the cause of this strong viscous interaction. By painting the airfoil surface with a mixture of solvent and Kaolin and running the wind tunnel at the desired condition several inferences can be made about the boundary layer flow. A photograph of the flow visualisation on the upper surface at the maximum lift condition is shown in Figure 41. The dark area in the first 30% of chord is a region of laminar flow where the surface coating remains fairly wet. Between 30% and 32% of chord the boundary layer undergoes transition to turbulent flow. With the greater skin friction and mixing in this fresh turbulent region the solvent evaporates quickly leaving the white deposit of Kaolin on the surface. The turbulent boundary layer quickly assumes a low skin friction, almost separating, velocity profile as was designed. The evaporation process then slows down leaving a wet patch. A fringe of liquid dribbles can be seen on the lower edge of the painted strip. These dribbles drop down vertically wherever they occur from the mid-chord point to the trailing edge. This indicates that the skin friction in this region is approximately zero. The fact that the dribbles do not progress upstream is an indication that no reverse flow exists.

To further examine the flow in the turbulent region a tuft, approximately 1% of chord long, was held next to the surface. The tuft

FIGURE 41 - UPPER SURFACE FLOW VISUALISATION, $Re = 10^6$, $\alpha = 16^o$.

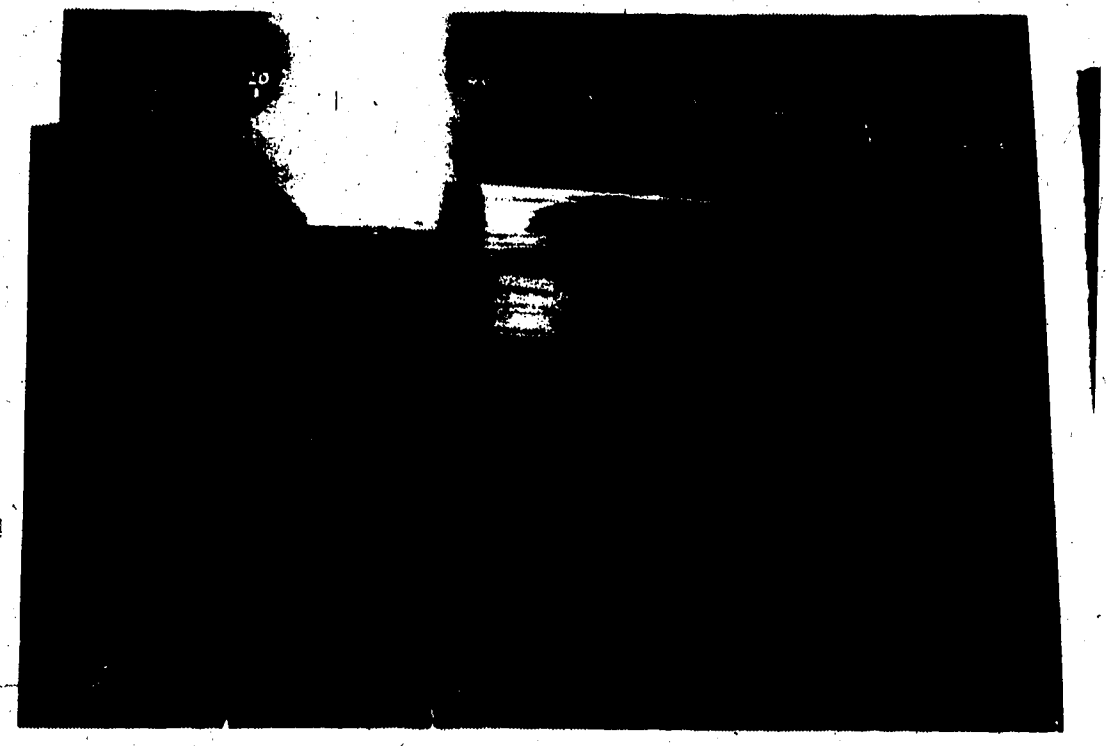

FIGURE 42 - UPPER SURFACE FLOW VISUALISATION, $Re = 10^6$, $\alpha = 12.5^o$

always pointed downstream. It did not however adhere firmly to the surface at the trailing edge which indicates that the boundary layer is certainly very close to separating. Sandborn and Liu [44] show that evaporation techniques of flow visualisation indicate the start of intermittent separation and not full flow separation as was previously believed. Some drying can be observed in Figure 41 over approximately the last 7% of chord. These experimental results therefore indicate that intermittent turbulent separation is occurring in this region.

At angles of attack greater than 16^{o} at this Reynolds number the flow broke down completely, stalling the section. At lower angles of attack the flow pattern was quite different from that at 16^{o}. A typical example is shown in Figure 42. This is the flow pattern at 12.5^{o} whose pressure distribution is given in Figure 40. A laminar separation bubble can be clearly seen separating from the surface at 35% of chord and reattaching at 40.5%. This is the region of the instability gradient and the airfoil section was designed to produce a laminar separation bubble in this region. The first long vertical dribble in Figure 42 shows the separation line and the last is the reattachment line where the local skin frictions are approximately zero. Inside the bubble dribbles of liquid can be seen clearly travelling upstream in the reverse flow of the bubble. The transition to turbulent flow occurs somewhere in the bubble and the reattaching boundary layer is turbulent. Immediately after the reattachment there is fast evaporation of the solvent indicating this. The wet region of almost zero skin friction turbulent flow continues to the trailing edge indicating completely attached flow to this point.

On the lower surface of the model the boundary layer remained attached for all angles shown in Figure 40. The transition point moved upstream from 75% to 62% of chord as the angle of attack was reduced from 16^{o} to 2.2^{o}. At angles below 2^{o} the transition point moved rapidly forward until at 0.1^{o} a laminar separation bubble was formed at about 20% of chord.

The model was tested at Reynolds numbers of 10^6, 1.5×10^6 and 2×10^6 to determine the effects this had on the pressure distributions. Up to the stalling angles the resulting pressure distributions were not greatly different from those shown in Figure 40. The upper surface pressure coefficients were, to within experimental accuracy, the same. On the lower surface the pressure coefficients were, on average slightly larger at larger Reynolds numbers. Comparing results at 10^6 and 2×10^6 Reynolds numbers at high angles of attack showed that there was an increase in loading at the trailing edge of approximately 0.1q.

6.5 Airfoil Characteristics

The lift and quarter chord pitching moment characteristics of the section at the three test Reynolds numbers are given in Figure 43 over the tested range of angles of attack. The scatter in the data at the lowest Reynolds number is due to errors in measuring the pressures around the section. The pressures in this case were approximately ¼ of those measured at 2×10^6 Reynolds number and the pressure transducers gave correspondingly larger errors. The lift curve slopes are constant from angles of attack from 4^{o} to within 1^{o} of the stall. Below 4^{o} the lower surface boundary layer transition point moved forward quickly. The thicker boundary layer eventually separated near the trailing edge and the resulting disturbance to the smooth flow over the trailing edge

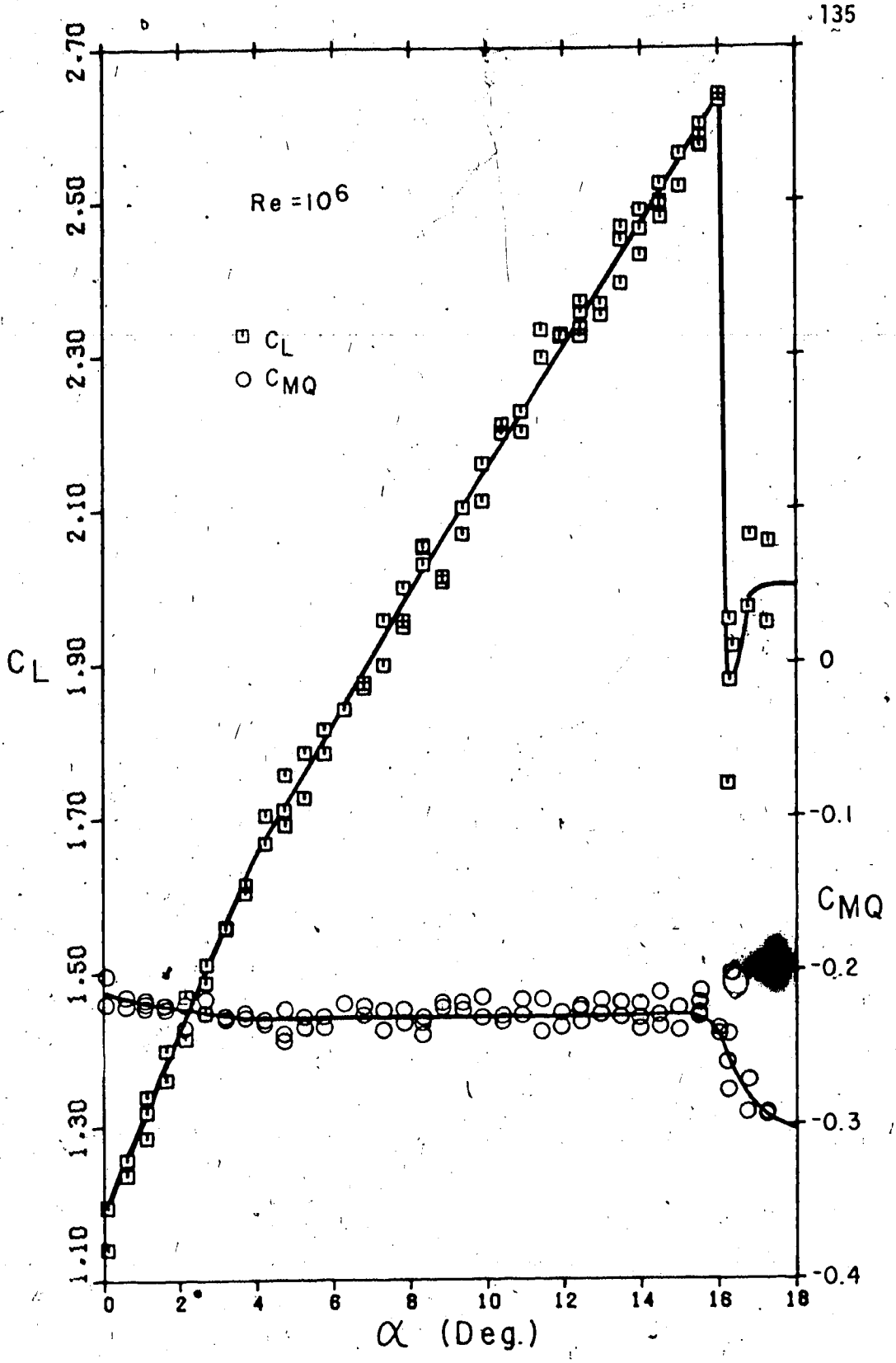

FIGURE 43 (a) - EXPERIMENTAL LIFT AND PITCHING MOMENT CHARACTERISTICS OF MODEL

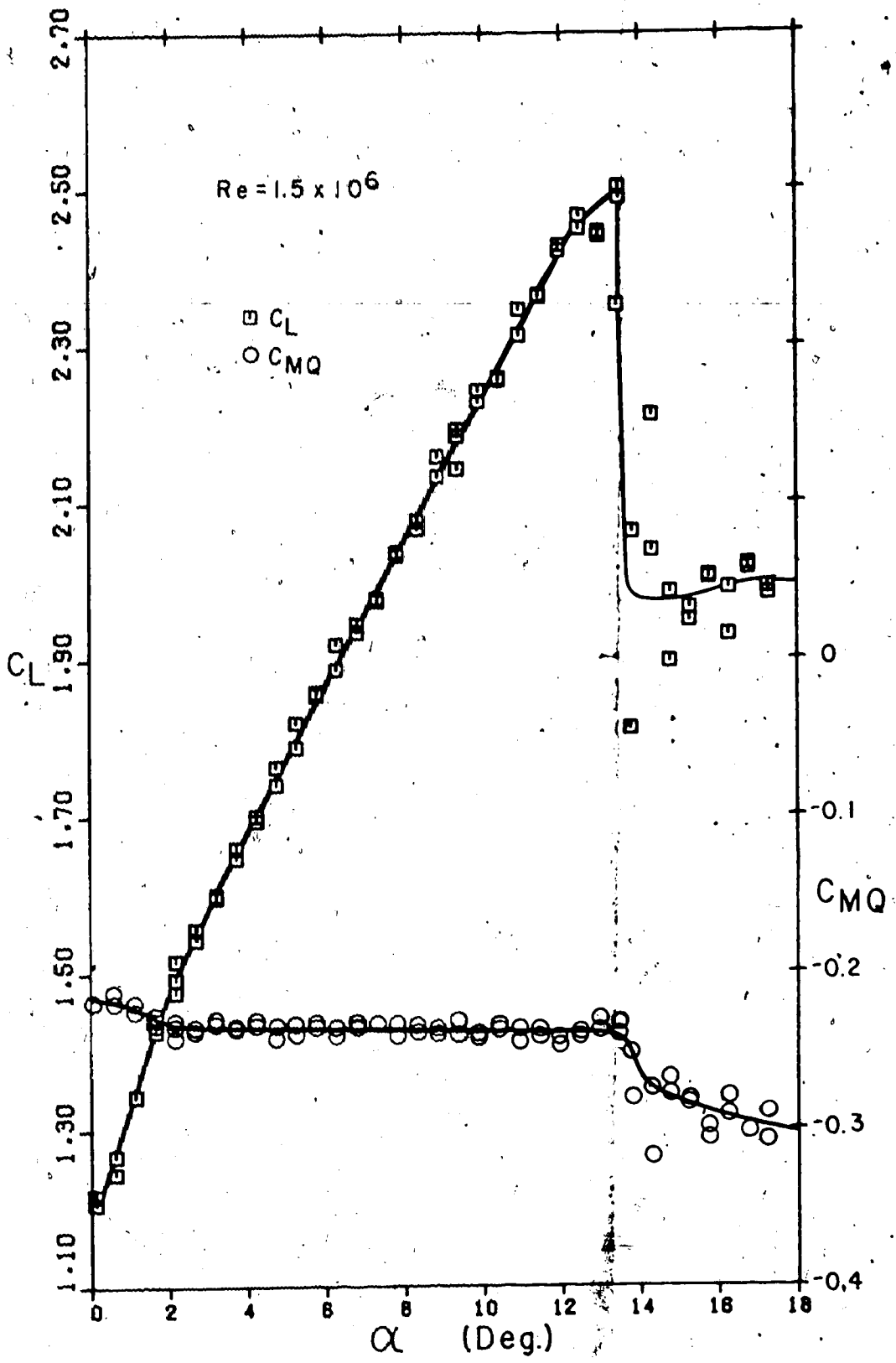

FIGURE 43 (b) - CONTINUED

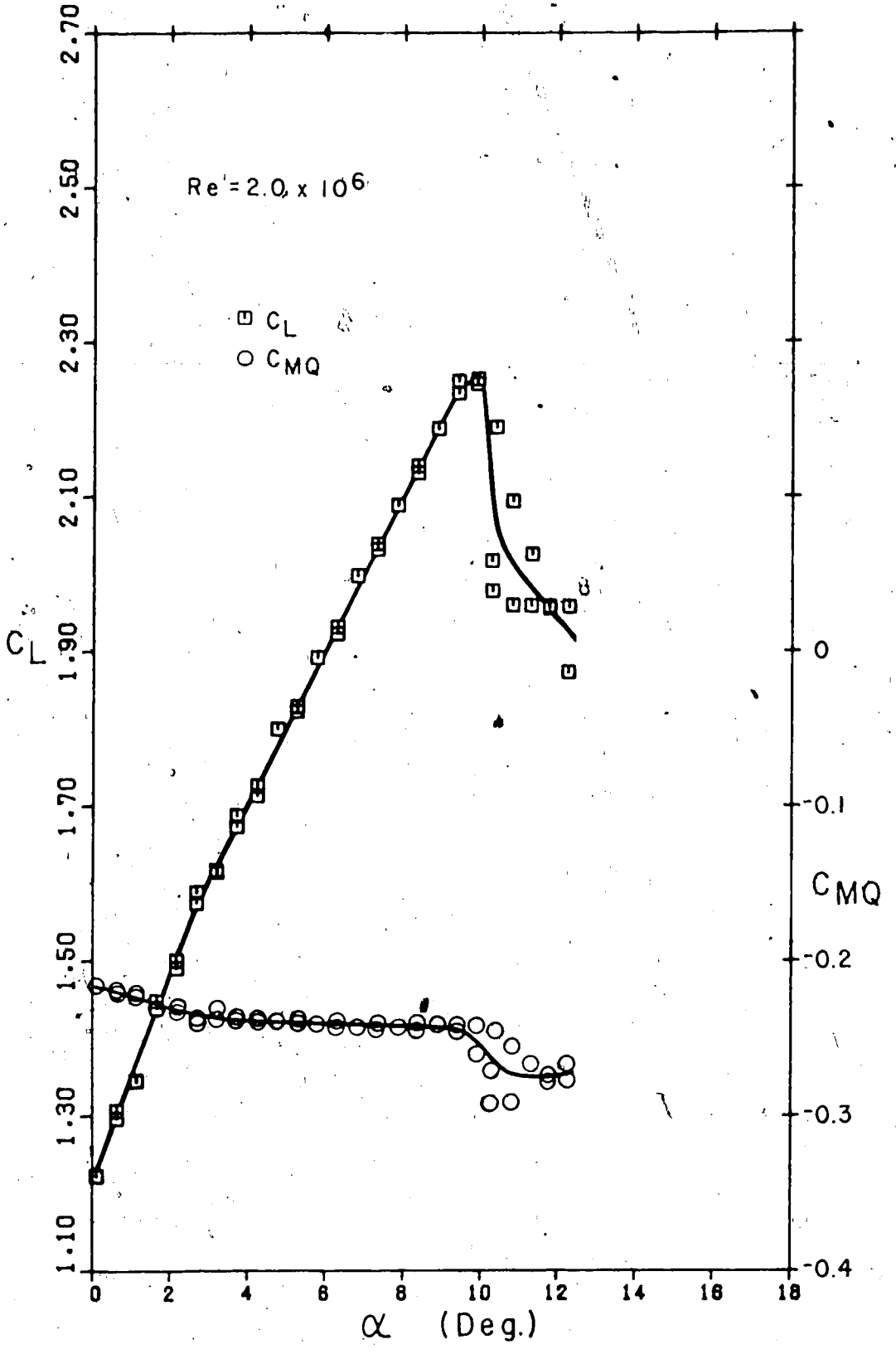

FIGURE 43 (c) - CONCLUDED

reduced the lift coefficient.

The lift curve slopes are 0.084, 0.093 and 0.101 per degree respectively for the three Reynolds numbers. This increase with Reynolds number is slightly larger than is usually observed on conventional airfoil sections. The boundary layers which develop on the upper surface are particularly thick due to the use of an almost separating pressure distribution, and the stronger than usual Reynolds number effect is attributed to these thicker than usual boundary layers.

The maximum lift coefficients were 2.64, 2.50 and 2.25 at Reynolds numbers of 10^6, 1.5×10^6 and 2×10^6 respectively. The stall in each case was caused by the upstream movement of the transition point on the upper surface. Flow visualisation studies taken at close to the stall showed that transition occurred ahead of 32% of chord for all Reynolds numbers. This earlier transition results in thicker downstream boundary layers which separate under the high adverse pressure gradients generated by the section. The stall was therefore a rapid form of trailing edge stall rather than due to the bursting of the laminar separation bubble.

High Reynolds numbers promoted earlier transition leading to earlier stalling of the section. This accounts for the observed decline in maximum lift coefficient with Reynolds number. A similar decline has been observed by Wortmann [50] on his high lift sections and the same phenomenon resulted in the failure of Liebeck's "laminar r[illegible]op" section [48] to operate successfully at Reynolds numbers in excess of 10^6.

The quarter chord pitching moment coefficients are also plotted in Figure 43. These are large and negative due mainly to the large amounts of rear loading on the section. The moment coefficients are

fairly constant over the linear range of the lift curve indicating that the quarter chord is approximately the aerodynamic centre of the section.

The measured drag coefficients are given in Figure 44 for all three Reynolds numbers. These drag coefficients are higher than those found on the high lift sections of Wortmann [50] or Liebeck [48]. The reason for this lies primarily in the high velocity at the trailing edge of the section. The Squire and Young drag formula (38) shows clearly the great dependancy of drag on this velocity. As the Reynolds number is increased the viscous effects are reduced and the thinner boundary layers give less drag. Because the experimental and theoretical pressure distributions are quite different no meaningful comparison can be made between actual and predicted drag coefficients.

The lift to drag ratio is an important parameter in estimating the performance of an airfoil section. The measured values for this section are given in Figure 45 for the three Reynolds numbers tested. As there is little difference between the lift curves at these Reynolds numbers the differences in glide ratio reflect mainly the improvements in drag as the Reynolds number increases. These results apply to wings of infinite aspect ratio. For a wing of reasonable aspect ratio the induced drag will be larger than the boundary layer drag at the angles tested.

6.6 Discussion

The experiments have shown that considerable rear loading can be developed on a single component airfoil section and this does lead to large lift coefficients. The section develops a lift coefficient of 2.64 at a Reynolds number of 10^6. By comparison Liebeck's section [48] gave a maximum lift coefficient of 2.2 and had no rear loading.

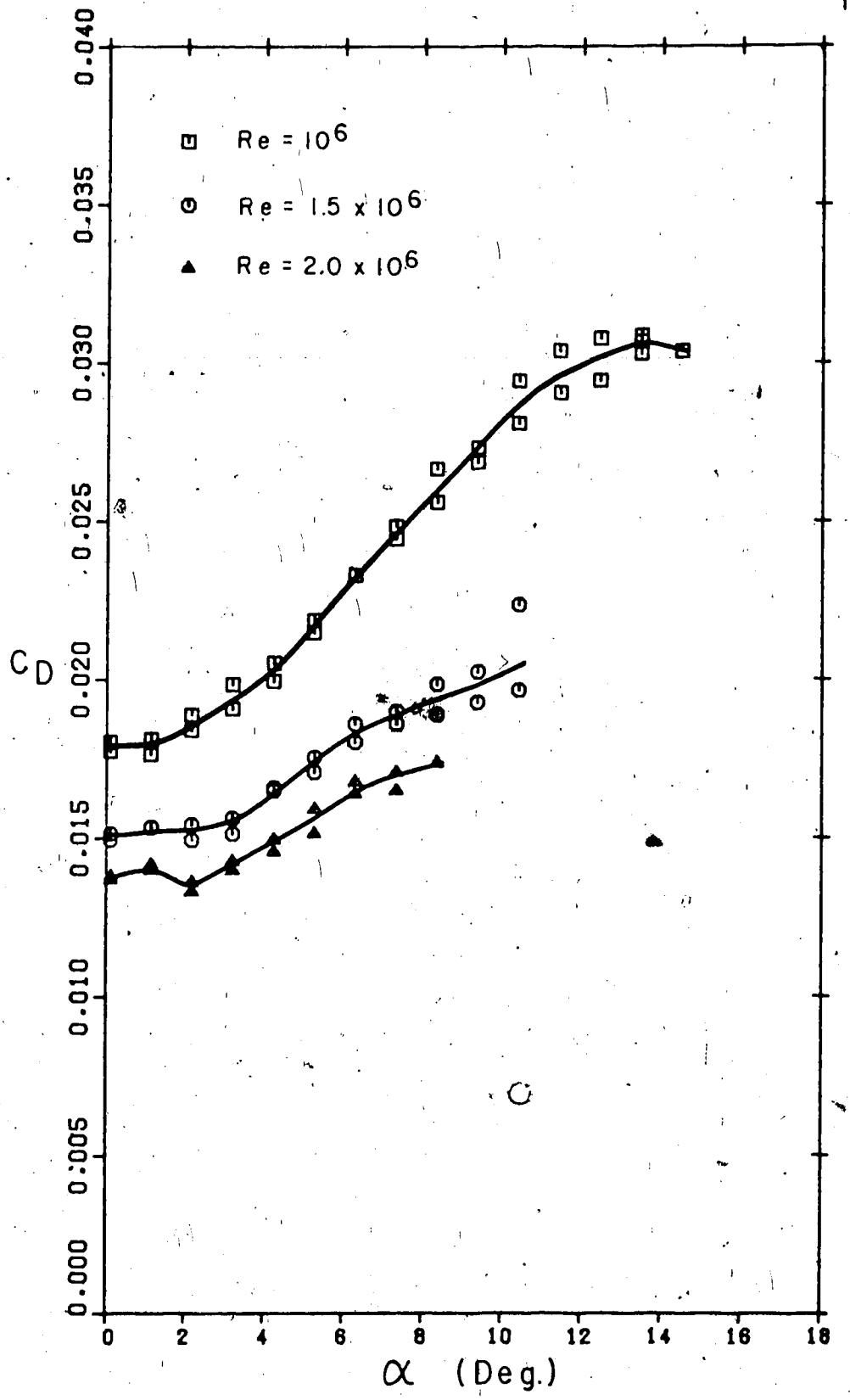

FIGURE 44 - EXPERIMENTAL DRAG COEFFICIENTS OF MODEL

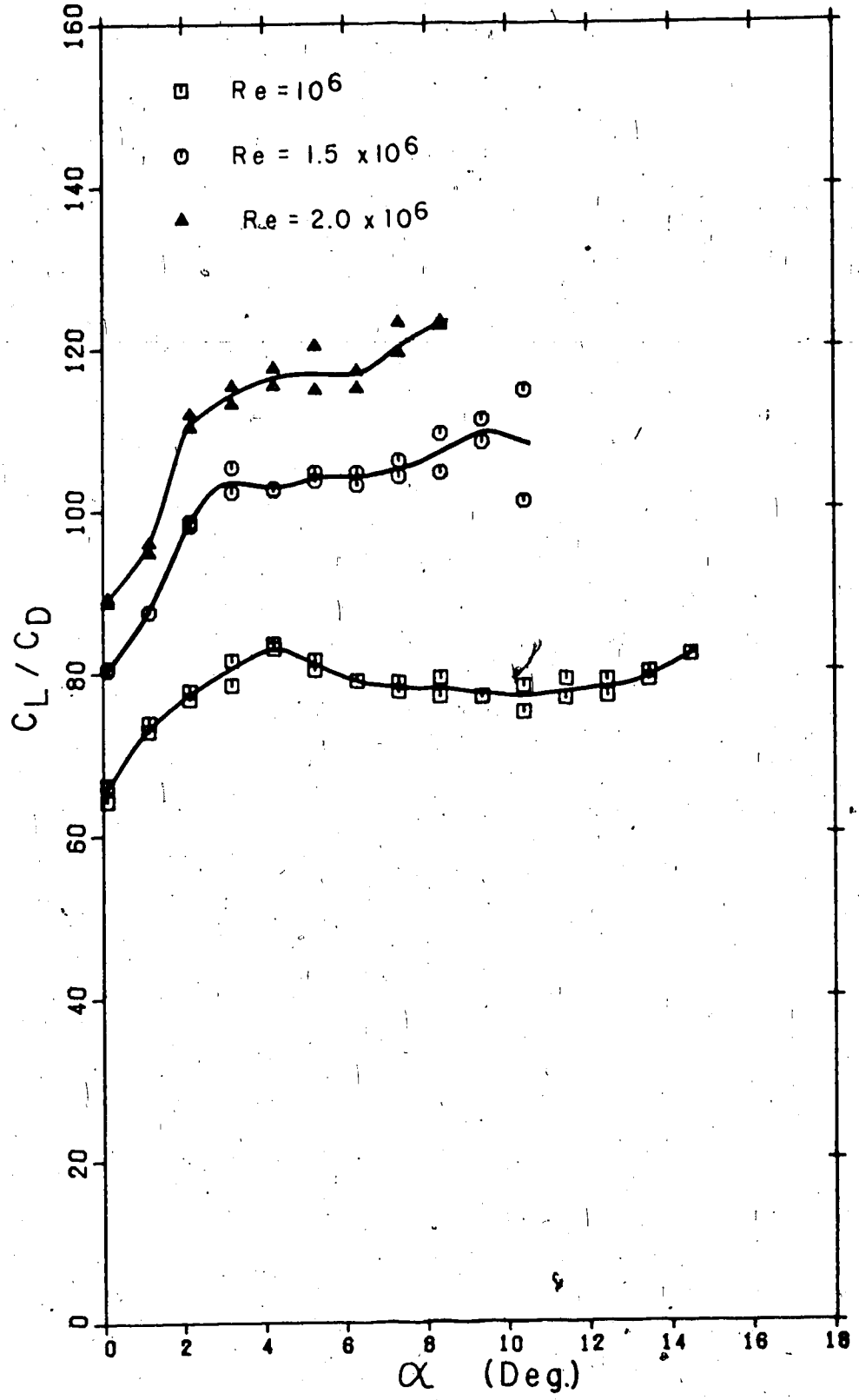

FIGURE 45 - EXPERIMENTAL GLIDE RATIOS OF MODEL

Wortmann's high lift section [50] achieved a lift coefficient of almost 2.4 and showed some rear loading in potential flow although the amount achieved in practice is not known.

It is a source of some disapointment that the viscous flow analysis was unable to correctly predict the pressure distribution about the section, and hence the lift coefficient. As the potential flow method and the boundary layer calculations have proven themselves to be correct in independent tests the errors lie in the matching of the two in the viscous flow model.

The large differences between theory and experiment could be attributed to the calculation of an incorrect camber line adjustment in the visous flow analysis. Various camber line modifications were therefore tried to attempt to find a theoretical solution which modelled the experiments. The most severe modification applied was to match the upper surface of the equivalent airfoil section to the calculated upper side displacement surface. This reduced the calculated lift coefficient from 3.71 to 3.28 at the design conditions. Employing the displacement thicknesses calculated from the experimental pressure coefficients gave little better results.

It is therefore interesting to speculate as to whether any equivalent airfoil of the type used in the viscous flow analysis can provide the experimental pressure distributions shown in Figure 40. The design technique provides a tool that can shed light on this issue. The design requirements were specified to be the pressure coefficients obtained experimentally at 16^{o} angle of attack at a Reynolds number of 10^{6}. The basic section used was the model itself and the calculations were terminated after 12 iterations. Figure 46 shows a comparison of

the model and the designed section. This is the effective section which most nearly approaches the experimental results. The agreement between the pressure coefficients on the effective section and the experiments was excellent up to the last 5% of chord.

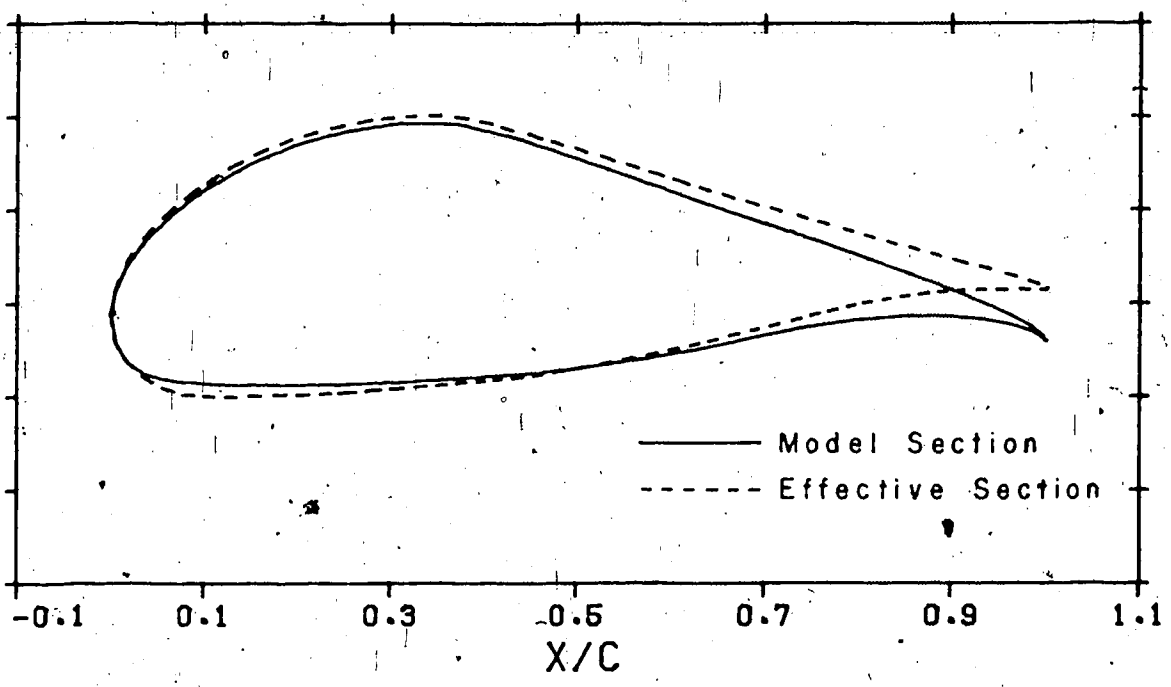

FIGURE 46 - COMPARISON OF MODEL AND EFFECTIVE SECTION

The effective section is considerably thicker than the model near the trailing edge and the camber of the section has been considerably reduced. This is approximately the geometry that the viscous flow calculations should have yielded by the displacement thickness changes. The trailing edge however has moved up by 5% of chord. This is approximately three times the calculated displacement thickness at that

point hence camber line adjustments calculated from displacement thickness could not yield this effective section.

In the viscous flow model both thickness effects and the influence of the wake were neglected. The increase in thickness of the effective section relative to the model suggests that thickness effects should be accounted for. Thickness effects could not however account for the large movement of the trailing edge. It is therefore thought that the effect of the wake must be considered in the viscous flow analysis of sections with very large rear loadings.

The boundary layer analysis, when applied to the measured pressure distributions, failed to indicate the forward movement of transition that causes the stall. However it can be used to demonstrate the mechanism that leads to the stall. On applying the boundary layer analysis to the upper surface pressure distribution at the maximum lift condition, laminar separation was predicted at 38% of chord. The values of the shape factor H for this analysis are plotted in Figure 47. Downstream of transition the minimum skin friction coefficient was calculated to be 7.26×10^{-4} at 85% of chord. By forcing transition to occur, as was observed, at approximately 32% of chord then the turbulent flow came much closer to separation. The shape factors H for this flow are also plotted in Figure 47 and in this case the minimum skin friction coefficient dropped to 3.44×10^{-4}. Any farther forward movement of transition caused the analysis to predict turbulent separation.

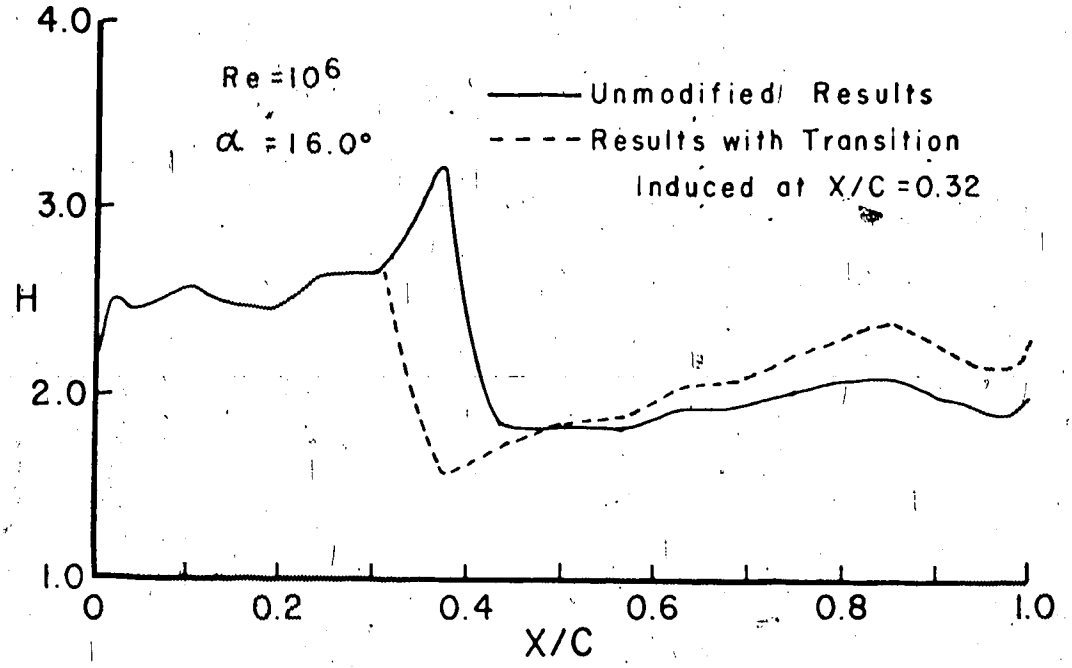

FIGURE 47 - THEORETICAL BOUNDARY LAYER ANALYSES OF EXPERIMENTAL PRESSURE DISTRIBUTION

The analysis method could not predict the early transition at high Reynolds numbers. This was true for all of the transition criteria (32) to (34) and for the Schlichting, Ulrich, Granville [35] method. This last method indicates that the surface waviness on the section, which shows up as irregularities in the theoretical and actual pressure distributions, can cause the laminar boundary layer to enter the unstable region ahead of the measured transition point. The growth of instabilities due to surface waviness is thought to be the most probable cause of early transition as both surface roughness and freestream turbulence levels were low.

The failure of the transition criteria on this airfoil section suggests that they must be re-examined. The present prediction methods are based mainly on data from previous airfoil sections. This section and Liebeck's are of a new type with long laminar rooftop velocity distributions and both exhibit the same unexpectedly early transition. They may therefore be experiencing a particular condition which was not present in previous airfoil sections. Hopefully this section could provide some information on this aspect of boundary layer theory.

When laminar separation bubbles were observed their location was predicted well by the boundary layer analysis. The turbulent separation criterion (37) appears from this exercise to be consistent with the onset of intermittent separation. From the results shown in Figure 47 it can be seen that the design value of $H = 1.8$ for the turbulent layer was conservative. Values of H of 2.1 are quite safe and higher values seem to be quite possible. This will enable designers to use larger adverse pressure gradients with consequent increases in the length of laminar rooftop flow. This could make possible the design of sections with higher lift coefficients than measured here.

CHAPTER VII

CONCLUSIONS

The determination of the properties of airfoil sections is based on the analysis of the section in potential flow. Such an analysis method was developed here and it was shown to be the most accurate to date. The principal reason for this accuracy is the correct formulation of the Kutta condition which determines the circulation about the section. This trailing point Kutta condition predicts correctly the loadings which occur near the trailing edge of airfoil sections. This is particularly important in the development of high lift sections and for multi-component sections for which forward components show large amounts of rear loading.

The practical application of a potential flow analysis method generally requires its use in an iterative procedure. Effiiciency is therefore very important. This method is simple, accurate and very efficient by comparison with other methods. It is therefore a very important practical tool for the aeronautical industry.

A technique of designing airfoil sections in potential flow was developed from this analysis method. By the application of this technique to various problems it was shown to be both powerful and flexible. The use of the trailing point Kutta condition greatly simplifies the calculation of the geometry of the designed airfoil section. This leads directly to the faster convergence of the iterative design procedure. All previous surface singularity techniques of airfoil design had used a Kutta condition which specified no loading near the trailing edge of the section. As the trailing point Kutta condition

does not have this restriction it permits the airfoil section designer to investigate the possibilities associated with large loadings near the trailing edge.

The novel use of the design technique to determine, from experimental pressure distributions, the effective airfoil in potential flow shows a further use of the design method. This application to experimental measurements may prove useful in the development of future viscous flow analyses.

A boundary layer analysis method which had proven accurate in the analysis of the boundary layers on airfoil sections was programmed. The accurate prediction of laminar separation, transition and turbulent separation are of crucial importance in airfoil sections and suitable criteria were chosen for each of these effects.

Combining the boundary layer method with the potential flow solutions a viscous flow analysis method was developed. This method uses the calculated displacement effects of the boundary layer to modify the camber line of the section to produce an equivalent airfoil section. This concept was shown to work well, giving accurate predictions of the viscous flow over a selection of airfoil sections.

A practical method for determining airfoil velocity distributions which yield maximum lift coefficient was developed using the boundary layer analysis technique. Employing this method the effects of raising the trailing edge velocity on the upper surface were examined. This is equivalent to raising the loading at the trailing edge in practical airfoil sections. The rooftop velocity for the optimum distribution was found to increase linearly with the trailing edge velocity. At the same time the optimum lift coefficient which the

section can produce rises nonlinearly.

An airfoil section with a high velocity on its upper surface at the trailing edge was designed to test the practical possibilities of achieving high lift coefficients by this technique. When this section was analyzed by the viscous flow method it was found to have a large amount of rear loading. This produced the desired high lift coefficient together with a large nose-down pitching moment coefficient and a large drag coefficient.

A model of the section was constructed and tested in the University of Alberta low turbulence wind tunnel at a series of angles of attack and at Reynolds numbers between 10^6 and 2×10^6. The test results show that the theoretically predicted lift coefficients were not obtained. The model also failed to develop the amount of rear loading which had been predicted. The rear loading which was achieved by this section was however much greater than that reported for any known section. This enabled the section to develop higher lift coefficients than had ever been reported for such single component sections.

The large rear loading on this section was found to be largely independent of Reynolds number and angle of attack, up to the stall. The lift curve slopes were, over a large range, linear although they were slightly less than those usually observed on modern sections. The strong viscous effects which account for this were also indicated by the relatively large drag coefficients of the section. The pitching moment was large and nose-down and, to within experimental accuracy, the quarter chord is the aerodynamic centre.

The experiments have shown that large rear loadings can be generated on single component sections. However the failure of the viscous flow analysis method to predict the experiments exactly implies that future sections designed to have large rear loadings cannot be analyzed with sufficient accuracy by this method. The design of such sections cannot be ignored as the contribution which they can make must be examined. However to proceed with experimental tests, on a trial and error basis, on sections whose characteristics cannot be accurately predicted will be expensive and will not likely lead to optimum airfoil designs. It is therefore advisable to extend the capability of the analysis method to handle such sections.

To develop the viscous flow analysis method from its present state to its full potential will require the consideration of the thickness effects of the boundary layer and of the wake. This would involve an analysis of the wake and the determination of the effect of the wake on the potential flow about the section. The transition criterion would also have to be re-examined as this plays a very important role in limiting the performance of sections with long laminar roof top flows. The solution to this problem may lie in obtaining detailed experimental results in the boundary layer. For this and for testing any viscous flow methods this section will provide an excellent test case.

Until such problems are solved it may be more practical to investigate other possibilities of more conventional, less highly loaded sections. For such sections the techniques which were developed here will provide the aerodynamicist with accurate analysis of airfoil sections which can be rapidly and efficiently designed. The computer analysis will then enable experimental testing of airfoil designs to be more productive.

REFERENCES

[1] LIEBECK, R.H., and Ormsbee A.I. - 'Optimisation of Airfoils for Maximum Lift', Journal of Aircraft, Vol. 7, No. 5 1970, pp 409-416.

[2] HESS, J.L., and Smith, A.M.O. - 'Calculation of Potential Flow about Arbitrary Bodies', Progress in Aeronautical Sciences, Vol. 8, Pergamon Press, 1967.

[3] CHEN, A.W. - 'The determination of the Geometries of Multiple-element Airfoils Optimised for Maximum Lift Coefficient', Thesis, University of Illinois, 1972.

[4] THEODORSEN, T. - 'Theory of Wing Sections of Arbitrary Shape', NACA Report No. 411, 1931.

[5] MARTENSEN, E. - 'Berechnung der Druckverteilung An Gitterprofilen in Ebener Potential Stromung mit einer Fredholmschen Integralgleichung', Arch. Rat. Mech. Anal., Vol. 3, 1959, pp 235-270.

[6] WILKINSON, D.H. - 'A Numerical Solution of the Analysis and Design Problems for the Flow Past One or More Aerofoils or Cascades', A.R.C. R & M 3545, 1967.

[7] GOLDSTEIN, A.W., and Jerison, M. - 'Isolated and Cascade Airfoils with Prescribed Velocity Distribution', NACA. Tech. Report No. 869, 1947.

[8] OELLERS, H.J. - 'Die Inkompressible Potentialstromung in der Ebenen Gitterstuffe', WGLR Jahrbuch, 1962, pp 349-353.

[9] MAVRIPLIS, F. - 'Aerodynamic Prediction and Design Methods of Aircraft High Lift Systems', N.R.C. of Canada, Proceedings of the Aerodynamics Seminar of May 15, 1974.

[10] MAVRIPLIS, F. 'Private Communication'.

[11] HESS, J. L. - 'Higher Order Numerical Solutions of the Integral Equation for the Two-dimensional Neumann Problem', Computer Methods in Applied Mechanics, Vol. 2, 1973, pp 1-15.

[12] MILNE-THOMSON, L.M., - 'Theoretical Aerodynamics', Dover Publications, 1973.

[13] PRANDTL, L., and Tietjens, O.G., 'Applied Hydro - and Aeromechanics', Dover Publications, 1957.

[14] BHATELEY, I.C., and Bradley, R.G. - 'A Simplified Mathematical Model for the Analysis of Multi-element Airfoils near the Stall', AGARD-CP-102, 1972.

[15] STEVENS, W.A., Goradia, S.H. and Braden, J.A. - 'Mathematical Model for Two-dimensional Multi-component Airfoils in Viscous Flow', NASA CR-1843, 1971.

[16] AHLBERG, J.H., Nilson, E.N., and Walsh, J.L. - 'The Theory of Splines and Their Applications', Mathematics in Science and Engineering, Vol. 38, Academic Press, 1967.

[17] WILLIAMS, B.R. - 'An Exact Test Case for the Plane Potential Flow about Two Adjacent Lifting Aerofoils', A.R.C. R & M 3717, 1971.

[18] SEEBOHM, T., and Newman, B.G. - 'A Numerical Method for Calculating Viscous Flow Round Multiple-Section Aerofoils', Aeronautical Quarterly, Vol. 26, Pt. 3, 1975, pp 176-188.

[19] MAVRIPLIS, F. - 'Comparison of Surface-Vorticity Method with Surface-Source Method and with an Exact Solution for Two dimensional Potential flow around Two Adjacent Lifting Airfoils'. C.A.S. Journal., Vol. 19, 1973, pp 411-413.

[20] BEATTY, T.D. and Narramore, J.C. - 'Inverse Method for the Design of Multielement High-Lift Systems', Journal of Aircraft, Vol. 13, No. 6, 1976, pp 393-398.

[21] ABBOTT, J.H. and VonDoenhoff, A.E. - 'Theory of Wing Sections', Dover Publications, 1959.

[22] POWELL, B.J. - 'The Calculation of the Pressure Distribution on a Thick Cambered Aerofoil at Subsonic Speeds including the Effects of the Boundary Layer', A.R.C. CP. No. 1005, 1967.

[23] CEBECI, T. and Smith, A.M.O. - 'Calculation of Profile Drag of Airfoils at Low Mach Numbers', Journal of Aircraft, Vol. 5, No. 6, 1968, pp 535-542.

[24] THWAITES, B. - 'Approximate Calculation of the Laminar Boundary Layer', Aeronautical Quarterly, Vol. 1, 1949, pp. 245-280.

[25] HEAD, M.R. - 'Entrainment in the Turbulent Boundary Layer', A.R.C. R & M. 3152, 1962.

[26] KLINE, S.J., (Editor) - 'Computations of Turbulent Boundary Layers', 1968 AFOSR-IFP-Stanford Conference.

[27] EPPLER, R. - 'Practische Berechnung Laminarer und Turbulenter Absuage - Grenzschichten', Ingenieur Archiv, Bd. 32, 1963, pp 222-245.

[28] FELSCH, K.O., Geropp, D. and Walz, A. - 'Method for Turbulent Boundary Layer Prediction', AFOSR-IFP-Stanford Conference, Vol. 1, 1968, pp 170-176.

[29] MILEY, S.J. - 'An analysis of the Design of Airfoil Sections for Low Reynolds Numbers', Thesis, Mississippi State University, 1972.

[30] NICOLL, W.B. and Escudier, M.P. - 'Empirical Relationships Between the Shape Factors H_{32} and H_{12} for Uniform Density Turbulent Boundary Layers and Wall Jets', A.I.A.A. Journal, Vol. 4, 1966, pp 940-942.

[31] FELSCH, K.O. - 'Beitrag zur Berechnung Turbulenter Grenzschichten in Zwei-dimensionaler Incompressibler Stromung', Deutsche Luft-und Raumfahrt, DLR-FB-66-46, 1966.

[32] SMITH, A.M.O. - 'Transition, Pressure Gradient and Stability Theory', Proc. 9th Int. Cong. Appl. Mech., Vol.4, 1957, pp 234-244.

[33] CEBECI, T., Mosinskis, G.J., Smith, A.M.O. - 'Calculation of Viscous Drag in Incompressible Flows', Journal of Aircraft, Vol. 9, No. 10, 1972, pp 691-692.

[34] WHITE, F.M. - 'Viscous Fluid Flow', McGraw-Hill, 1974.

[35] SCHLICHTING, H. - 'Boundary Layer Theory', McGraw-Hill, 1968.

[36] CURLE, N., and Skan, S.W. - 'Approximate Methods for Predicting Separation Properties of Laminar Boundary Layer', Aeronautical Quarterly, Vol. 8, 1957, pp 257-268.

[37] LIU, C.Y., and Sandborn, V.A. - 'Evaluation of the Separation Properties of Laminar Boundary Layers', Aeronautical Quarterly, Vol. 19, 1968, pp 235-242.

[38] TANI, I. - 'On the Solution of the Laminar Boundary Layer Equations', Journal of the Physical Society of Japan, Vol. 4, 1949, pp 149-154.

[39] OWEN, P.R., and Klanfer, L. - 'On the Laminar Boundary Layer Separation from the Leading Edge of a Thin Aerofoil', R.A.E. Report No. Aero 2508, 1953.

[40] GASTER, M. - 'The Structure and Behaviour of Laminar Separation Bubbles', A.R.C., Report 28-226.

[41] HORTON, H.P. - 'A Semi-empirical Theory for the Growth and Bursting of Laminar Separation Bubbles', A.R.C., C.P. No. 1073, 1967.

[42] CHANG, P.K. - 'Separation of Flow', Pergamon Press, 1970.

[43] STRATFORD, B.S. - 'The Prediction of Separation of the Turbulent Boundary Layer', Journal of Fluid Mechanics, Vol. 5, 1959, pp 1-16.

[44] SANDBORN, V.A., and Liu, C.Y. - 'On Turbulent Boundary-layer Separation', Journal of Fluid Mechanics, Vol. 32, 1968, pp 293-304.

[45] SMITH, A.M.O., and Cebeci, T. - 'Remarks on Methods for Predicting Viscous Drag', AGARD- CP-124, 1973.

[46] RASPET, A., and Gyorgyfalvy, D. - 'Boundary Layer Studies on the Phoenix Sailplane', 8th OSTIV Congress, Cologne, 1960.

[47] LOFTIN, L.K., and Smith, H.A. - 'Aerodynamic Characteristics of 15 NACA Airfoil Sections at Seven Reynolds Numbers from 0.7 x 10^6 to 9.0 x 10^6, NACA Technical Note 1945, 1949.

[48] LIEBECK, R.H. - 'A Class of Airfoils Designed for High Lift in Incompressible Flow', Journal of Aircraft, Vol. 10, No. 10, 1973, pp 610-617.

[49] BINGHAM, G.J. and CHEN, A.W. - 'Low-speed Aerodynamic Characteristics of an Airfoil Optimised for Maximum Lift Coefficient', NASA TND-7071, 1972.

[50] WORTMANN, F.X. - 'The Quest for High Lift', AIAA paper No. 74-1018, 2nd Int. Symposium on Technology and Science of Low Speed and Motorless Flight, 1974.

[51] SMITH, A.M.O. - 'High Lift Aerodynamics', Journal of Aircraft, Vol. 12, No. 6, 1975, pp 501-530.

[52] WORTMANN, F.X. - 'A Contribution to the Design of Laminar Profiles for Gliders and Helicopters', Z. Flugw., 3(10), 1955, pp 333-345., also, Great Britain, Ministry of Aviation, TIL/T.4903, 1960.

[53] GARNER, H.C. - 'Subsonic Wind Tunnel Wall Corrections', AGARD 109, 1966.

[54] POPE, A., and Harper, J.J. - 'Low Speed Wind Tunnel Testing', John Wiley & Sons, 1966.

[55] JONES, B.M. - 'Measurement of Profile Drag by the Pitot-Traverse Method', A.R.C. R & M 1688, 1936.

APPENDIX 1

EVALUATION OF THE INTEGRAL IN EQUATION (7)

The most straight forward method of evaluating the integral in equation (7) is to do so using a numerical integration procedure. This replaces the exact integral with the sum of weighted values of the integrand calculated at certain points in the range of integration. This is, effectively the procedure used by Wilkinson [6] in his method of analysis. The better solutions which are obtained by the method of Hess and Smith [2] can be partly explained by the use of exact integration formula over approximate, straight line, surface elements. Following this approach Hess [11] has considered the exact evaluation of the integral for the Hess and Smith method using higher order terms including surface curvature and variations in the strength of the singularity over the element. The improvement which Hess obtained suggests that higher order solutions for this analysis method should be examined.

The surface element is therefore chosen to be curved and the velocity distribution, or the vorticity distribution, can vary over the element. The influence of this distribution on one element on the control point of another element is calculated by the integral

$$I = \frac{1}{2\pi} \int_{S1}^{S2} \gamma(S) \ln r(C_i, S)\, dS. \qquad (45)$$

A coordinate system (ξ,η) is set up with it origin at the control point of the influencing element as shown in Figure 48. The influenced control point is located at (b,a) in this co-ordinate system.

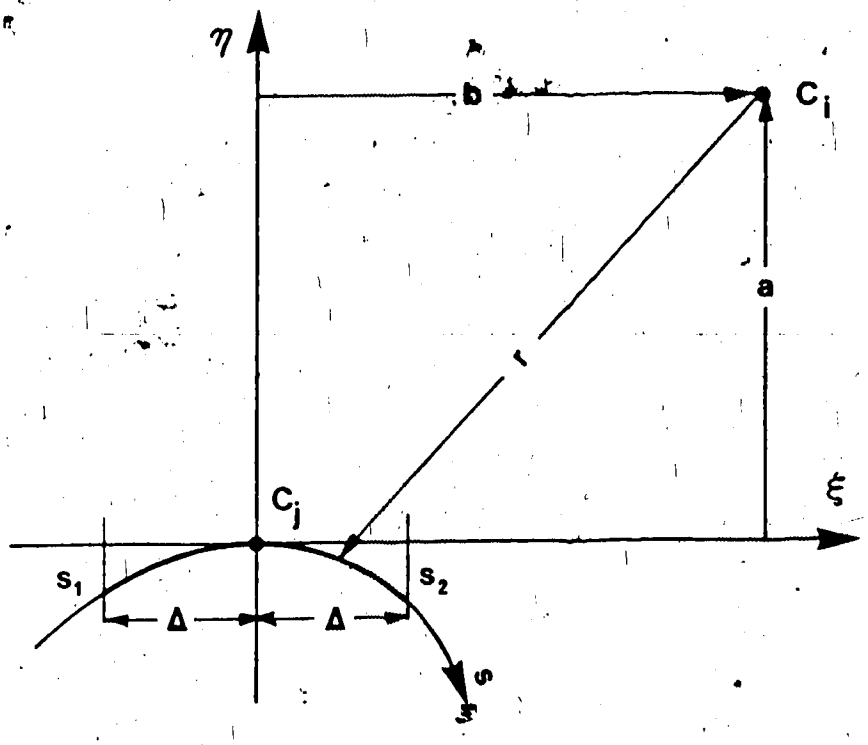

FIGURE 48 - GEOMETRY FOR CALCULATION OF HIGHER ORDER TERMS

The surface element is defined by $\eta = \eta(\xi)$. In the neighbourhood of the origin a power series expansion is used,

$$\eta = c\,\xi^2 + e\,\xi^3 + \ldots \qquad (46)$$

The integral is taken over the surface distance and it is convenient to use:

$$\frac{dS}{d\xi} = \left[1 + \frac{d\eta^2}{d\xi}\right]^{\frac{1}{2}} \qquad (47)$$

On expanding (47) as a series about $\xi = 0$,

$$\frac{dS}{d\xi} = 1 + 2\,c^2\,\xi^2 + 6\,ce\,\xi^3 + \ldots \qquad (48)$$

The vortex density can also be written as a series defined by,

$$\gamma(S) = \gamma^{(0)} + \gamma^{(1)}S + \gamma^{(2)}S^2 + \gamma^{(3)}S^3 + \ldots \quad (49)$$

Applying (48) to (49),

$$\gamma(\xi) = \gamma^{(0)} + \gamma^{(1)}\xi + \gamma^{(2)}\xi^2 + \left(\frac{2}{3}c^2\gamma^{(1)} + \gamma^{(3)}\right)\xi^3 + \ldots \quad (50)$$

The distance $r(c_i,S)$ from the control point to the surface is,

$$r(c_i,S) = [(a-n)^2 + (b-\xi)^2]^{\frac{1}{2}} . \quad (51)$$

At this point it is necessary to employ the technique used by Hess [11]. Instead of expanding this term directly a modification is used which permits the basic, flat element, term to appear as the first term of the series. By writing,

$$r_f^2 \equiv a^2 + (b-\xi)^2 , \quad (52)$$

the distance to the flat surface $n = 0$, the remaining terms are expanded and,

$$r^2 = r_f^2 - 2ac\,\xi^2 - 2ae\,\xi^3 + \ldots . \quad (53)$$

Substituting (53) in the logarithm term and expanding all but the r_f^2 term about $\xi = 0$ yields,

$$\ln r = \frac{1}{2}\left[\ln(r_f^2) - \frac{2ac}{r_f^2}\xi^2 - \frac{2ae}{r_f^2}\xi^3 + \ldots\right] . \quad (54)$$

The integral (45) can now be evaluated to as high a degree of accuracy as is desired. In this case only the first few terms are retained, higher-order terms being of diminishing importance. Equation

(45) then becomes,

$$I = \frac{1}{4\pi} \int_{-\Delta}^{\Delta} \left[\gamma^{(0)} \ln r_f^2 + \gamma^{(1)} \ln r_f^2 \, \xi - \frac{2ac}{r_f^2} \gamma^{(0)} \xi^2 + \ldots \right] d\xi \tag{55}$$

The first term is the flat element, constant velocity case, the second term introduces a linear velocity distribution and the third introduces the surface curvature.

Each term in (55) can be integrated separately.

$$\int_{-\Delta}^{\Delta} \ln r_f^2 \, d\xi = \int_{-\Delta}^{\Delta} \ln [a^2 + (b - \xi)^2] \, d\xi$$

$$= \left[(b+\Delta) \ln (a^2 + (b+\Delta)^2) - (b-\Delta) \ln (a^2 + (b-\Delta)^2) \right.$$

$$\left. + 2a \, \mathrm{Tan}^{-1} \left(\frac{b+\Delta}{a}\right) - 2a \, \mathrm{Tan}^{-1} \left(\frac{b-\Delta}{a}\right) - 4\Delta \right]$$

$$= \left[(b+\Delta) \ln r_1^2 - (b-\Delta) \ln r_2^2 - 4\Delta \right.$$

$$\left. + 2a \, \mathrm{Tan}^{-1} \left(\frac{2a\Delta}{a^2+b^2-\Delta^2}\right) \right], \tag{56}$$

$$\int_{-\Delta}^{\Delta} \ln r_f^2 \, \xi \, d\xi = \frac{a^2-b^2+\Delta^2}{2} \ln \left(\frac{r_2}{r_1}\right) - 2b\Delta$$

$$- 2ab \, \mathrm{Tan}^{-1} \left(\frac{2a\Delta}{a^2+b^2-\Delta^2}\right), \tag{57}$$

$$\int_{-\Delta}^{\Delta} \frac{\xi^2}{r_f^2} \, d\xi = (b^2-a^2) \, \mathrm{Tan}^{-1} \left(\frac{2a\Delta}{a^2+b^2-\Delta^2}\right) + 2a\Delta$$

$$+ a \, b \, \ln \left(\frac{r_2}{r_1}\right) \tag{58}$$

For higher order terms involving surface curvature the constant C must be determined. In this case this was done by fitting parabolas through sets of three adjacent element end points. The curvature thus determined was assumed to be the airfoil surface curvature at the centre of the three points. The curvature at the control points were then found by interpolation. The values at the elements adjacent to the trailing edge were found by extrapolation. Having determined the curvature of the element the location of the control point can be calculated as this point is no longer on the straight line joining the element end points.

In employing variations in the singularity strength the term $\gamma^{(1)}$ is an unknown and must be related to the $\gamma^{(0)}$. Various schemes are available to do this and the technique used by Hess [11] is followed here. The derivitives of the γ distribution on the j^{th} element are determined by assuming a parabolic distribution through the three successive values $\gamma^{(0)}_{j-1}$, $\gamma^{(0)}_{j}$, $\gamma^{(0)}_{j+1}$. The linear vortex density term, unlike the other two terms, is therefore comprised of terms that involve the vortex densities of adjacent elements.

The application of the higher order methods to the solution involves the calculation of the extra terms (57) and (58). The curvature terms are simply added to the influence coefficient K_{ij} calculated for the basic case. The linear velocity terms must be added to the coefficients $K_{i,j-1}$, K_{ij}, $K_{i,j+1}$. Although this is not difficult to do, the extra calculations involved do take considerable amounts of time to perform.